Phase transitions and multifractal properties of random field Ising models

Von der Fakultät für Physik und Geowissenschaften

der Universität Leipzig

genehmigte

DISSERTATION

zur Erlangung des akademischen Grades

doctor rerum naturalium

(Dr. rer. nat.)

vorgelegt

von *Diplom-Physiker Thomas Nowotny*

geboren am *17. September 1971* in *Kassel*

Gutachter: *Prof. Dr. U. Behn, Universität Leipzig*

Prof. Dr. V. A. Zagrebnov, CNRS Luminy, Marseille

Prof. Dr. F. Iglói, SZFKI Budapest

Tag der Verleihung *26. November 2001*

Bibliographische Beschreibung

Nowotny, Thomas
Phase transitions and multifractal properties of random field Ising models
Universität Leipzig, Dissertation
128 S., 152 Lit., 35 Abb., 1 Tab.

Referat

In dieser Arbeit werden Zufallsfeld-Ising-Modelle mit einem eingefrorenen dichotomen symmetrischen Zufallsfeld für den eindimensionalen Fall und das Bethe-Gitter untersucht. Dabei wird die kanonische Zustandssumme zu der eines einzelnen Spins in einem effektiven Feld umformuliert. Im ersten Teil der Arbeit werden das mulktifraktale Spektrum dieses effektiven Feldes untersucht, Übergänge im Spektrum erklärt und Ungleichungen zwischen lokalen und globalen Dimensionsbegriffen bewiesen, die eine weitgehend vollständige Charakterisierung des multifraktalen Spektrums durch eine Reihe von Schranken erlauben. Ein weiterer Teil der Arbeit beschäftigt sich mit einer ähnlichen Charakterisierung des Maßes der lokalen Magnetisierung, das aus dem Maß des effektiven Feldes durch Faltung hervorgeht. In diesem Zusammenhang wird die Faltung von Multifraktalen in einem allgemeineren Rahmen behandelt und Zusammenhänge zwischen den multifraktalen Eigenschaften der Faltung und denen der gefalteten Maße bewiesen. Im dritten Teil der Dissertation wird der Phasenübergang von Ferro- zu Paramagnetismus im Modell auf dem Bethe Gitter untersucht. Neben verbesserten exakten Schranken für die Eindeutigkeit des paramagnetischen Zustands werden im wesentlichen drei Kriterien für die tatsächliche Lage des Übergangs angegeben und numerisch ausgewertet. Die multifraktalen Eigenschaften des effektiven Felds im Modell auf dem Bethe-Gitter schließlich erweisen sich als trivial, da die interessanten Dimensionen nicht existieren.

Bibliographic Information

Nowotny, Thomas
Phase transitions and multifractal properties of random field Ising models
Universität Leipzig, Dissertation
128 p., 152 ref., 35 fig., 1 tab.

Abstract

In this work random field Ising models with quenched dichotomous symmetric random field are considered for the one-dimensional case and on the Bethe lattice. To this end the canonical partition function is reformulated to the partition function of one spin in an effective field. In the first part of the work the multifractal spectrum of this effective field is investigated, transitions in the spectrum are explained and inequalities between local and global generalized fractal dimensions are proven which allow to characterize the multifractal spectrum bei various bounds. A further part of the work is dedicated to the characterization of the measure of the local magnetization which is obtained by convolution of the measure of the effective field with itself. In this context the convolution of multifractals is investigated in a more general setup and relations between the multifractal properties of the convolution and the multifractal properties of the convoluted measures are proven. The phase transition from ferro- to paramagnetismus for the model on the Bethe lattice is investigated in the third part of the thesis. Apart from improved exact bounds for the uniqueness of the paramagnetic state essentially three criteria for the transition are developped and numerically evaluated to determine the transition line. The multifractal properties of the effective field for the model on the Bethe lattice finally turn out to be trivial because the interesting dimensions do not exist.

Contents

Chapter 1

Introduction

Whenever different fields of physics have a common intersection, interesting results are obtained from the interaction of the different typical methods of the intersecting fields. The random field Ising models considered in this work are a typical example. They combine aspects of the theory of disordered systems, multifractality in discrete dynamical systems and statistical physics of Ising-type spin models.

Disorder effects are present in practically all experimental systems. Crystals have misalignments and vacant sites, materials have impurities of foreign atoms, the different types of atoms in alloys are not evenly but randomly distributed or the structure of a material is even completely random like in structural glasses, to name but a few. For a long time the disorder was treated as a perturbation of ideally ordered and therefore less complicated situations. For example, scattering of electrons at impurities in otherwise strictly periodic crystals was treated in this way leading to corrections for transport coefficients. In the same way defects were seen to lead to modified material constants.

The view of disorder as a small secondary effect changed dramatically with the discovery of the Anderson localization [And58, LR85] in which disorder effects lead to a metal-insulator transition. The disorder therefore can change the properties of a material qualitatively not only quantitatively. In addition, the effect occurs already at small amplitudes of the disorder such that it is definitely not accessible by perturbative methods.

Other famous effects of disorder are, e. g., non-zero ground state entropies, critical slowing down and aging effects in spin glasses [BY86, FH91, Rya92]. With the years disordered systems have thus become a field of research on its own.

Sets with non-intuitive properties have been known in mathematics at least since the introduction of the Weierstraß function [Wei72], the Cantor sets [Can83, Can32] and the Peano curves [Pea90, Pea73] at the end of the 19th century. The also well-known Koch curve was introduced somewhat later [vK04]. Tools like the Hausdorff dimension [Hau19] to characterize dimensional aspects of such strange sets have also long been known.

It was the merit of Benoît B. Mandelbrot to observe that similar sets appear practically everywhere in nature, especially in physics, and to promote this idea through his by now famous book [Man83]. Some examples of the occurrence of fractal sets are snow flakes, cloud and rock formations, coast lines and even star and galaxy distributions in the universe. In theoretical physics the typical examples are strange attractors in dynamical systems [Ott93], the structure of turbulent flows and pattern formation in diffusion limited aggregation.

In the wake of Mandelbrot's observation the new field of fractal geometry arose. The main ingredients of this theory are various notions of fractal dimensions of point sets in $\mathbb{R}^n$ as, e. g., the well-known Hausdorff dimension, box counting dimensions and packing dimensions. For an introduction cf [Fal90, Bar93].

Often not only fractal sets but also measures on these sets are encountered like, e. g., the natural measure on chaotic attractors [FOY83, GP87], escape rates from chaotic repellers [ST86, Tél86, Tél87], dissipation fields of turbulent flow [BPPV84] or the harmonic measure in diffusion limited aggregates [HMP86]. To obtain a more comprehensive description of these systems the fractal geometry of sets was generalized to a multifractal geometry of measures. In particular, one-parameter sets of generalized box dimensions D_q, $q \in \mathbb{R}$, [HP83, GP83] and the so-called $f(\alpha)$-spectrum, $\alpha \in \mathbb{R}$, [HJK$^+$86] were introduced. By now, multifractal generalizations for practically all fractal dimensions exist [Ols95].

The Ising model [Cip87, Dom74, LB99] was proposed as a simple model of statistical mechanics to describe the phase transition between paramagnetic and ferromagnetic behaviour. It was first proposed by Lenz [Len20] and solved for the one-dimensional case by Ising [Isi24]. As the one-dimensional model has no phase transition for finite temperatures Ising was deeply disappointed and completely retired from research in physics to become a highschool teacher. In the meantime the Ising model named after him became popular for all kinds of applications. With Onsager's exact solution [Ons44] of the two-dimensional Ising model [MW73, Bax89] one of the few known exact solutions of models with phase transitions was found. Even though most properties of the three-dimensional model [Wu82] are well known on a numerical level [FL91, CPRV99] an exact solution of this model or higher dimensional models has not been found.

The Ising model became even more popular when it was formulated with random couplings or in an external random field [Bel98, Nat98]. Well known models of the spin glasses mentioned above are, e. g., the Edwards-Anderson model [EA75] and its mean field version the Sherrington-Kirkpatrick [SK75] or Thouless-Anderson-Palmer [TAP77] model which are variations of a random exchange Ising model.

The random field Ising models considered in this work combine all three aspects. They are Ising models, are disordered by a quenched external random field and the probability distributions of, e. g., the local magnetization with respect to the disorder probability space turns out to be a multifractal. In particular, models with symmetric dichotomous random field will be considered for a one-dimensional chain (chapter 3 and chapter 4) and on the Bethe lattice (chapter 5). The absence of loops in both geometries is essential for the iterative relations used. Random exchange spin glass models on the Bethe lattice can be analysed with similar iteration relations [CCC$^+$90, CCST90].

In early work on one-dimensional disordered systems [Dys53, Sch57, Hal67] variations of transfer matrix methods were used to obtain quantities like the cumulative density of states [Hal67] or the frequency spectrum of coupled oscillators [Sch57]. The one-dimensional random field Ising model however can be reformulated to a one-spin system in an effective field [Ruj78, GR84, BG78, BA83] which is characterized by a contractive random iterated function system of first order. This simplifies its treatment considerably in comparison to standard transfer matrix methods which can only be formulated as iterated function systems of *second order*.

The random iterated function system obtained has a unique invariant measure [Hut81, BZ87a, BZ87b, AC90] which is the probability measure of the effective field in the thermodynamic limit. Similar random iterated function systems also appear in the context of learning in neural networks [vHKK88, BvHK$^+$93, RSW93].

The distribution function corresponding to the invariant measure is a so-called devil's staircase [GR84] for discrete random fields with large amplitude but is smooth for continuous random fields [And86] or small amplitudes. The same transition from a devil's staircase to a smooth distribution function was also found in quasi-one-dimensional Ising models [NMO85]. In terms of fractal geometry the transition is from a fractal support of the invariant measure for discrete random field distributions and sufficiently large random field amplitude [SB87, Sat87, BZ88b] to a set of dimension one for small field amplitudes. As already stated above, models with continuous random field distributions do not exhibit a fractal support of the invariant measure in a strict sense. Strongly peaked continuous distributions with peaks of width δ lead however to invariant measures with a support *resembling* a fractal set down to a scale of the order of δ but are not fractal below that scale [And86].

The ground state energy per spin and the ground state entropy per spin had been calculated with transfer matrix methods early on [DVP78]. It turns out that the ground state has a residual entropy which can be explained by flips of microscopic spin clusters [BPZ90]. Similar frustration effects have also been observed in the one-dimensional Ising chain in a quasi-periodic potential [Luc87]. The connected correlation functions at zero temperature for the random exchange Ising model were later also obtained [Igl94].

The D_q-spectrum was numerically calculated for the invariant measure of the effective field [BS88, BvHK+94, BL92] soon after its introduction [HP83] while other authors concentrated on related concepts like the order q free energy [TFI89, TFI90] or correlation functions [LN89]. For some combinations of the temperature and the random field strength the limits $D_\infty = \lim_{q\to\infty} D_q$ and $D_{-\infty} = \lim_{q\to-\infty} D_q$ could even be calculated analytically [Eva87]. The D_q-spectrum undergoes several transitions [BL92, BvHK+94, PBL95] in dependence on the random field strength, cf also figure 3.2. The transitions for small random field were explained by changes of the pointwise dimension at the boundary of the support of the measure and these pointwise dimensions were explicitly calculated [BL92].

The most striking transition is the collapse of the D_q-spectrum for $q < 0$ at some critical field strength $h_c^{(2)}$, cf figure 3.2. It was explained on a phenomenological level by the disappearance of deep cuts in the measure density [BvHK+94] observed in numerically generated measure densities [BL92]. Similar transitions have been found in the superposition of multifractals [Rad93, Rad95, SS97]. The disappearance of deep cuts was later explained by the analysis of the orbit structure of the random iterated function system defining the effective field [PBL95, Pat97].

After some introduction into the notions of multifractal geometry in chapter 2 and into the one-dimensional random field Ising model in the first part of chapter 3 the explanation of the transition at $h_c^{(2)}$ is made more precise in sections 3.3 and 3.4. To this end the concept of orbits and their pointwise dimension is discussed in detail and it is proven that the pointwise dimension of the invariant measure at the points of periodic orbits which do not touch the overlap exists. Furthermore, the explicit formula for the pointwise dimension of periodic orbits given in [Pat97] is rigorously proven.

The condition determining the critical field strength for the transition which results from the analysis of the orbit structure is solved to an explicit form.

Generalizing the arguments formerly applied to the periodic $\{+-\}$ orbit in order to explain the transition at $h_c^{(2)}$ to a certain family of orbits, a hitherto unnoticed further transition in the D_q-spectrum for $q < 0$ is explained. The condition for the corresponding critical field strength $h_c^{(2a)}$ is solved numerically. The new transition was detected through numerical calculations of the D_q-spectrum with increased numerical precision also performed as part of this work.

The last section in chapter 3 is dedicated to the investigation of general relations between pointwise dimensions and D_q-spectra. Two different types of general inequalities are proven. Applied to the invariant measure of the effective field the inequalities provide bounds which characterize the D_q-spectrum very precisely and allow to calculate $D_{-\infty}$ and D_∞ explicitly. This generalizes the results of [Eva87].

The original D_q-spectrum [HP83] turned out to be not well-defined for $q < 0$. The problem was fixed by the introduction of an improved multifractal formalism [Rie95]. Surprisingly, most earlier results remain or sometimes even just become valid in the improved formalism. Throughout this work the improved formalism is always used if it does not coincide with the classical definition. The main results of chapter 3 have been published in [NPB01a].

It should not go unmentioned that there is still a considerable amount of other ongoing research on aspects of the one-dimensional random field Ising model. Examples are the investigations of the randomly driven Ising magnet [HR99a, HR99b], of the dynamical Ising model [SC00] and of mathematical aspects such as the uniqueness of Gibbs states and the structure of ground state revisited in the formalism of Gibbs measures [BRZ96]. Other authors concentrate on disordered *quantum* Ising spin chains which is a separate field in its own right, cf e. g. [IJR99, KJTI99] and related work.

The mathematical research on (random) iterated function systems has also been a quite active field. Some examples are the investigation of parabolic iterated function systems [SSU98a, SSU98b, SSU00], multifractal formalism for self-similar functions [Sli99] and multi-scaled multinomial measures [GR00] and measures on self-affine sets [Fal99]. A connection to domain theory has been established [Eda95, Eda96, Eda97] and wavelets can be used for the analysis of multifractal properties as well [MBA94, ABJM97, ABJM98]. A related field is the investigation of Bernoulli convolutions [PSS00] with respect to multifractal aspects [LP94, LP96a, LP96b, Pat97].

It has long been regretted that most results focused on the effective field which is not a directly measurable physical quantity even though it is related to the local magnetization at the boundary of the Ising chain, cf chapter 3. Therefore, chapter 4 is dedicated to the investigation of the measure of the local magnetization which in principle can be measured e. g. by neutron scattering. As the local magnetization is essentially the sum of two effective fields from the left and from the right [GR84, BZ87a, BZ88b] its measure is essentially the convolution of the invariant measure with itself, cf also [AB83].

To exploit the extensive knowledge of the properties of the effective field for the local magnetization, the relations between the multifractal properties of two measures and the multifractal properties of their convolution are investigated. There are two main results. Firstly, the pointwise dimension at the boundary of the support of the convolution is the sum of the pointwise dimensions at the corresponding boundaries of the two convoluted measures. Secondly, the D_q-

spectrum of the convolution is bounded from above by the sum of the D_q-spectra of the convoluted measures.

The results are applied to the measure of the local magnetization. Together with the bounds and numerical results for the effective field of chapter 3 a precise characterization of the D_q-spectrum of the measure of the local magnetization is achieved.

The numerically generated spectrum is in perfect agreement with the analytical bounds. Some difficulties arise in a certain parameter range leading to numerical instabilities in the preferred algorithm of the new natural partition. These effects can be understood in terms of the band structure of the approximations to the measure densities of the effective fields used to approximate the measure of the local magnetization. It turns out that the numerical instability is of principal nature and indicates a sensitive dependence of the D_q-spectrum for $q < 0$ on the temperature and the random field strength.

From an experimentalists point of view however, the scale of observation is always bounded from below. Therefore, it is adequate to use box counting methods which also have a minimal resolution defined by the smallest box size in contrast to the methods based on new natural partitions which can have arbitrary small scale already at finite iteration depths. Following this approach, the D_q-spectra are calculated by box methods in the problematic regions which leads to meaningful results. All obtained results can qualitatively be understood in terms of overlap structures of the natural partition of the effective field in the process of the convolution.

As a byproduct of the numerical calculation of D_q-spectra, approximations of the invariant measure densities for various values of the random field strength h are obtained. One can directly see a gradual transition from a strongly peaked monomodal distribution for small random field amplitude to a strongly peaked bimodal distribution for large random field strengths. This resembles a phase transition from paramagnetic to ferromagnetic behavior. Because it is only a local effect and the symmetry is not broken it is not a physical phase transition though. After the quenched average over all random field configurations the magnetization is always zero.

Sums of independent random variables appear in a wide variety of applications. Therefore, the general results on the convolution of multifractals obtained in chapter 4 are also of interest beyond the characterization of the local magnetization of the one-dimensional random field Ising model. The main results are submitted for publication [NB01].

The reason of Ising's disappointment, the absence of phase transitions at finite temperature in the one-dimensional model, is of course not lifted by the introduction of a random field. In order to study disorder effects on phase transitions or even disorder-driven phase transitions one needs to consider models with a different underlying geometry. The Bethe lattice or Cayley tree is uniquely characterized by the two properties that it is a graph with constant vertex degree and that it contains no loops. The latter property allows to reformulate the random field Ising model on the Bethe lattice to a (generalized) random iterated function system in close analogy to the one-dimensional case [Bra80, Bru84, Pat97]. In contrast to the one-dimensional case the iterated function system is no longer necessarily contractive. The loss of contractivity leads to a phase transition from paramagnetic to ferromagnetic behaviour in dependence on the temperature and the strength of the random field.

The research on the Ising model on the Bethe lattice with and without random fields has not been as extensive as for the one-dimensional model. There are only seemingly disconnected sets of works on this subject.

Early work considered correlation functions of spins in the classical Ising model on the Bethe lattice without external field [Fal75, vHT74, Mat74, MHZ74, Egg74] which has also been investigated for the model with homogeneous external field recently [IH98, HI98]. It was shown that the magnetic susceptibility diverges below a critical temperature thus giving rise to phase transition. This phase transition was also found in the model with random field [Bru84] which will be discussed in more detail below. Later, the possible phase diagram topologies were investigated numerically [SMCB94].

Recently, the phase diagram of analogues of the anisotropic next nearest neighbours Ising model [AS97, AS99] and the phase diagram of the standard Ising model on a two layer Bethe lattice [HIO99] were considered. The ground state structure has also attracted some interest. Examples are the investigation of the residual entropy and hysteresis loops [DSS97, Shu01] as well as of the single spin flip dynamics [SSD00] at zero temperature. The Ising spin glass (random exchange Ising model) on the Bethe lattice also is still under investigation [MP01].

After the treatment of the purity of the paramagnetic limiting Gibbs state of the Ising model without random field [Ble90, BRZ95] the uniqueness of Gibbs measures compatible with the Ising Hamiltonian with dichotomous random field has been investigated [BRZ98]. Among other results the authors were able to give an exact upper bound for the uniqueness of the Gibbs measure for all random field configurations and a tighter upper bound for the uniqueness of the Gibbs state for almost all random field configurations. The latter can be improved by iterating the original argument. This is explained in detail in section 5.1 and the resulting bound is presented. Though being a considerable improvement of the earlier result the bound is still far from the region where the transition is suspected.

As mentioned above, Bruinsma also investigated the phase transition in the random field Ising model on the Bethe lattice. He proposed a lower bound for the existence of a stable ferromagnetic phase [Bru84]. In section 5.2 three numerical criteria are developed to detect the position of the phase transition numerically. In subsection 5.2.1 the expectation value of the local magnetization is calculated. The regions in which the magnetization is increasing with increasing distance to the boundary are identified as regions with a stable ferromagnetic and an unstable paramagnetic phase whereas the regions with decreasing magnetization have at least a stable paramagnetic phase. The investigation of the average contractivity in subsection 5.2.2 also results in the identification of two such regions leading to an upper bound for the stability of the paramagnetic state. The analysis of the average contractivity goes back to [Pat97]. Finally, the calculation of the dependence of the effective field at the center of the Bethe lattice on boundary conditions which are close to zero in subsection 5.2.3 gives an estimate on the stability of the paramagnetic phase with respect to small perturbations at the boundary. This also results in an upper bound on the stability of the paramagnetic phase. All estimates for the transition line are in good agreement with each other but significantly disagree with Bruinsma's bound.

As Bruinsma's argument rests on the differentiability of the density of the invariant measure which was only proven for small h and near T_c there are two possible interpretations. Either Bruinsma's bound is not true outside the proven region of validity and the transition from ferromagnetic to paramagnetic behaviour takes place at the smaller random field values found in the numerical investigation or there is a region of coexistence of stable ferromagnetic phases with a stable paramagnetic phase implying a phase transition of first order in this region. The second scenario seems less likely as the random iterated function system is less contractive for small boundary conditions than for large ones such that it is to be expected that the paramagnetic state becomes unstable before ferromagnetic phases emerge.

The successful characterization of the multifractal properties of the effective field as well as the local magnetization in the one-dimensional case motivates to treat the measure of the effective field for the model on the Bethe lattice in a similar way. It turns out however that the measure of the effective field for this model is a left-sided multifractal, i. e., that the generalized box dimensions D_q do not exist for negative q. Therefore, the transition in the fractal dimension of the support is the only one of the transitions discussed for the one-dimensional case also existing on the Bethe lattice. The left-sidedness of the measure of the effective field and the transition in D_0 are discussed in section 5.3. The D_q-spectrum for positive q is obtained numerically.

The results of chapter 5 are submitted for publication [NPB01b]. All results are summarized in the conclusions in chapter 6 and some outlook is given.

Chapter 2

Multifractal measures

In fractal geometry point sets in $\mathbb{R}^n$ are characterized by fractal dimensions such as box counting dimensions, packing dimensions and the Hausdorff dimension. When considering strange attractors of dynamical systems however one encounters not only a point set (the attractor) but also a measure supported by this set (the natural measure). Other examples are the effective field and the local magnetization of the random field Ising model considered in this work. They are not only characterized by the set of values they can take on but also by the probability measure governing the occurrence of the possible values. A measure is only very roughly characterized by the fractal dimension of its support. It is therefore important to find quantities which also characterize the varying strength of the measure on different parts of its support. Ideas like this led to the development of generalized versions of practically all fractal dimensions.

2.1 Generalized fractal dimensions

The generalization of the box counting dimension are the generalized box dimensions or generalized Rényi dimensions D_q with parameter $q \in \mathbb{R}$ which are based on the idea of Rényi entropies [Rén60, Rén61, Rén70]. They were first introduced by Hentschel and Procaccia [HP83], Grassberger and Procaccia [GP83] and Grassberger [Gra83] in the following way.

Definition 2.1 Classical generalized box dimensions *Let μ be a bounded Borel measure on $\mathbb{R}^n$, $\{b_i^\varepsilon\}_{i\in\mathbb{N}}$ a mesh of cubes of side length ε covering $\mathbb{R}^n$ and $q \in \mathbb{R}$, $q \neq 1$. Then the* lower *and* upper classical generalized box dimensions *of μ are defined as*

$$\underline{D}_q^{\mathrm{cl}}(\mu) := \frac{1}{q-1} \liminf_{\varepsilon\to 0} \frac{\log \sum_{i\in\mathbb{N}} \mu(b_i^\varepsilon)^q}{\log \varepsilon} \quad \textit{and} \tag{2.1}$$

$$\overline{D}_q^{\mathrm{cl}}(\mu) := \frac{1}{q-1} \limsup_{\varepsilon\to 0} \frac{\log \sum_{i\in\mathbb{N}} \mu(b_i^\varepsilon)^q}{\log \varepsilon} . \tag{2.2}$$

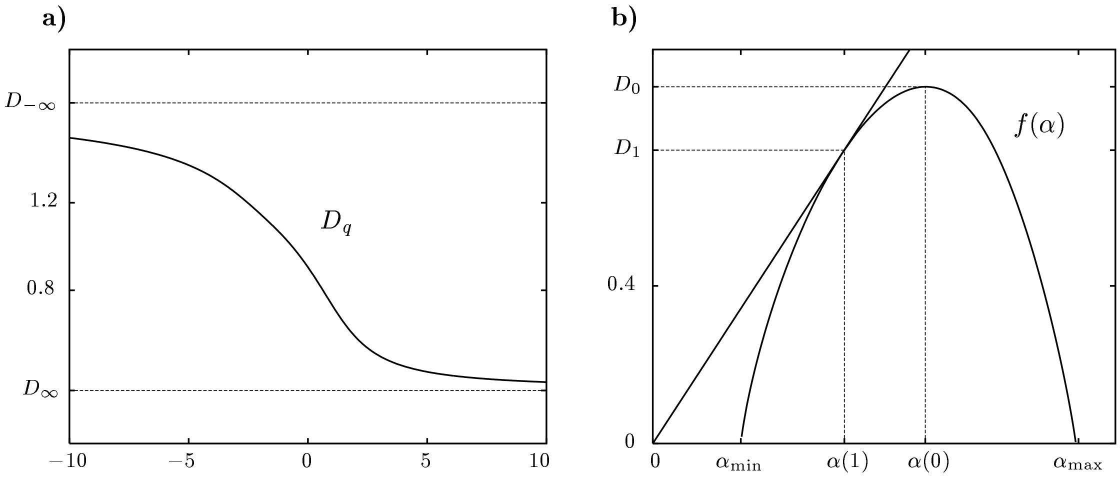

Figure 2.1 a) Typical D_q-spectrum. It was obtained for the measure of the effective field of the one-dimensional random field Ising model through the method based on the new natural partition, cf appendix A.1 at iteration depth 10 and $\beta = J = h = 1$. b) Typical $f(\alpha)$-spectrum generated as the Legendre transform of the $\tau(q)$ obtained from the D_q-spectrum of figure a.

For the case $q = 1$ the limit $q \to 1$ of (2.1) and (2.2) yields

$$\underline{D}_1^{\mathrm{cl}}(\mu) = \liminf_{\varepsilon \to 0} \frac{\sum_{i \in \mathbb{N}} \mu(b_i^\varepsilon) \log \mu(b_i^\varepsilon)}{\log \varepsilon} \quad \text{and} \tag{2.3}$$

$$\overline{D}_1^{\mathrm{cl}}(\mu) = \limsup_{\varepsilon \to 0} \frac{\sum_{i \in \mathbb{N}} \mu(b_i^\varepsilon) \log \mu(b_i^\varepsilon)}{\log \varepsilon} \tag{2.4}$$

which is used as the definition of $\underline{D}_1^{\mathrm{cl}}$ and $\overline{D}_1^{\mathrm{cl}}$ respectively. If the upper and the lower dimension coincide then $D_q^{\mathrm{cl}} := \underline{D}_q^{\mathrm{cl}} = \overline{D}_q^{\mathrm{cl}}$ is the *classical generalized box dimension of μ.*

The sums in definition 2.1 and all similar sums in this work tacitly only extend over boxes b_i^ε with $\mu(b_i^\varepsilon) \neq 0$. Figure 2.1a shows a typical D_q-spectrum.

When calculating limits of the form encountered in (2.1) through (2.4) it is often useful to restrict the calculation to *admissible sequences*. A sequence $(\varepsilon_n)_{n \in \mathbb{N}}$ is admissible if all $\varepsilon_n > 0$ and $k' \geq \varepsilon_{n+1}/\varepsilon_n \geq k$ for some $1 > k' \geq k > 0$. For admissible sequences it is not difficult to show that if the second limit exists, so does the first and

$$\lim_{\varepsilon \to 0} \frac{\log f(\varepsilon)}{\log \varepsilon} = \lim_{n \to \infty} \frac{\log f(\varepsilon_n)}{\log \varepsilon_n} \tag{2.5}$$

for any function $f : \mathbb{R} \to \mathbb{R}$, cf e. g. [Fal90, 3.1].

It took quite a while until it was noticed that for $q < 0$ the generalized box dimensions of definition 2.1 are not well-defined. The effect can easily be seen in the following example taken from [LN99].

Example 2.1 Let μ be the Lebesgue measure restricted to $[0,1]$ and $b_i^{\varepsilon_n} := [i\varepsilon_n, (i+1)\varepsilon_n]$ where $\varepsilon_n = (1-2^{-n})/n$, $i \in \mathbb{N}$. The sequence $(\varepsilon_n)_{n\in\mathbb{N}}$ is admissible. The interval $b_n^{\varepsilon_n}$ has measure $\mu(b_n^{\varepsilon_n}) = 2^{-n}$ and thus $\sum_{i\in\mathbb{N}} \mu(b_i^{\varepsilon_n})^q > 2^{-nq}$ such that for $q < 0$

$$\overline{D}_q^{\mathrm{cl}} \geq \underline{D}_q^{\mathrm{cl}} = \frac{1}{q-1} \liminf_{\varepsilon\to 0} \frac{\log \sum_{i\in\mathbb{N}} \mu(b_i^{\varepsilon})^q}{\log \varepsilon} \tag{2.6}$$

$$= \frac{1}{q-1} \liminf_{n\to\infty} \frac{\log \sum_{i=0}^{n} \mu(b_i^{\varepsilon_n})^q}{\log \varepsilon_n} = \infty\,. \tag{2.7}$$

On the other hand, if choosing $\varepsilon_n = 1/n$ instead, one obtains $D_q^{\mathrm{cl}} = 1$ for all $q < 0$ as one rather would have expected. By adequate choice of the box sizes one can obtain *any* value in the interval $[1, \infty]$.

The example shows that D_q^{cl} depends on the choice of the boxes with which it is calculated and that this effect already occurs for the most simple measures. The problem was solved by Riedi [Rie95] by proposing an improved multifractal formalism. Obviously, the main difficulties are caused by boxes with unnaturally small weight caused by an only marginal overlap with the support of the measure. This can be excluded by the use of enlarged boxes.

Definition 2.2 Improved generalized box dimensions *Let μ be a bounded Borel measure on $\mathbb{R}^n$ and $\{b_i^{\varepsilon}\}_{i\in\mathbb{N}}$ a mesh of cubes of side length ε which cover $\mathbb{R}^n$ and are centered around points $\{x_i\}_{i\in\mathbb{N}}$. Let $\{\overline{b}_i^{\varepsilon}\}_{i\in\mathbb{N}}$ be cubes centered around the same points $\{x_i\}_{i\in\mathbb{N}}$ but of side length $\varepsilon\,(1+\delta)$ with some fixed $\delta > 0$. Furthermore, define*

$$\mu_i := \begin{cases} \mu(\overline{b}_i^{\varepsilon}) & (\textit{if } \mu(b_i^{\varepsilon}) > 0) \\ 0 & (\textit{otherwise}) \end{cases}\,. \tag{2.8}$$

Then the lower *and* upper improved generalized box dimensions *of μ for $q \in \mathbb{R}$, $q \neq 1$ are defined by*

$$\underline{D}_q(\mu) := \frac{1}{q-1} \liminf_{\varepsilon\to 0} \frac{\log \sum_{i\in\mathbb{N}} \mu_i^q}{\log \varepsilon} \quad \textit{and} \tag{2.9}$$

$$\overline{D}_q(\mu) := \frac{1}{q-1} \limsup_{\varepsilon\to 0} \frac{\log \sum_{i\in\mathbb{N}} \mu_i^q}{\log \varepsilon}\,. \tag{2.10}$$

For the case $q = 1$ the definition is accordingly

$$\underline{D}_1(\mu) := \liminf_{\varepsilon\to 0} \frac{\sum_{i\in\mathbb{N}} \mu_i \log \mu_i}{\log \varepsilon} \quad \textit{and} \tag{2.11}$$

$$\overline{D}_1(\mu) := \limsup_{\varepsilon\to 0} \frac{\sum_{i\in\mathbb{N}} \mu_i \log \mu_i}{\log \varepsilon}\,. \tag{2.12}$$

If the upper and the lower dimension coincide then $D_q(\mu) := \underline{D}_q(\mu) = \overline{D}_q(\mu)$ is the *improved generalized box dimension of μ.*

Although the modification of the definition of the D_q-spectrum at first glance seems to be more of conceptual nature than of practical interest, it turns out that it is also very important for numerical approximations. This is due to the fact that already at finite box sizes 'misplaced' boxes can strongly affect the results such that numerical estimates can strongly depend on the choice of boxes. The D_q of definition 2.2 however are independent of the orientation and position of the mesh cubes as well as the choice of the factor of enlargement δ.

Sometimes the quantity $\tau(q) := (1-q)D_q$ is also used. This definition follows [Fal90, Rie95]. Note that other authors choose a different sign cf e. g. [HJK$^+$86]. It is know that $\tau(q)$ is continuous in q, convex and non-increasing if finite valued, cf [Rie95]. Therefore, D_q is also continuous in q except for possibly at $q = 1$. If D_1 exists and is finite though, the limits $\lim_{q\nearrow 1} D_q$ and $\lim_{q\searrow 1} D_q$ are identical and D_q is everywhere continuous. Furthermore, it is not difficult to see that it also is non-increasing, cf appendix B.1. For $q > 0$ definitions 2.1 and 2.2 are equivalent and will be used interchangeably throughout this work whereas for $q < 0$ always the improved formalism will be used.

The generalized box dimension D_0 is by definition the usual box counting dimension of the support of the measure under consideration. In this sense the D_q are direct generalizations of the usual box counting dimension.

Another important property of the D_q-spectrum is its invariance with respect to bi-Lipschitz maps in the following sense.

Definition 2.3 Induced mapping of Borel measures *Let $f : \mathbb{R}^n \to \mathbb{R}^n$ be a Borel measurable function. Then f also defines a function $f_\#$ on the Borel measures on $\mathbb{R}^n$ by*

$$f_\#(\mu)(X) := \mu(f^{-1}(X)) \tag{2.13}$$

where X is an arbitrary measurable set. For more details cf e. g. [Bau90].

Lemma 2.4 Invariance of D_q with respect to bi-Lipschitz maps *Let μ be a bounded Borel measure on $\mathbb{R}^n$ and f a bi-Lipschitz map on $\mathbb{R}^n$, i.e. there exists a number $L > 1$ such that $L^{-1}\|y-x\| \leq \|f(y)-f(x)\| \leq L\|y-x\|$. Then*

$$D_q(f_\#(\mu)) = D_q(\mu)\,. \tag{2.14}$$

The proof is given in [Rie95]. It is easy to see that it is sufficient that the function f is bi-Lipschitz on the support of the measure μ which will be the case in the treatment of the measure of the local magnetization of the one-dimensional random field Ising model in chapter 4.

An entity related to the D_q-spectrum but measuring the local scaling properties rather than the global singularity structure of the measure is the pointwise dimension. It sometimes also is called local dimension, Hölder exponent or singularity.

Definition 2.5 Pointwise dimension *Let μ be a bounded Borel measure on $\mathbb{R}^n$ and $x \in \operatorname{supp} \mu$. Then the* upper *and* lower pointwise dimension *of μ at x are given by*

$$\underline{D}_p(x;\mu) = \underline{\alpha}_\mu(x) := \liminf_{\varepsilon\to 0} \frac{\log \mu(B_\varepsilon(x))}{\log \varepsilon} \quad \textit{and} \tag{2.15}$$

$$\overline{D}_p(x;\mu) = \overline{\alpha}_\mu(x) := \limsup_{\varepsilon\to 0} \frac{\log \mu(B_\varepsilon(x))}{\log \varepsilon}\,. \tag{2.16}$$

In the usual case that both values are identical $D_p(x;\mu) := \underline{D}_p(x;\mu) = \overline{D}_p(x;\mu)$ is the *pointwise dimension of μ at x.*

The intuition behind the definition of the pointwise dimension is that the *lower* the value of $D_p(x;\mu)$ is the *stronger* the measure μ scales at the point x. For example, a Dirac measure $\delta(x)$ at $x \in \mathbb{R}$ has the pointwise dimension $D_p(x;\delta(x)) = 0$, the Lebesgue measure on $\mathbb{R}$ has $D_p(x;\lambda) = 1$ at any $x \in \mathbb{R}$ and a measure on $\mathbb{R}$ with vanishing density at x has $D_p(x;\mu) \geq 1$. The definition of the pointwise dimension does not need to be refined with enlarged boxes as unnaturally small overlaps with the support of the measure are a priori excluded.

The pointwise dimension is if not invariant then at least 'covariant' with respect to bi-Lipschitz maps.

Lemma 2.6 Covariance of D_p with respect to bi-Lipschitz maps *Let μ be a bounded Borel measure on $\mathbb{R}^n$ and $x \in \operatorname{supp} \mu$ such that $D_p(x;\mu)$ exists. Furthermore, let $f : \mathbb{R}^n \to \mathbb{R}^n$ be a bi-Lipschitz map. Then*

$$D_p(f(x); f_\#(\mu)) = D_p(x;\mu)\,. \tag{2.17}$$

The result is also true for the upper and lower pointwise dimensions separately if they are not equal. The covariance of D_p will also play an important role in chapter 4. The proof is given in B.2. As for the invariance of the D_q-spectrum with respect to bi-Lipschitz maps it is sufficient that the function f is bi-Lipschitz on the support of the measure μ.

An alternative to the D_q-spectrum is the so-called $f(\alpha)$-spectrum which is more popular in the mathematical community. It was first introduced by Halsey, Jensen, Kadanoff, Procaccia and Shraiman [HJK+86] but various different and not always equivalent definitions have been used since then. The following definition was taken from [Fal90].

Definition 2.7 $f(\alpha)$-spectrum *Let μ be a bounded Borel measure on $\mathbb{R}^n$ and $\{b_i^\varepsilon\}_{i\in\mathbb{N}}$ the usual mesh of cubes covering $\mathbb{R}^n$. For any $\alpha \geq 0$ let $N_\varepsilon(\alpha) := \#\{i : \mu(b_i^\varepsilon) \geq \varepsilon^\alpha\}$, i. e. the number of boxes which have at least measure ε^α. If the twofold limit exists it defines*

$$f(\alpha) := \lim_{\delta\to 0} \lim_{\varepsilon\to 0} \frac{\log(N_\varepsilon(\alpha+\delta) - N_\varepsilon(\alpha-\delta))}{-\log \varepsilon}\,. \tag{2.18}$$

This definition is also sometimes referred to as the coarse multifractal spectrum*, cf [Fal97].*

The definition already suggests the interpretation that $f(\alpha)$ characterizes the fractal dimension of sets with a given pointwise dimension. In many examples this can be made precise in the sense that

$$f(\alpha) = D^{\mathrm{H}}(\{x \in \mathbb{R}^n : D_p(x;\mu) = \alpha\}) \tag{2.19}$$

in which D^{H} denotes the usual Hausdorff dimension of point sets in $\mathbb{R}^n$. Some authors use this as a definition of $f^{\mathrm{H}}(\alpha)$ and refer to it as the *fine multifractal spectrum*.

The D_q-spectrum and the $f(\alpha)$-spectrum are in some sense equivalent as for many examples they are Legendre transforms of each other. This is sometimes called the multifractal formalism [Rie95, LN99].

Theorem 2.8 *For large classes of measures, including self-similar and self-affine measures with certain disjointness conditions of the support and cookie cutters*[1] *without overlap, $\tau(q) = (1-q)D_q$ is the Legendre transform of $f(\alpha)$, i.e.*

$$\tau(q) = \inf_{\alpha \geq 0} \left(f(\alpha) - q\,\alpha\right). \tag{2.20}$$

The proof of this statement for different classes of measures can be found in [Ols95, Rie95, RM95, LN99, Fal90, Fal97, PW97] and related articles. On the other hand there are also exceptions, cf e. g. [RM98]. In typical examples the $f(\alpha)$-spectrum is differentiable in α, concave and identically zero outside some interval $[\alpha_{\min}, \alpha_{\max}]$. Exceptions to this rule are the so-called left-sided measures, cf [MEH90, HGH00]. For differentiable $f(\alpha)$ and $\tau(q)$ the Legendre transform can be written as

$$\tau(q) = f(\alpha(q)) - q\,\alpha(q) \quad \text{with} \quad \alpha(q) = -\frac{d}{dq}\,\tau(q)\,. \tag{2.21}$$

From this one easily deduces $f(\alpha(1)) = \alpha(1) = D_1$ and $f(\alpha(0)) = D_0$ such that the typical $f(\alpha)$-spectrum has the form shown in figure 2.1b.

As it inspires one of the numerical techniques to obtain D_q-spectra used below the definition of D_q^{H} according to [HJK⁺86] should also be mentioned.

Definition 2.9 Generalized Hausdorff dimensions *Let μ be a bounded Borel measure on $\mathbb{R}^n$, $\{S_i^\varepsilon\}_{i\in\mathbb{N}}$ a disjoint ε-covering of* supp μ*, i. e. $\varepsilon_i := |S_i^\varepsilon| \leq \varepsilon\ \forall\, i \in \mathbb{N}$, and $p_i^\varepsilon := \mu(S_i^\varepsilon)$. Let $\Gamma(q,\tau,\{S_i^\varepsilon\},\varepsilon) := \sum_{i\in\mathbb{N}} p_i^q \cdot \varepsilon_i^\tau$ and*

$$\Gamma(q,\tau,\varepsilon) := \begin{cases} \sup_{\{S_i^\varepsilon\}} \Gamma(q,\tau,\{S_i^\varepsilon\},\varepsilon) & (q \geq 1, \tau \leq 0) \\ \inf_{\{S_i^\varepsilon\}} \Gamma(q,\tau,\{S_i^\varepsilon\},\varepsilon) & (q \leq 1, \tau \geq 0) \end{cases}. \tag{2.22}$$

[1] Non-linear analog of Cantor sets, cf [Fal97]

Finally, $\Gamma(q,\tau) := \lim_{\varepsilon\to 0}\Gamma(q,\tau,\varepsilon)$*. Then there is a unique function* $\tau(q)$ *with*

$$\Gamma(q,\tau) = \begin{cases} \infty & (\tau < \tau(q)) \\ 0 & (\tau > \tau(q)) \end{cases} \tag{2.23}$$

and the generalized Hausdorff dimension is defined by

$$D_q^{\mathrm{H}} := \frac{1}{1-q}\,\tau(q)\,. \tag{2.24}$$

The missing cases $q \geq 1$, $\tau \geq 0$ *and* $q \leq 1$, $\tau \leq 0$ *in (2.22) are of no significance as for any choice of* $\{S_i^\varepsilon\}$, $\Gamma(q,\tau,\{S_i^\varepsilon\},\varepsilon)$ *tends to* 0 *and* ∞ *for* $\varepsilon \to 0$ *respectively in these cases.*

For $q = 0$ the definition is exactly the definition of the Hausdorff dimension of the support of the measure μ, i. e. $D_0^{\mathrm{H}}(\mu) = D^{\mathrm{H}}(\mathrm{supp}\ \mu)$ and therefore D_q^{H} is a generalization of the Hausdorff dimension as suggested by the notation. Already the usual box counting dimension and the Hausdorff dimension are not equivalent. Therefore, D_q and D_q^{H} are in general not equivalent but in full analogy with the dimensions of point sets they coincide in many examples. Like the improved generalized box dimensions D_q correspond to the coarse multifractal spectrum $f(\alpha)$, the generalized Hausdorff dimensions D_q^{H} correspond to the fine multifractal spectrum $f^{\mathrm{H}}(\alpha)$. In chapter 3 and 4 the idea of a stationary partition function $\Gamma(q,\tau,\varepsilon)$ for decreasing ε will be used for numerical estimates of D_q^{H}.

There are also generalized dimensions based on packing dimensions which are similar to the improved generalized box dimensions D_q presented here. For more details cf [Ols95, LN99, Fal97].

2.2 Random iterated function systems

Typical examples of multifractal measures are invariant measures of iterated function systems and random iterated function systems. A random iterated function system consists of N measurable functions $f_i : \mathbb{R}^n \to \mathbb{R}^n$ and N probabilities $\rho_i > 0$, $\sum_{i=1}^N \rho_i = 1$. The functions f_i are applied iteratively to an initial value x_0, each f_i with probability ρ_i, i. e. $x_n = f_i(x_{n-1})$ with probability ρ_i.

Viewing x_n as a random variable on $\mathbb{R}^n$ this iteration induces an iteration for the probability measure μ_n of x_n which is the Frobenius-Perron or Chapman-Kolmogorov equation

$$\mu_n(X) = \sum_{i=1}^N \rho_i f_{i\#}\mu_{n-1}(X) = \sum_{i=1}^N \rho_i \mu_{n-1}(f_i^{-1}(X)) \tag{2.25}$$

for any Borel measurable set X. The equation is sometimes formulated with a Frobenius-Perron operator, $\mu_n(X) = \mathcal{F}\mu_{n-1}(X)$. $\mathcal{F}$ is a linear operator on the vector space of bounded Borel measures on $\mathbb{R}^n$.

It is sometimes convenient to use densities and in the case of measures on $\mathbb{R}$ distribution functions as well. The densities will be denoted by p_n and the distribution functions by P_n. The Frobenius-Perron equations for these read

$$p_n(x) = \sum_{i=1}^{N} \rho_i \frac{p_{n-1}(f_i^{-1}(x))}{\left|f_i'(f_i^{-1}(x))\right|} \quad \text{and} \quad P_n(x) = \sum_{i=1}^{N} \rho_i \, P_{n-1}(f_i^{-1}(x)) \,. \tag{2.26}$$

A measure μ is invariant with respect to — or a fixed point of — the Frobenius-Perron equation if $\mu = \mathcal{F}\mu$. Such invariant measures are typically multifractal measures.

An important tool to investigate the convergence of the sequence of measures μ_n of a random iterated function system to an invariant measure μ and of the uniqueness of the invariant measure is the Hutchinson metric introduced by Hutchinson [Hut81].

Definition 2.10 Hutchinson metric *Let μ and ν be Borel probability measures on $\mathbb{R}^n$. Then the Hutchinson metric is defined by*

$$d_{\mathrm{Hutch}}(\mu, \nu) := \sup \left\{ \left| \int f d\mu - \int g d\nu \right| : \mathrm{Lip}(f) \leq 1 \right\} \tag{2.27}$$

where $\mathrm{Lip}(f)$ *is the Lipschitz constant of* $f : \mathbb{R}^n \to \mathbb{R}$.

The Hutchinson metric is indeed a metric and the induced topology is equivalent to the weak topology of measures for probability measures with compact support, cf [Hut81].

The following theorem is useful for characterizing the measure of the effective field of the one-dimensional random field Ising model.

Theorem 2.11 Existence and uniqueness of the invariant measure
If all f_i, $i = 1, \ldots, N$, are contractions then the Frobenius-Perron operator $\mathcal{F}$ is a global contraction with respect to the Hutchinson metric and by virtue of Banach's fixed point theorem a unique invariant measure μ exists.

The proof can be found in [Hut81] for the case of similitudes but directly generalizes to arbitrary contractions f_i in an obvious way. The uniqueness of the invariant measure implies ergodicity in the sense that the invariant measure can not be decomposed into two non-trivial invariant measures. Furthermore, the support of the invariant measure is the attractor of the random iterated function system.

The definitions and relations presented in this chapter are of course only a tiny fraction of the existing multifractal theory and the theory of iterated function systems. Nevertheless the material presented should be sufficient to understand the investigations of the random field Ising model in the following chapters.

Chapter 3

Multifractal properties of the effective field of the one-dimensional random field Ising model

In this chapter the one-dimensional random field Ising model with quenched disorder is considered. For N spins the Hamiltonian is

$$H_N(\{s\}_N) = -J \sum_{i=a}^{b-1} s_i s_{i+1} - \sum_{i=a}^{b} h_i s_i \tag{3.1}$$

with $a < 0 < b$ and $b - a + 1 = N$. The symbol s_i denotes the classical spin at site i taking values ± 1, J is the coupling strength between spins and h_i is the random field at site i. The random fields are independent identically distributed random variables with probability density

$$\rho(h_i) = \frac{1}{2}\delta(h_i - h) + \frac{1}{2}\delta(h_i + h), \quad h \in \mathbb{R}^+, \tag{3.2}$$

i. e. the random fields are h or $-h$ with probability $\frac{1}{2}$.

The canonical partition function $Z_N = \sum_{\{s\}_N} \exp(-\beta H_N(\{s\}_N))$ can be reformulated to the partition function of the spin s_a at the left boundary of the chain in an effective field $x_a^{(N)}$. This reformulation was first introduced by Ruján [Ruj78] and is explained in more detail in appendix B.3. It results in

$$Z_N = \sum_{s_a = \pm 1} \exp \beta \Big(x_a^{(N)} s_a + \sum_{i=a+1}^{b} B\big(x_i^{(N)}\big) \Big) \tag{3.3}$$

$$x_i^{(N)} = A(x_{i+1}^{(N)}) + h_i, \quad x_{b+1}^{(N)} = 0 \tag{3.4}$$

where

$$A(x) = (2\beta)^{-1}\log(\cosh\beta(x+J)/\cosh\beta(x-J)) \tag{3.5}$$
$$B(x) = (2\beta)^{-1}\log(4\cosh\beta(x+J)\cosh\beta(x-J))\,. \tag{3.6}$$

The initial condition $x_{b+1}^{(N)} = 0$ corresponds to free boundary conditions. Equation (3.4) defines a random iterated function system with functions $\{f_- = A-h, f_+ = A+h\}$ and probabilities $\rho_- = \rho_+ = \frac{1}{2}$. When viewing (3.4) as a random iterated function system, x_n instead of $x_i^{(N)}$ will be used to denote the effective field after $n = N-i+1$ iterations of (3.4). The effective fields x_n are random variables on the probability space of the random fields and $p_n^{(x)}(x)$ denotes their induced probability density, $P_n^{(x)}(x) = \int_0^x p_n^{(x)}(\xi)d\xi$ their distribution function and $\mu_n^{(x)}(X) = \int_X p_n^{(x)}$ their measures following the nomenclature of random iterated function systems introduced in section 2.2. The Frobenius-Perron or Chapman-Kolmogorov equation for the distribution functions then is

$$P_n^{(x)}(x) = \int dh\ \rho(h) P_{n-1}^{(x)}\big(A^{-1}(x-h)\big) = \sum_{\sigma=\pm}\frac{1}{2}P_{n-1}^{(x)}\big(f_\sigma^{-1}(x)\big) \tag{3.7}$$

where $P_0^{(x)}(x) = \Theta(x)$. Here $\Theta : \mathbb{R} \to \{0,1\}$ is the Heaviside function. The choice of $P_0^{(x)}$ decodes the free boundary conditions corresponding to $x_{b+1}^{(N)} = 0$. The densities and measures obey corresponding Frobenius-Perron equations. As the functions f_- and f_+ are global contractions for all $T > 0$, the Frobenius-Perron equation has a unique invariant measure $\mu^{(x)}$ and the measures $\mu_n^{(x)}$ converge to $\mu^{(x)}$ in the weak topology of Borel measures on $\mathbb{R}$ for any initial probability measure $\mu_0^{(x)}$, cf section 2.2. The invariant measure $\mu^{(x)}$ therefore is the measure of the effective field x in the thermodynamic limit $b \to \infty$ ($n \to \infty$ in the notation of the random iterated function system) for arbitrary boundary conditions and the support of $\mu^{(x)}$ is the attractor of the random iterated function system, cf section 2.2.

The case $T = 0$ is discussed in detail in [BZ87b, BZ88b, BPZ90, Igl94] and will not be considered in this work.

The effective field can directly be interpreted as the local magnetization *at the boundary* because the latter is given by

$$m^{\text{boundary}} = \langle s_a \rangle = \tanh\beta x. \tag{3.8}$$

The probability measure of the local magnetization at the boundary is thus $\tanh\beta_{\#}\mu^{(x)}$ which has the same D_q-spectrum as the effective field itself because $x \mapsto \tanh\beta x$ is bi-Lipschitz on any bounded set and the support of the invariant measure of the effective field is compact, cf lemma 2.4. The physically more interesting magnetization *in the bulk* on the other hand has a much more complicated structure and will be treated in chapter 4.

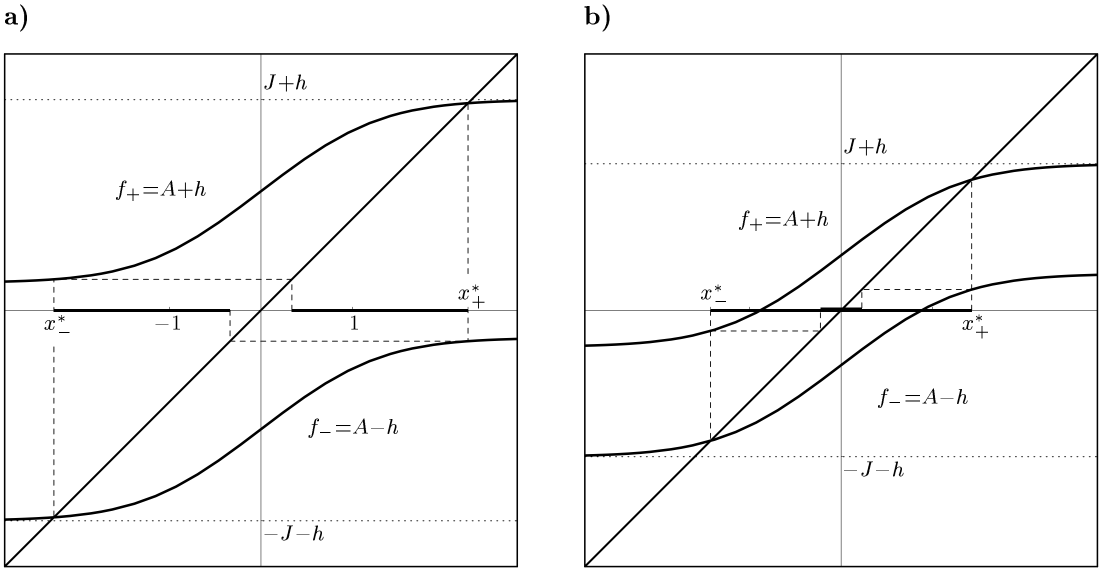

Figure 3.1 a) Iterated function system in the non-overlapping case ($\beta = J = 1$, $h = 1.3$). The first order bands do not overlap leaving the (first order) ***gap*** in the support. The dotted lines are the asymptotic values of f_+ and f_- for $x \to \infty$ and $x \to -\infty$ respectively. b) Overlapping case ($\beta = J = 1$, $h = 0.6$). The first order bands overlap in the middle forming the (first order) ***overlap*** $\mathcal{O}$. The dotted lines are again the asymptotic values of f_+ and f_-.

3.1 Basic properties and notations

Before the multifractal structure of the effective field is investigated in detail it is necessary to delineate some basic properties of the random iterated function system (3.4) and to fix some notations.

The functions f_- and f_+ are shown in figure 3.1. They are smooth, strictly monotonically increasing, globally contracting and have unique attracting fixed points x_-^* and x_+^* respectively. Because of the symmetry of the distribution of the random fields (3.2) and as $A(x) = -A(-x)$ the fixed points are symmetric to the origin, i. e. $x_+^* = -x_-^*$.

It turns out to be extremely useful to introduce a symbolic dynamic for the random iterated function system. $\Sigma_n := \{-,+\}^n$ denotes the set of n-tuples $\{\sigma\}_n$ of symbols $-$ and $+$ and Σ the set of infinite sequences $\{\sigma\}$ of such symbols. Note that the n-tuples as well as the infinite sequences are *ordered* despite the notation with curly brackets. This slightly non-standard notation was chosen for consistency with earlier work, e. g. [BZ87a, BZ87b, BZ88b]. For a given $\{\sigma\} \in \Sigma$ the *head* of the n leftmost symbols is denoted by $\{\sigma\}_n$ and is viewed as an element of Σ_n in the obvious way.

The notation $f_{\{\sigma\}_n}$ is used for the composition $f_{\{\sigma\}_n}(x) = f_{\sigma_1} \circ f_{\sigma_2} \circ \ldots \circ f_{\sigma_n}(x)$ of the functions f_+ and f_-. For any n-tupel $\{\sigma\}_n \in \Sigma_n$ the composite function $f_{\{\sigma\}_n}$ is smooth, strictly monotonically increasing and globally contracting because f_- and f_+ have these properties. It thus also has a unique fixed point $x^*_{\{\sigma\}_n} \in I$.

With the notation of composite functions the n-th iterate of the Frobenius-Perron equation (3.7) can be written as

$$P_n^{(x)}(x) = \sum_{\{\sigma\}_n} \frac{1}{2^n} P_0^{(x)}\big(f^{-1}_{\{\sigma\}_n}(x)\big) \tag{3.9}$$

which in the limit $n \to \infty$ is a path integral in the space of symbolic dynamics.

The interval $I := [x^*_-, x^*_+]$ is called *invariant interval* and fulfills $f_-(I) \cup f_+(I) \subseteq I$. The images $I_{\{\sigma\}_n} := f_{\{\sigma\}_n}(I)$ of the composite functions $f_{\{\sigma\}_n}$ are called *bands* of order n and play an important role in the analysis of pointwise dimensions of the invariant measure $\mu^{(x)}$. The fixed points $x^*_{\{\sigma\}_n}$ are elements of the corresponding bands $I_{\{\sigma\}_n}$. Let now $\{\sigma\} \in \Sigma$ be some fixed symbolic sequence. As $f_\pm(I) \subset I$ and $f_{\{\sigma\}_{n+1}} = f_{\{\sigma\}_n} \circ f_{\sigma_{n+1}}$ the higher order band $I_{\{\sigma\}_{n+1}} = f_{\{\sigma\}_n}(f_{\sigma_{n+1}}(I))$ is contained in $I_{\{\sigma\}_n}$ and inductively $I_{\{\sigma\}_m} \subseteq I_{\{\sigma\}_n}$ for $m > n$.

If the first order bands do not overlap, i. e. $I_- \cap I_+ = \emptyset$ then the (first order) *gap* is denoted by $\Delta := I \backslash (I_- \cup I_+) = [f_-(x^*_+), f_+(x^*_-]$. If they do overlap the (first order) *overlap* is denoted by $\mathcal{O} := I_- \cap I_+ = [f_+(x^*_-), f_-(x^*_+)]$. The structure of the first order bands is repeated in higher orders such that if the first order bands do not overlap neither do the higher order bands and if they overlap the higher order bands also do. The first case is called the *non-overlapping case* and the second one the *overlapping case*, cf also figure 3.1.

The limit $\lim_{n\to\infty} f_{\{\sigma\}_n}(x_0)$ exists for any $\{\sigma\} \in \Sigma$ and $x_0 \in I$ and does not depend on x_0. It therefore is meaningful to define $x^*_{\{\sigma\}} := \lim_{n\to\infty} f_{\{\sigma\}_n}(x_0)$ and the (constant) function $f_{\{\sigma\}} : I \to I$, $f_{\{\sigma\}}(x) = x^*_{\{\sigma\}}$. By this definition $x^*_{\{\sigma\}}$ is the unique fixed point of $f_{\{\sigma\}}$. If $\{\sigma\}$ is periodic, i. e. $\{\sigma\} = (\{\sigma\}_n)_\infty$ then $x^*_{\{\sigma\}} = x^*_{\{\sigma\}_n}$. In this sense the fixed points $x^*_{\{\sigma\}}$ to arbitrary sequences $\{\sigma\}$ are a direct generalization of the fixed points $x^*_{\{\sigma\}_n}$ of finite iterations $f_{\{\sigma\}_n}$.

In the same way as for every $\{\sigma\} \in \Sigma$ the fixed point $x^*_{\{\sigma\}} \in \operatorname{supp} \mu^{(x)}$ exists the reverse statement is also true. For any $x \in \operatorname{supp} \mu^{(x)}$ a symbolic sequence $\{\sigma\} \in \Sigma$ exists such that $x = x^*_{\{\sigma\}}$. In the non-overlapping case this relation is one to one. For more details cf appendix B.5

3.2 Known transitions in the D_q-spectrum

In this section previous work on transitions in the D_q-spectrum of the invariant measure $\mu^{(x)}$ and its measure density is briefly summarized. For large random field amplitude h the support of $\mu^{(x)}$ is totally disconnected and is similar to a multi-scale Cantor set [BZ88b].

At a critical value $h_c^{(1)}$ of h the support of $\mu^{(x)}$ becomes connected for all $h \le h_c^{(1)}$ [NMO85]. The value of $h_c^{(1)}$ is determined by the overlap condition for

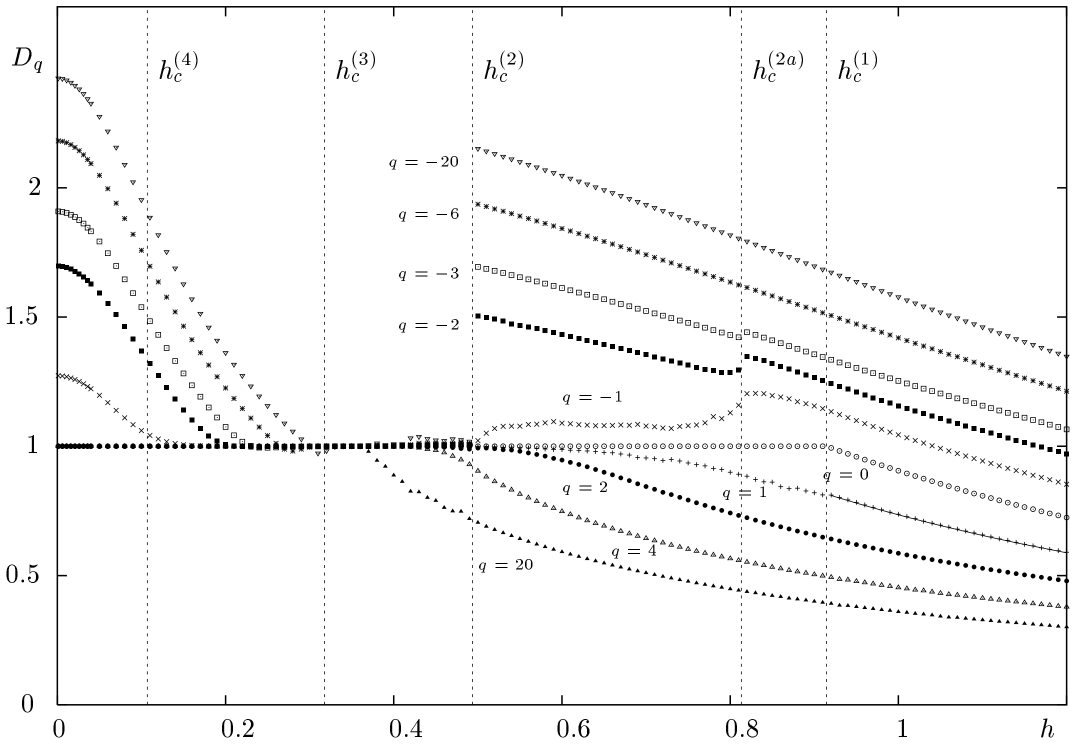

Figure 3.2 Generalized fractal dimensions D_q of the invariant measure of the effective field for $q = -20, -6, -3, -2, -1, 0, 1, 2, 4, 20$ versus the amplitude h of the random field for $\beta = J = 1$. The results were computed with the method of the new natural partition, cf appendix A.1. At the critical values $h_c^{(n)}$, $n = 1, \ldots, 4$, and $h_c^{(2a)}$ transitions take place in the D_q-spectrum. The details are explained in sections 3.2 and 3.4. The solid line coinciding with the values of D_1 for $h > h_c^{(1)}$ was obtained using $D_1 = \hat{D}_p$ and (3.37) evaluated as an R-integral, cf [Eda95]. The details are given in subsection 3.3.1.

the first bands, $f_-(x_+^*) = f_+(x_-^*)$. This results in [BL92]

$$h_c^{(1)} = \frac{1}{2\beta} \operatorname{arcosh}\left((e^{2\beta J} - 1)/2\right). \tag{3.10}$$

The transition can be seen in the densities $p_n^{(x)}$ of the approximations $\mu_n^{(x)}$ of the invariant measure $\mu^{(x)}$ [BL92]. In the D_q-spectrum the transition is visible as the point where D_0 becomes 1, cf figure 3.2. The critical temperature beyond which a transition of this type ceases to exist is given by the condition $h_c^{(1)} = 0$ leading to

$$\frac{1}{k_B T_c^{(1)}} = \beta_c^{(1)} = \frac{1}{2J} \log 3\,. \tag{3.11}$$

All D_q with $q < 0$ collapse to the value 1 at a critical field strength $h_c^{(2)}$ of the random field. This has been explained by changes in the pointwise dimension of certain orbits [PBL95, Pat97] leading to the condition

$$f_-(x_+^*) = x_{\{+-\}}^* \quad \text{at } h = h_c^{(2)}. \tag{3.12}$$

The pointwise dimension of orbits and the explanation of this transition are discussed in detail below.

The approximating densities $p_n^{(x)}$ of the invariant measure diverge at $x_\pm^*$ in the limit $n \to \infty$ for $h > h_c^{(3)}$ and converge to 0 for $h < h_c^{(3)}$ where $h_c^{(3)} < h_c^{(1)}$ is another critical random field amplitude, cf [BL92]. Divergence occurs for $f'_\pm(x_\pm^*) < \frac{1}{2}$ and convergence to 0 for $f'_\pm(x_\pm^*) > \frac{1}{2}$. Therefore, the critical value $h_c^{(3)}$ is [BL92]

$$h_c^{(3)} = \frac{1}{\beta} \operatorname{arsinh}\left(2^{-\frac{3}{2}}(1 - 9e^{-4\beta J})^{\frac{1}{2}}\right). \tag{3.13}$$

In terms of the pointwise dimension the corresponding condition is $D_p(x_\pm^*) = 1$. The transition can be observed in numerically generated densities $p_n^{(x)}$ [BL92]. In [BvHK+93] it was shown that $D_{-\infty} = 1$ at $h_c^{(3)}$ and $D_{-\infty} > 1$ for $h < h_c^{(3)}$. Therefore, the transition also is visible in the D_q-spectrum as the value of h at which $D_{-\infty}$ starts to grow beyond 1 again for decreasing h, cf figure 3.2. The critical temperature for this transition is determined by $h_c^{(3)} = 0$ yielding

$$\frac{1}{k_B T_c^{(3)}} = \beta_c^{(3)} = \frac{1}{2J} \log 3 \tag{3.14}$$

i. e. the critical temperature $T_c^{(3)}$ is always the same as $T_c^{(1)}$.

The fourth known transition occurs at $h_c^{(4)} \leq h_c^{(3)}$ where the slope of the approximating measure densities $p_n^{(x)}$ at $x_\pm^*$ converges to 0 for $h < h_c^{(4)}$ and diverges for $h > h_c^{(4)}$ in the limit $n \to \infty$. The condition for this transition is $f'_\sigma(x_\sigma^*) = 2^{-1/2}$ [BvHK+94] resulting in [BL92]

$$h_c^{(4)} = \frac{1}{\beta} \operatorname{arsinh}\left(3 \cdot 2^{-\frac{5}{2}} - \tfrac{1}{2} - (3 \cdot 2^{-\frac{5}{2}} + \tfrac{1}{2})e^{-4\beta J}\right)^{\frac{1}{2}}. \tag{3.15}$$

In terms of the pointwise dimension the condition for the transition is $D_p(x_\pm^*) = 2$. The transition is visible in numerically generated densities $p_n^{(x)}$ [BL92] but not in the D_q-spectrum, cf figure 3.2. Again, $D_{-\infty}$ can be calculated analytically and is $D_{-\infty} = 2$. In fact, $D_{-\infty}$ can be calculated analytically for all $h < h_c^{(3)}$ because for this parameter region the scaling of the invariant measure at its boundary is weaker than at any other point and it therefore is possible to give lower and upper bounds on D_q which for $q \to -\infty$ converge to a common value, cf [Eva87] and section 3.5. The critical temperature for the transition at $h_c^{(4)}$ is determined by $h_c^{(4)} = 0$ resulting in

$$\frac{1}{k_B T_c^{(4)}} = \beta_c^{(4)} = \frac{1}{4J}(\log(3 + 2\sqrt{2}) - \log(3 - 2\sqrt{2})). \tag{3.16}$$

Note that the third and fourth transition discussed in this section only depend on the measure at the boundary of its support and therefore are sometimes not viewed as real multifractal effects.

3.3 Pointwise dimension of orbits

The points of supp $\mu^{(x)}$ can be grouped into *orbits* in a natural way. This concept is extremely useful in the investigation of the pointwise dimensions of the invariant measure $\mu^{(x)}$.

Definition 3.1 Orbit *The* orbit *to a given sequence* $\{\sigma\} \in \Sigma$ *consists of the preimages* $f^{-1}_{\{\sigma\}_n}(x^*_{\{\sigma\}})$ *of the corresponding fixed point* $x^*_{\{\sigma\}}$.

In the case of a periodic sequence $\{\sigma\} = (\{\sigma\}_n)_\infty$ the orbit consists of the n fixed points of the finite compositions $f_{\pi\{\sigma\}_n}$ where π denotes a cyclic permutation. Any point $x = x^*_{\{\sigma\}}$ is contained in at least all orbits $\{\tilde{\sigma}\}_n\{\sigma\}$ with arbitrary *head* $\{\tilde{\sigma}\}_n$ and fixed *tail* $\{\sigma\}$. This implies that it belongs to at least countably infinitely many orbits.

3.3.1 Pointwise dimension of orbits outside the overlap

The following technical lemma is very useful for the calculation of the pointwise dimension at the points of a certain class of orbits.

Lemma 3.2 *Let* $(x_i^{(n)} \in I_{\{\sigma\}_i})_{i=1,\dots,n}$ *and* $(\tilde{x}_i^{(n)} \in I_{\{\sigma\}_i})_{i=1,\dots,n}$ *be given for all* $n \in \mathbb{N}$ *and a fixed symbol sequence* $\{\sigma\}$. *Then, for any strictly positive differentiable function* ϕ,

$$\lim_{n\to\infty} \frac{1}{n} \sum_{i=1}^{n} \left(\log \phi(x_i^{(n)}) - \log \phi(\tilde{x}_i^{(n)}) \right) = 0\,. \tag{3.17}$$

If the limit $\lim_{n\to\infty} \frac{1}{n} \sum_{i=1}^{n} \log \phi(x_i^{(n)})$ exists the lemma implies that it is independent of the choice of $\{x_i^{(n)} : i = 1, \dots, n;\ n \in \mathbb{N}\}$ provided each $x_i^{(n)}$ is an element of $I_{\{\sigma\}_i}$. The lemma will be used with $\phi = A'$ below. The proof is given in appendix B.7.

For periodic orbits which never touch the overlap $\mathcal{O}$ the pointwise dimension exists and can be calculated explicitly.

Lemma 3.3 *Let* $\{\sigma\} \in \Sigma$ *be a periodic sequence* $\{\sigma\} = (\{\sigma\}_n)_\infty$ *with period* n *such that no point of the corresponding orbit is in the overlap. Then the pointwise dimension at* $x^*_{\{\sigma\}} = x^*_{\{\sigma\}_n}$ *exists and*

$$D_p(x^*_{\{\sigma\}_n}; \mu^{(x)}) = \frac{-\log 2}{\frac{1}{n} \sum_{i=1}^{n} \log A'\left(f^{-1}_{\{\sigma\}_i}(x^*_{\{\sigma\}_n})\right)}\,. \tag{3.18}$$

Proof. Let throughout this proof x^* denote $x^*_{\{\sigma\}_n}$ for simplicity of notation. Note that the sum in the denominator extends exactly over all points of the periodic orbit. As the overlap is a closed set its complement is open and because the orbit $\{\sigma\}_n$ has a finite number of points there exists $\varepsilon > 0$ such that all preimages $f^{-1}_{\{\sigma\}_i}(f_{\{\sigma\}_n}(B_\varepsilon(x^*)))$, $i = 1, \ldots, n$, do not intersect the overlap $\mathcal{O}$. Therefore, the n-fold application of the Frobenius-Perron equation (3.7) has only one term for this ε and yields

$$\mu^{(x)}\big(f_{\{\sigma\}_n}(B_\varepsilon(x^*))\big) = \frac{1}{2^n}\,\mu^{(x)}(B_\varepsilon(x^*))\,. \tag{3.19}$$

As $f_{\{\sigma\}_n}$ is a contraction

$$|f_{\{\sigma\}_n}(x) - x^*| = |f_{\{\sigma\}_n}(x) - f_{\{\sigma\}_n}(x^*)| < |x - x^*| \tag{3.20}$$

implying

$$f_{\{\sigma\}_n}(B_\varepsilon(x^*)) \subset B_\varepsilon(x^*)\,. \tag{3.21}$$

Therefore, $f^{-1}_{\{\sigma\}_i}(f_{\{\sigma\}_{kn}}(B_\varepsilon(x^*))) \cap \mathcal{O} = \emptyset$ for $i = 1, \ldots, kn$ and any $k \in \mathbb{N}$. This allows to iterate equation (3.19) to obtain

$$\mu^{(x)}\big(f_{\{\sigma\}_{kn}}(B_\varepsilon(x^*))\big) = \frac{1}{2^{kn}}\,\mu^{(x)}(B_\varepsilon(x^*))\,. \tag{3.22}$$

Now define

$$\delta_k^{\max} := \max_{x \in B_\varepsilon(x^*)} \big(f_{\{\sigma\}_{kn}}\big)'(x)\,\varepsilon \tag{3.23}$$

$$\delta_k^{\min} := \min_{x \in B_\varepsilon(x^*)} \big(f_{\{\sigma\}_{kn}}\big)'(x)\,\varepsilon\,. \tag{3.24}$$

Using $\big(f_{\{\sigma\}_{kn}}\big)'(x) = \prod_{i=1}^{kn} f'_{\sigma_i}\big(f^{-1}_{\{\sigma\}_i}(f_{\{\sigma\}_{kn}}(x))\big)$ and $f'_{\sigma_i} = A'$ leads to

$$\delta_k^{\max} = \max_{x \in B_\varepsilon(x^*)} \prod_{i=1}^{kn} A'\big(f^{-1}_{\{\sigma\}_i}(f_{\{\sigma\}_{kn}}(x))\big)\,\varepsilon \tag{3.25}$$

and the same with the minimum instead of the maximum for $\delta_k^{\min}$. As an immediate consequence

$$\frac{\delta_{k+1}^{\max}}{\delta_k^{\max}} \geq \big(A'_{\min}\big)^n \quad \text{and} \quad \frac{\delta_{k+1}^{\min}}{\delta_k^{\min}} \geq \big(A'_{\min}\big)^n \tag{3.26}$$

where $A'_{\min} := \min_{x \in I} A'(x) > 0$ such that $(\delta_k^{\max})_{k \in \mathbb{N}}$ and $(\delta_k^{\min})_{k \in \mathbb{N}}$ are admissible sequences. On the other hand the mean value theorem applied to $f_{\{\sigma\}_{kn}}$ implies

$$B_{\delta_k^{\min}}(x^*) \subseteq f_{\{\sigma\}_{kn}}(B_\varepsilon(x^*)) \subseteq B_{\delta_k^{\max}}(x^*) \tag{3.27}$$

such that

$$\mu^{(x)}(B_{\delta_k^{\min}}(x^*)) \le \mu^{(x)}\big(f_{\{\sigma\}_{kn}}(B_\varepsilon(x^*))\big) \le \mu^{(x)}(B_{\delta_k^{\max}}(x^*))\,. \tag{3.28}$$

Therefore,

$$\overline{D}_p(x^*;\mu^{(x)}) = \limsup_{\delta\to 0} \frac{\log \mu^{(x)}(B_\delta(x^*))}{\log\delta} = \limsup_{k\to\infty} \frac{\log \mu^{(x)}(B_{\delta_k^{\max}}(x^*))}{\log \delta_k^{\max}} \tag{3.29}$$

$$\le \limsup_{k\to\infty} \frac{\log \mu^{(x)}\big(f_{\{\sigma\}_{kn}}(B_\varepsilon(x^*))\big)}{\log \delta_k^{\max}}\,. \tag{3.30}$$

Inserting (3.22) and (3.25) leads to

$$\overline{D}_p(x^*;\mu^{(x)}) \le \limsup_{k\to\infty} \frac{-kn\log 2 + \log\mu^{(x)}(B_\varepsilon(x^*))}{\max\limits_{x\in B_\varepsilon(x^*)} \sum_{i=1}^{kn} \log A'\big(f^{-1}_{\{\sigma\}_i}(f_{\{\sigma\}_{kn}}(x))\big) + \log\varepsilon} \tag{3.31}$$

$$= \limsup_{k\to\infty} \frac{-\log 2}{\max\limits_{x\in B_\varepsilon(x^*)} \frac{1}{kn}\sum_{i=1}^{kn} \log A'\big(f^{-1}_{\{\sigma\}_i}(f_{\{\sigma\}_{kn}}(x))\big)}. \tag{3.32}$$

The points $f^{-1}_{\{\sigma\}_i}(f_{\{\sigma\}_{kn}}(x))$, $i = 1,\dots,kn$, are elements of $I_{\{\sigma_{i+1},\dots,\sigma_{kn}\}}$. Therefore, the average $\frac{1}{kn}\sum_{i=1}^{kn} \log A'\big(f^{-1}_{\{\sigma\}_i}(f_{\{\sigma\}_{kn}}(x))\big)$ in the denominator does in the limit $k\to\infty$ not depend on the choice of x according to lemma 3.2 such that one can choose $x = x^*$, drop the maximum and use $f_{\{\sigma\}_{kn}}(x^*) = x^*$ for any $k\in\mathbb{N}$ to obtain

$$\overline{D}_p(x^*;\mu^{(x)}) \le \limsup_{k\to\infty} \frac{-\log 2}{\frac{1}{kn} k \sum_{i=1}^{n} \log A'\big(f^{-1}_{\{\sigma\}_i}(x^*)\big)} \tag{3.33}$$

$$= \frac{-\log 2}{\frac{1}{n}\sum_{i=1}^{n} \log A'\big(f^{-1}_{\{\sigma\}_i}(x^*)\big)}\,. \tag{3.34}$$

Repeating the calculation with the sequence $(\delta_k^{\min})_{k\in\mathbb{N}}$ instead of $(\delta_k^{\max})_{k\in\mathbb{N}}$ and the limes inferior yields the opposite inequality for $\underline{D}_p$ such that D_p exists and is equal to (3.34). □

Even though the main idea, the void intersection of neighbourhoods of the points of a periodic orbit with the overlap and the consequences for the Frobenius-Perron equation, is the same as in the clever argument given in [PBL95, Pat97] which was somewhat refined also presented in [NPB01a], the rather tedious proof given here is clearly more general. It does not depend on the a priori assumption of existence of the pointwise dimension nor does it need the assumption of strong scaling[1]. On the contrary, it is *proved* that the pointwise dimension exists for all points of periodic orbits which do not touch the overlap.

[1] The assumption of strong scaling means that not only the existence of $D_p(x;\mu)$ but also the existence of the limit $\lim_{\varepsilon\to 0}\mu(B_\varepsilon(x))/\varepsilon^{D_p}$ is assumed which is a considerably stronger assumption.

head (finite)	tail (infinite)
	generic
$+-+++--+-$	$+-+++--+-++---+\ldots$
$\{\sigma\}_n$	$\{\tilde{\sigma}\}$
	periodic (here period 3)
$-++-++-++$	$-++-++-++-++-++\ldots$
$\{\sigma\}_9 = \{-++\}_3$	$\{-++\}_\infty$
	offshoot (arbitrary head, periodic tail)
$+-++---++$	$-++-++-++-++-++\ldots$
$\{\sigma\}_n$	$\{-++\}_\infty$
head determines the interval $I_{\{\sigma\}_n} \ni x^*_{\{\sigma\}}$	tail determines scaling at $x^*_{\{\sigma\}}$

Table 3.1 Illustration of the terminology of symbolic sequences and the different roles played by head and tail. Note, that the head consists of the symbols belonging to the functions applied last and the infinite tail to those applied first. This notation corresponds to the consideration of so-called α-limits which is often the most useful approach.

Equation (3.18) is invariant with respect to cyclic permutations of $\{\sigma\}_n$. Therefore, the invariant measure has the same pointwise dimension at all points of a periodic orbit for which lemma 3.3 applies. A short calculation using the Frobenius-Perron equation (3.7) shows that the pointwise dimension at arbitrary points x and $f_\sigma(x)$ are the same provided $f_\sigma(x)$ is not in the overlap, cf appendix B.6. The argument can be iterated such that $\mu^{(x)}$ has the same pointwise dimension at x and all its images $f_{\{\tilde{\sigma}\}_m}(x)$ if no point $f^{-1}_{\{\tilde{\sigma}\}_i}(f_{\{\tilde{\sigma}\}_m}(x))$, $i = 1, \ldots m$ is in $\mathcal{O}$. Therefore, not only the pointwise dimension at all points of a periodic orbit are the same but also the pointwise dimensions at all points of non-periodic orbits in case the orbit does not touch the overlap $\mathcal{O}$. For this reason the terms *the pointwise dimension of an orbit* or *the local dimension of an orbit* are sometimes used.

For orbits of the form $\{\tilde{\sigma}\}_m(\{\sigma\}_n)_\infty$ the pointwise dimension is determined by the periodic tail $(\{\sigma\}_n)_\infty$. Non-periodic orbits of this type will be called *offshoots* of the corresponding periodic orbit. The roles played by the head and the tail of a sequence $\{\sigma\} \in \Sigma$ are summarized in table 3.1. Note that the choice of the length of the head is arbitrary, in a sense. Similar structures have been considered in [BL90].

In the non-overlapping case the pointwise dimension of an even larger class of orbits can be calculated due to the fact that in this case all predecessors of points with respect to the iteration of (3.4) are unique.

Lemma 3.4 *If there is no overlap and the limit*

$$\lim_{n\to\infty} \frac{1}{n} \sum_{i=1}^{n} \log A'\big(f^{-1}_{\{\sigma\}_i}(x^*_{\{\sigma\}})\big) \tag{3.35}$$

exists for $\{\sigma\} \in \Sigma$ *then the pointwise dimension at* $x^*_{\{\sigma\}}$ *also exists and is given by*

$$D_p(x^*_{\{\sigma\}}; \mu^{(x)}) = \lim_{n\to\infty} \frac{-\log 2}{\frac{1}{n}\sum_{i=1}^{n} \log A'\big(f^{-1}_{\{\sigma\}_i}(x^*_{\{\sigma\}})\big)}\,. \tag{3.36}$$

Even though the proof is very similar to the proof of lemma 3.3 it is not quite the same. It is given in full detail in appendix B.8. Elton's ergodic theorem [Elt87] implies that the assumption of the existence of (3.35) is fulfilled for almost all $\{\sigma\}$ which corresponds to $\mu^{(x)}$-almost sure existence of the pointwise dimension $D_p(x; \mu^{(x)})$. Elton's ergodic theorem together with (3.36) further implies that for $\mu^{(x)}$-almost all x the pointwise dimension has the same value

$$D_p(x; \mu^{(x)}) \overset{\mu^{(x)}\text{-a.s.}}{=} \frac{-\log 2}{\int \log A'(\xi)\, \mu^{(x)}(d\xi)} =: \hat{D}_p. \tag{3.37}$$

This result has direct consequences for the information dimension D_1. Proposition 2.1. in [You82] implies that

$$f(\hat{D}_p) = D^{\mathrm{H}}(\{x \in I : D_p(x) = \hat{D}_p\}) = \hat{D}_p \tag{3.38}$$

in which D^{H} denotes the Hausdorff-dimension. General properties of the multifractal $f(\alpha)$-spectrum imply that $\alpha(1)$ is the only fixed point of $f(\alpha)$ and that $\alpha(1) = D_1$, cf section 2.1 and [Fal90]. Therefore, (3.38) implies $\alpha(1) = \hat{D}_p$ and thus $\hat{D}_p = D_1$. This is illustrated by the solid line in figure 3.2 on page 23 which coincides with the numerically obtained values of D_1 for $h > h_c^{(1)}$. It was obtained by calculation of (3.37) using Edalat's R-integration [Eda95] for the integral in the denominator.

It also easily can be checked that using a randomly chosen sequence $\{\sigma\}$ the value obtained from (3.36) yields the same value with probability 1.

Note that the restriction to almost all $\{\sigma\}$ above is necessary because the sum in (3.35) does not converge for all $\{\sigma\} \in \Sigma$ as the following example shows.

Example 3.1 Let $\{\sigma\} := \{(+)_{i_k}(+-)_{j_k}\}_{k\in\mathbb{N}}$ with $i_k = 2^{2^{2k}}$ and $j_k = 2^{2^{2k+1}}$. Furthermore, denote $n_k := \sum_{l=1}^{k} i_l + \sum_{l=1}^{k-1} j_l$ and $m_k := \sum_{l=1}^{k} i_l + \sum_{l=1}^{k} j_l$ such that n_k are the positions at the end of the $(+)$ series in $\{\sigma\}$ and m_k the positions at the end of the $(+-)$ series. Then

$$s_{n_k} := \frac{1}{n_k} \sum_{i=1}^{n_k} \log A'\big(f^{-1}_{\{\sigma\}_i}(x^*_{\{\sigma\}})\big) \tag{3.39}$$

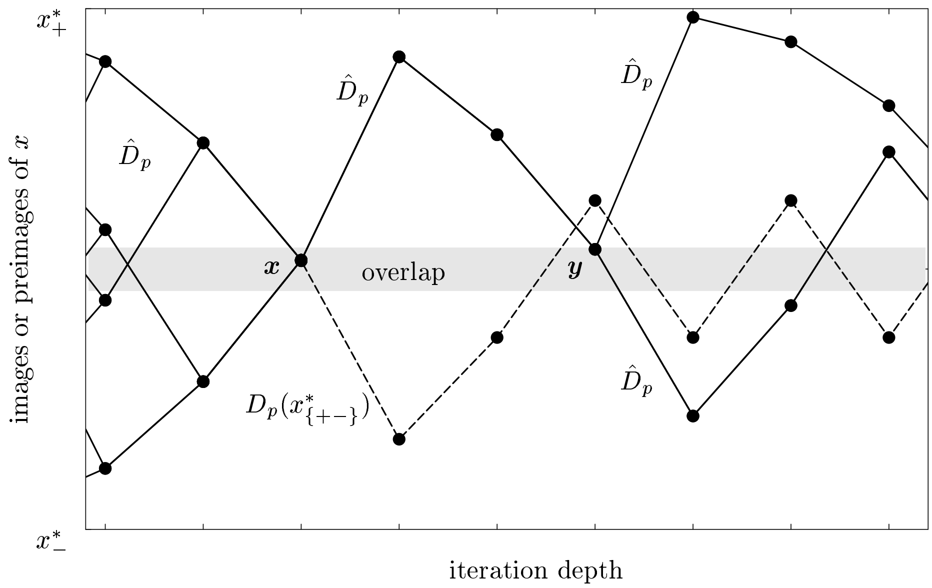

Figure 3.3 Illustration of the intricate structure of orbits and how larger pointwise dimensions are superseded by smaller ones. The point $x = x^*_{\{+--(+-)_\infty\}}$ is in the overlap at $\beta = J = 1$, $h = 0.74$ ($h_c^{(2)} < h < h_c^{(2a)}$). This figure shows x, all its predecessors up to 6-fold application of $f_\pm^{-1}$ and all its successors up to 2-fold application of $f_\pm$. The points are the predecessors/successors whereas the connecting lines illustrate which point is mapped onto which. Note that the backward trajectory of x branches each time a point is in the overlap whereas the predecessor is unique if the overlap is not touched. The dashed line connects points of the orbit $\{+--(+-)_\infty\}$ which is an offshoot of the $\{+-\}$ orbit and therefore has $D_p(x^*_{\{+-\}}) \approx 1.982$. The solid lines connect points of two other orbits which meet at $y \in \mathcal{O}$, both having the generic pointwise dimension $\hat{D}_p \approx 0.943$. At x the larger pointwise dimension $D_p(x^*_{\{+-\}})$ is superseded by $\hat{D}_p$. The offshoots emerging from x all have the smaller pointwise dimension $\hat{D}_p$.

$$\sim \frac{1}{n_k} \sum_{i=1}^{m_{k-1}} \log A'\big(f^{-1}_{\{\sigma\}_i}(x^*_{\{\sigma\}})\big) + \frac{i_k}{n_k} \log A'(x^*_+) \tag{3.40}$$

as the repeated application of f_+ brings the orbit close to x^*_+ very fast. The limit of the first term for $k \to \infty$ is 0 as the sum has only m_{k-1} terms and m_{k-1}/n_k converges to 0. The second term converges to $\log A'(x^*_+)$ as i_k/n_k converges to 1. Therefore, $\lim_{k\to\infty} s_{n_k} = \log A'(x^*_+)$. On the other hand $\lim_{k\to\infty} s_{m_k} = \log A'(x^*_{\{+-\}})$ by a similar argument. Therefore, the limit $\lim_{n\to\infty} s_n$ does not exist.

3.3.2 Pointwise dimension of points in the overlap

In lemmata 3.3 and 3.4 it was essential that no point of the orbit under consideration was in the overlap $\mathcal{O}$ such that the Frobenius-Perron equation (3.7) had only one term. If some point x is in the overlap $\mathcal{O}$ though the Frobenius-Perron equation has two terms corresponding to the two predecessors of x. If the pointwise dimension exists at the two predecessors then it also exists at x and is the minimum of the dimensions at the predecessors.

Lemma 3.5 *Let $x \in \mathcal{O}$ such that $D_p(f_-^{-1}(x);\mu^{(x)})$ and $D_p(f_+^{-1}(x);\mu^{(x)})$ exist. Then the pointwise dimension $D_p(x;\mu^{(x)})$ exists and is given by*

$$D_p(x;\mu^{(x)}) = \min\{D_p(f_-^{-1}(x);\mu^{(x)}), D_p(f_+^{-1}(x);\mu^{(x)})\}\,. \tag{3.41}$$

Sketch of proof. Writing $x_1 := f_-^{-1}(x)$, $x_2 := f_+^{-1}(x)$, $\alpha_1 := D_p(x_1;\mu^{(x)})$ and $\alpha_2 := D_p(x_2;\mu^{(x)})$ the invariant measure scales like

$$\mu^{(x)}(B_\varepsilon(x_1)) \sim \varepsilon^{\alpha_1} \quad \text{and} \quad \mu^{(x)}(B_\varepsilon(x_2)) \sim \varepsilon^{\alpha_2} \tag{3.42}$$

such that the measure at x scales according to the Frobenius-Perron equation roughly like

$$\mu^{(x)}(B_\varepsilon(x)) \sim \tfrac{1}{2}(\varepsilon^{\alpha_1} + \varepsilon^{\alpha 2}) \sim \varepsilon^{\min\{\alpha_1,\alpha_2\}}. \tag{3.43}$$

This implies $D_p(x;\mu^{(x)}) = \min\{\alpha_1,\alpha_2\}$. □

The sketch of proof was taken from [PBL95, Pat97, NPB01a]. The exact proof is rather tedious and can be found in appendix B.9. The mechanism of such *superseding of pointwise dimensions* for points in the overlap is illustrated in figure 3.3 for the example of an orbit which will be important in the next section.

When investigating the dependence of the D_q-spectrum on the physical parameters β, J and h it is most convenient to fix β and J and study the effects of decreasing random field strength h because the structure in the non-overlapping case, i. e. for large h, is rather well understood. With decreasing h the overlap grows and more orbits have points in it. For orbits with pointwise dimension smaller than or equal to the pointwise dimension of the additional predecessor the entry into the overlap has no consequences. For orbits with large pointwise dimension though the pointwise dimension is abruptly changed with the entry into the overlap. In fact, at the value of h where the orbit first touches the overlap the pointwise dimension of the additional predecessor is the pointwise dimension of the fixed points $x^*_\pm$ which is rather small because $A'(x^*_\pm)$ is small. Therefore, orbits with pointwise dimension larger than the local dimension of $x^*_\pm$ are guaranteed to change their pointwise dimension as soon as they touch the overlap. This change in the pointwise dimension may have a major impact on the D_q-spectrum if some or all of the large pointwise dimensions have already been superseded.

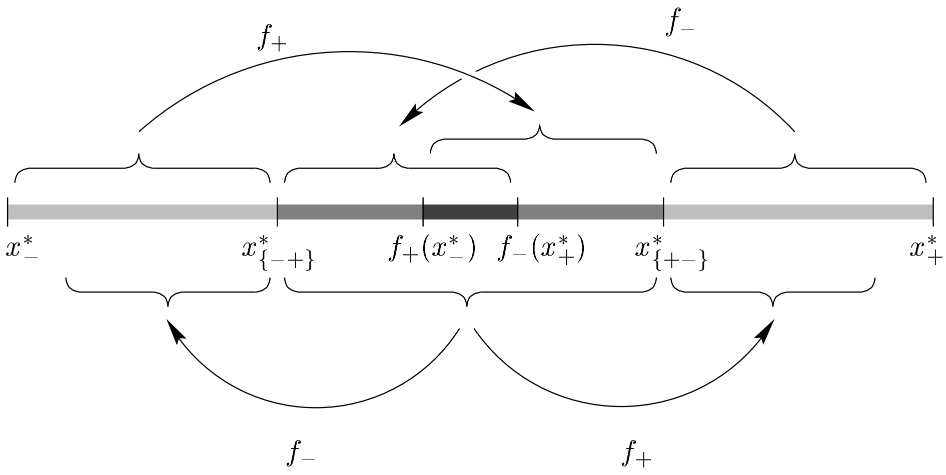

Figure 3.4 Mapping of subintervals of $I = [x^*_-, x^*_+]$ by f_+ and f_- elucidating the importance of the interval $[x^*_{\{-+\}}, x^*_{\{+-\}}]$. The latter is mapped onto parts of the outer intervals $[x^*_-, x^*_{\{-+\}}]$ and $[x^*_{\{+-\}}, x^*_+]$ by f_- and f_+ while these outer intervals are themselves preimages of parts of $[x^*_{\{-+\}}, x^*_{\{+-\}}]$. The points in the overlap $[f_+(x^*_-), f_-(x^*_+)]$ have two predecessors, one stemming from the left by f_+ and one from the right by f_- (all in the case of moderate overlap).

3.4 Further transitions in the D_q-spectrum

3.4.1 Transition at $h_c^{(2)}$

A special role in the mechanism described above is played by the 1-orbits $\{+\}$ and $\{-\}$, because they never touch the overlap $\mathcal{O}$, and by the 2-orbit $\{+-\}$. At moderate overlap (small $|\mathcal{O}|$) the situation is like illustrated in figure 3.4. Since $x^*_{\{+-\}}$ is mapped to $x^*_{\{-+\}}$ and vice versa and because f_σ is monotonic, all points to the right of $x^*_{\{+-\}}$ are mapped to the right of $x^*_{\{-+\}}$ and all points to left of $x^*_{\{-+\}}$ are mapped to points left of $x^*_{\{+-\}}$. Therefore, any periodic n-orbit with $n > 2$ must have at least one point inside $[x^*_{\{-+\}}, x^*_{\{+-\}}]$. Hence, the $\{+-\}$ orbit is the last periodic orbit to touch $\mathcal{O}$.

The $\{+-\}$ orbit and its offshoots have a comparably large pointwise dimension as the $\{+-\}$ orbit always stays in regions with comparably large A', cf equation (3.18). For β and J in the vicinity of $\beta = J = 1$ one can show that the orbit $\{+-\}$ even has the largest pointwise dimension of all periodic orbits [Pat97]. Because of its large pointwise dimension and the fact that all other periodic orbits and their offshoots touch the overlap before $x^*_{\{+-\}}$ does, the $\{+-\}$ orbit and its offshoots practically solely determine all D_q with $q < 0$ if h is close to the value for which $x^*_{\{+-\}}$ gets into the overlap. As soon as $\mathcal{O}$ includes $x^*_{\{+-\}}$, i. e. $f_-(x^*_+) \geq x^*_{\{+-\}}$, the large pointwise dimension of the $\{+-\}$ orbit and its offshoots is superseded by a smaller one and, as all other periodic orbits have been reached by $\mathcal{O}$ before, all D_q with $q < 0$ collapse to $D_q = 1$ at this point. The critical value $h_c^{(2)}$ at

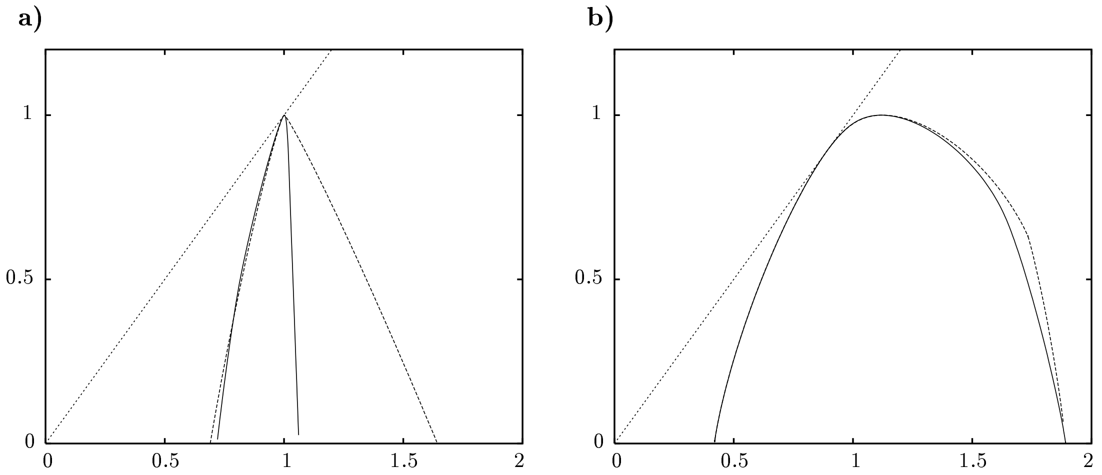

Figure 3.5 Collapse of the right part of the $f(\alpha)$-spectrum at $h_c^{(2)}$ and $h_c^{(2a)}$. In a) the spectra at $h = 0.49385 > h_c^{(2)}$ (dashed line) and $h = 0.4938 < h_c^{(2)}$ (solid line) are shown. In b) the spectra are at $h = 0.8136 > h_c^{(2a)}$ (dashed line) and $h = 0.8128 < h_c^{(2a)}$ (solid line). The spectra were obtained by a numerical Legendre transform of the corresponding D_q-spectra. These were generated with the same algorithm as in figure 3.2 with a recursion depth of 21. ($\beta = J = 1$)

which the collapse takes place is thus given by the condition [Pat97, NPB01a]

$$f_-(x_+^*) = x_{\{+-\}}^* \,. \tag{3.44}$$

The collapse is clearly visible in the numerically generated D_q-spectra, cf figure 3.2 on page 23.

So far only periodic orbits and their offshoots were discussed. Other, non-periodic orbits do not play a major role because they generically have the rather small pointwise dimension $\hat{D}_p = D_1$ and also generically have points inside $[x_{\{-+\}}^*, x_{\{+-\}}^*]$ such that they touch $\mathcal{O}$ before the $\{+-\}$ orbit does.

The drastic change in the D_q-spectrum has a counterpart in the $f(\alpha)$-spectrum. For all $h < h_c^{(2)}$ the right part of the spectrum has vanished since the large pointwise dimensions have all been superseded by smaller ones, cf figure 3.5a. A similar collapse of parts of the multifractal spectrum has previously been observed in the superposition of equal-scale [Rad95] and multi-scale [RS96, SS97] Cantor sets showing that effects of this type appear in a wide variety of applications.

The value of $h_c^{(2)}$ can be calculated explicitly. In a first step explicit expressions for $x_+^* = -x_-^*$ and $x_{\{+-\}}^* = -x_{\{-+\}}^*$ are needed. The fixed point x_+^* is defined by $f_+(x_+^*) = x_+^*$. With the notation $z = e^{2\beta x_+^*}$ this yields the equation

$$z^2 - (e^{2\beta J}(e^{2\beta h} - 1))z - e^{2\beta h} = 0 \tag{3.45}$$

with the solution

$$x_+^* = \frac{1}{2\beta} \log\left(K + \sqrt{K^2 + e^{2\beta h}}\right) \tag{3.46}$$

where $K = e^{2\beta J}(e^{2\beta h} - 1)/2$. To obtain $x^*_{\{+-\}}$ one can exploit $x^*_{\{+-\}} = -x^*_{\{-+\}} = -f_-(x^*_{\{+-\}})$. With $z = e^{2\beta x^*_{\{+-\}}}$ this yields

$$z^2 + e^{-2\beta J}(e^{2\beta h} - 1)z - e^{2\beta h} = 0 \tag{3.47}$$

and therefore

$$x^*_{\{+-\}} = \frac{1}{2\beta} \log\left(\tilde{K} + \sqrt{\tilde{K}^2 + e^{2\beta h}}\right) \tag{3.48}$$

with $\tilde{K} = e^{-2\beta J}(e^{2\beta h}-1)/2$. The condition (3.44) is equivalent to $x^*_+ = x^*_{\{+-\}}+2h$. With the explicit expressions for x^*_+ and $x^*_{\{+-\}}$ this yields after some elementary algebra

$$k^2(1 + 3z + 3z^2 + 4z^3 + 3z^4 + 3z^5 + z^6) - z^3 - k^4 z^3 = 0 \tag{3.49}$$

in the variables $k = e^{2\beta J}$ and $z = e^{2\beta h_c^{(2)}}$. Dividing by z^3 and regrouping then leads to

$$2\big(\cosh(2\beta h_c^{(2)})\big)^3 + 3\big(\cosh(2\beta h_c^{(2)})\big)^2 = \big(\cosh(2\beta J)\big)^2. \tag{3.50}$$

This equation has exactly one real solution for $\cosh\left(2\beta h_c^{(2)}\right)$ resulting in

$$h_c^{(2)} = \frac{1}{2\beta} \operatorname{arcosh}\left(\cosh(\tfrac{4}{3}\beta J) - \tfrac{1}{2}\right). \tag{3.51}$$

There is a critical temperature $(k_B T_c^{(2)})^{-1} = \beta_c^{(2)}$ such that no phase transition of this type is possible for all $\beta < \beta_c^{(2)}$. It is given by the condition $h_c^{(2)} = 0$ corresponding to

$$\frac{1}{k_B T_c^{(2)}} = \beta_c^{(2)} = \frac{3}{4J} \operatorname{arcosh}(\tfrac{3}{2}) = \frac{1}{2J} \log\left(2 + \sqrt{5}\right). \tag{3.52}$$

With (3.44), (3.51) and (3.52) a complete analytical understanding of the occurrence *and the position* of the transition at $h_c^{(2)}$ is achieved. The results are in perfect agreement with the numerical data, cf figure 3.2 on page 23.

3.4.2 Transition at $h_c^{(2a)}$

The key to the explanation of the transition at $h_c^{(2)}$ was the knowledge of the pointwise dimension of the $\{+-\}$ orbit and its significance for the generalized dimensions D_q with $q < 0$. In the numerically generated D_q-spectrum another smaller collapse of the D_q with $q < 0$ is visible at some critical field strength $h_c^{(2a)}$. It is due to a similar mechanism as the one described in the previous subsection but whereas a single orbit and some of its offshoots caused the transition at $h_c^{(2)}$, the transition at $h_c^{(2a)}$ is due to changes in the pointwise dimension of a *family* of periodic orbits and some of their offshoots.

Consider the family $\{\{+--(+-)_n\} : n \in \mathbb{N}\}$ of periodic orbits. It has the following properties.

- For large n most points of the $\{+--(+-)_n\}$ orbit are close to $x^*_{\{+-\}}$ and $x^*_{\{-+\}}$. Provided no point of the orbit is in $\mathcal{O}$ its pointwise dimension is therefore by virtue of (3.18) comparably large.
- The larger n the larger is the fraction of points in the vicinity of $x^*_{\{+-\}}$ and $x^*_{\{-+\}}$ such that the pointwise dimension of the orbits is increasing with n.
- For each orbit $\{+--(+-)_n\}$ the point $z_n := x^*_{\{+--(+-)_n\}}$ is the one closest to the origin and therefore the first one to get into $\mathcal{O}$ with decreasing h.
- The sequence of points $(z_n)_{n\in\mathbb{N}}$ is monotonically growing with n.
- $f_{\{+--(+-)_n\}}(x_0^{(n)})$ converges to $x^*_{\{+--(+-)_\infty\}}$ for any choice of initial values $x_0^{(n)} \in I$ in the limit $n \to \infty$. Furthermore, $f_{\{+--(+-)_n\}}(z_n) = z_n$ by definition of z_n. Therefore, with $x_0^{(n)} := z_n$ one immediately deduces $\lim_{n\to\infty} z_n = x^*_{\{+--(+-)_\infty\}}$.

Combining these properties it is clear that each orbit $\{+--(+-)_n\}$ is affected by the overlap as soon as $z_n \in \mathcal{O}$ and that therefore the orbits with larger pointwise dimension are affected later than the ones with lesser pointwise dimension for decreasing h. From the last point it is clear that as long as $x^*_{\{+--(+-)_\infty\}} \notin \mathcal{O}$ there are countably infinitely many orbits $\{+--(+-)_n\}$ left which have no points in $\mathcal{O}$ but as soon as $x^*_{\{+--(+-)_\infty\}} \in \mathcal{O}$ all of the orbits have points in the overlap and there pointwise dimension is therefore superseded. Thus, the pointwise dimension at a considerable amount of points changes from a large value to a smaller one at a sharp critical value. This causes the small collapse in all D_q with $q < 0$ at $h_c^{(2a)}$ and the critical field strength for this transition is therefore determined by

$$f_-(x^*_+) = x^*_{\{+--(+-)_\infty\}} = f_{\{+-\}}(x^*_{\{-+\}})\,. \tag{3.53}$$

The result is in perfect agreement with the numerically obtained positions of the small collapse in the D_q-spectrum for $q = -1$, -2 and -3, cf figure 3.6.

The transition is also visible in the $f(\alpha)$-spectrum. For $h \searrow h_c^{(2a)}$ a cusp develops and the spectrum collapses to a smooth form again at $h_c^{(2a)}$, cf figure 3.5b.

So far only the periodic orbits $\{+--(+-)_n\}$ were considered neglecting their offshoots. Each such orbit has countably many offshoots. From these offshoots those originating from points left of $\mathcal{O}$ and containing exclusively additional $-$ as well as those originating from points to the right of $\mathcal{O}$ and only containing

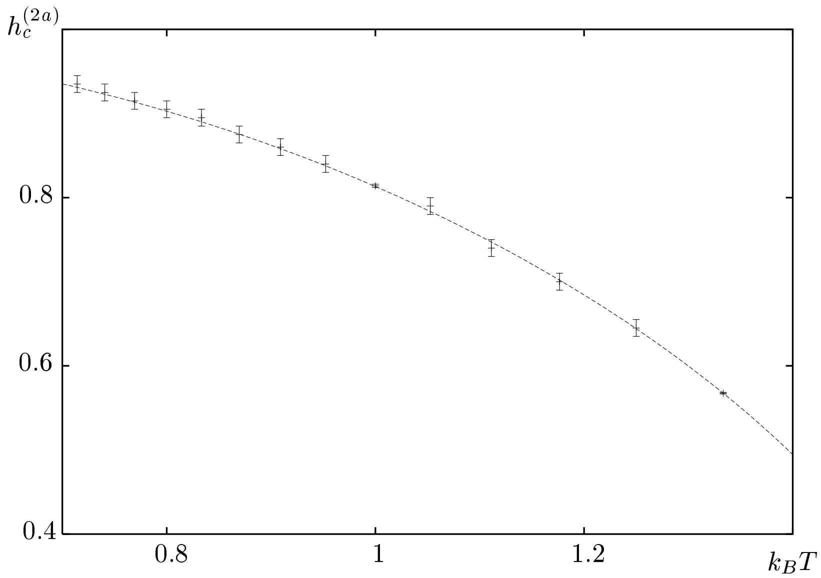

Figure 3.6 $h_c^{(2a)}$ obtained from the analytical condition (3.53) (dashed line) compared to the location of the small drops in D_q (error-bars), cf figure 3.2. The errors are estimated and mainly due to the error in reading off the exact location of the collapse in the numerically obtained D_q-spectra. The points were read off the D_q-spectra for $q = -1$, -2 and -3, equally spaced in β. Points with small error bars correspond to numerical data with especially fine steps in the random field strength. ($J = 1$)

additional $+$ are not touching the overlap as long as the corresponding periodic orbit is not. Thus, at $h_c^{(2a)}$ countably infinitely many periodic orbits with each countably infinitely many offshoots of the described form lose their large pointwise dimension at once. This gives a clue why this transition is visible in the D_q-spectrum in contrast to events of single orbits (and their offshoots) changing their local dimension at their entry into the overlap occurring at various values of h.

The fact that the transition is not visible in D_q with large negative q is also easily understood in this framework. As the pointwise dimension of all $\{+--(+-)_n\}$ orbits is similar to but somewhat smaller than the pointwise dimension of the $\{+-\}$ orbit, the $\{+-\}$ orbit and its offshoots dominate D_q for large negative q and the transition is not visible.

There is also a critical temperature for this transition which is determined by the condition $h_c^{(2a)} = 0$. Even though an explicit expression for $h_c^{(2a)}$ could not be found so far the explicit form of the critical temperature can be obtained after some basic algebra. It is

$$\frac{1}{k_B T_c^{(2a)}} = \beta_c^{(2a)} = \frac{1}{4J} \log\left(\tfrac{19}{3} + \tfrac{8}{3}\sqrt{7}\cos(\tfrac{\pi}{3} - \tfrac{1}{3}\arctan(3\sqrt{3}))\right). \tag{3.54}$$

Note that the symmetry of the system allows the same reasoning as above

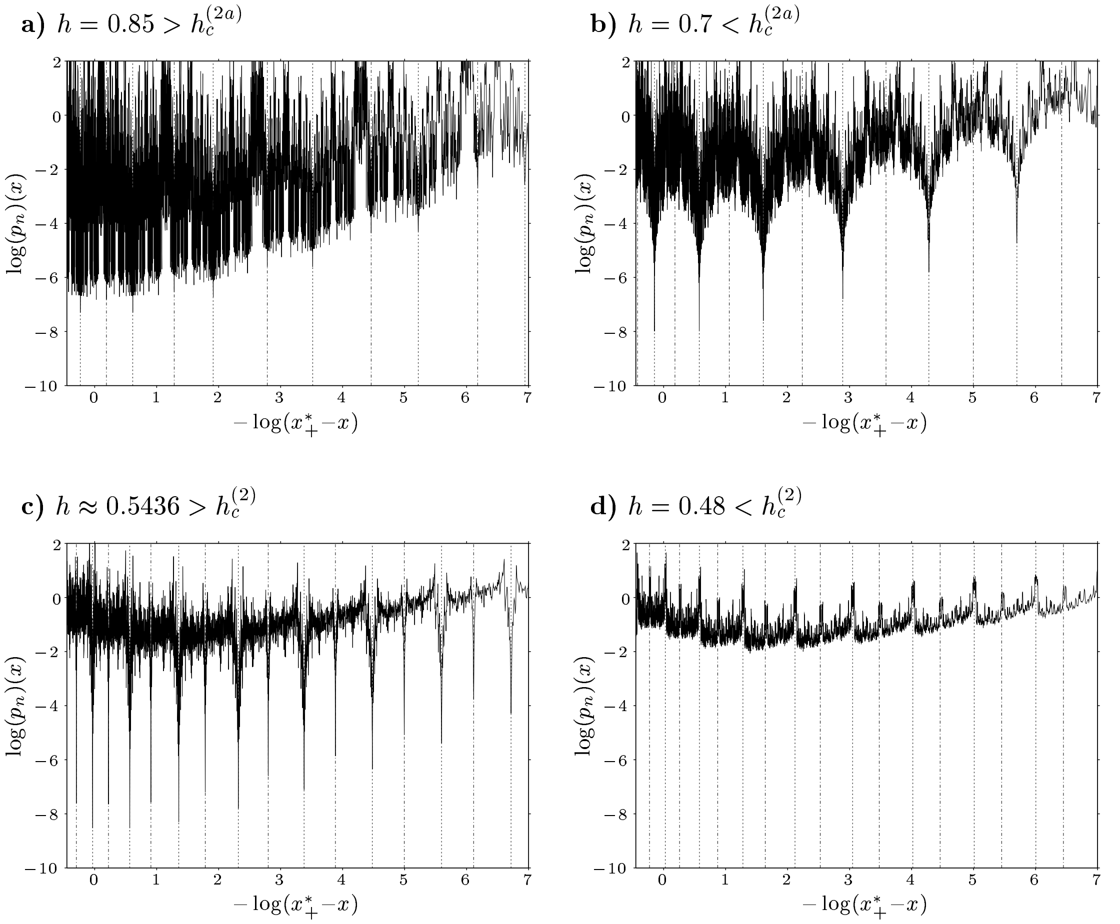

Figure 3.7 Double logarithmic plot of p_n generated with the algorithm based on the new natural partition, cf appendix A.1, at iteration depth 21. The negative peaks correspond to deep cuts in p_n. The dotted lines mark the position of $x^*_{\{(+)_k(+-)_\infty\}}$, i.e. the points of the $\{+-\}$ orbit and its offshoots, and the dash-dotted lines the positions of $x^*_{\{(+)_k+--(+-)_\infty\}}$, i.e. the points of the $\{+--(+-)_\infty\}$ orbit and its offshoots. In a) at random field $h > h_c^{(2a)}$ deep cuts are visible at all marked positions whereas in b) for $h < h_c^{(2a)}$ the deep cuts at $x^*_{\{(+)_k+--(+-)_\infty\}}$ have vanished. They reappear in c) at a critical field strength $h \approx 0.5436$ as is discussed in the text whereas in d) for $h < h_c^{(2)}$ all deep cuts have vanished. ($\beta = J = 1$)

with the ‘opposite’ orbits $\{-++(-+)_n\}$ resulting in an equivalent result.

Even though the effect is due to the periodic orbits $\{+--(+-)_n\}$ and their offshoots, the orbit entering into condition (3.53) is an offshoot of the $\{+-\}$ orbit, namely $\{+--(+-)_\infty\}$. This orbit thus plays a similar role as the $\{+-\}$ orbit for the transition at $h_c^{(2)}$.

In numerically generated approximations of p_n a bunch of weakly scaling points (deep cuts in the measure density) in the vicinity of $x^*_{\{+-\}}$ and its offshoots $\{(+)_m(+-)_\infty\}$ as well as $x^*_{\{+--(+-)\infty\}}$ and its offshoots $x^*_{\{(+)_m+--(+-)_\infty\}}$ can be

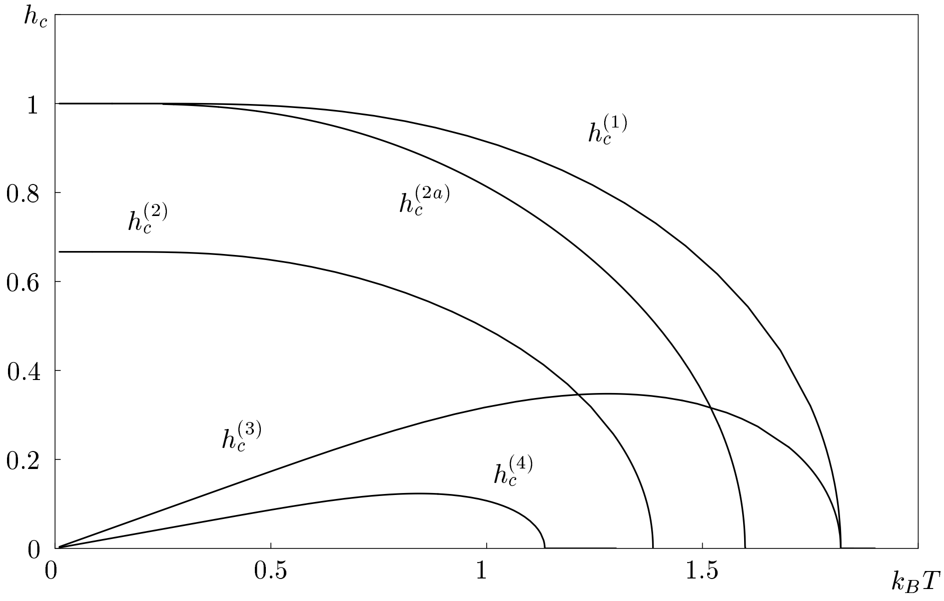

Figure 3.8 Phase diagram for the transitions in the invariant measure of the one-dimensional random field Ising model. The critical random field strengths $h_c^{(n)}$ are defined in the text. The remarkable fact that the lines of $h_c^{(2)}$ and $h_c^{(3)}$ as well as the lines of $h_c^{(2a)}$ and $h_c^{(3)}$ intersect shows that there is a variety of different scenarios depending on the choice of T. For example, at $k_BT = 1.3$, the transition at $h_c^{(2)}$ precedes the one at $h_c^{(3)}$ while the transition at $h_c^{(4)}$ is non-existent. ($J = 1$)

seen for $h > h_c^{(2a)}$, cf figure 3.7a. For $h_c^{(2)} < h < h_c^{(2a)}$ the weakly scaling points around $x^*_{\{+--(+-)\infty\}}$ and its offshoots have vanished, cf figure 3.7b. For $h < h_c^{(2)}$ all weakly scaling points have vanished, cf figure 3.7d.

The attentive reader will have noticed that it was argued that the large local dimension of an orbit which touches the overlap $\mathcal{O}$ for some h_0 but not for $h > h_0$ is superseded by the small pointwise dimension of the $\{+\}$ or the $\{-\}$ orbit. For smaller h the pointwise dimension of the second predecessor will be D_1 in the generic case and thus also rather small. It is not excluded though that *two large pointwise dimensions* are combined resulting in a large pointwise dimension even though the orbit touches the overlap. A prominent example of this effect is the value of h for which $x^*_{\{+--(+-)_\infty\}} = x^*_{\{-++(-+)_\infty\}} = 0$. At this random field amplitude new deep cuts in the approximated measure density appear at $x^*_{\{+--(+-)_\infty\}}$ and its offshoots, cf figure 3.7c. The effect on the D_q-spectrum is negligible though as this is a rare event only affecting a single orbit and its offshoots and only appearing at an isolated value of h.

To summarize, the crucial feature for a visible transition in the D_q-spectrum is that a non-negligible fraction of orbits with large pointwise dimension is affected by the overlap at one sharp critical value $h_c^{(2a)}$ resulting in a collapse of D_q with negative q. It is not excluded that there are more transitions of this type which might become observable with further increase in numerical accuracy in the

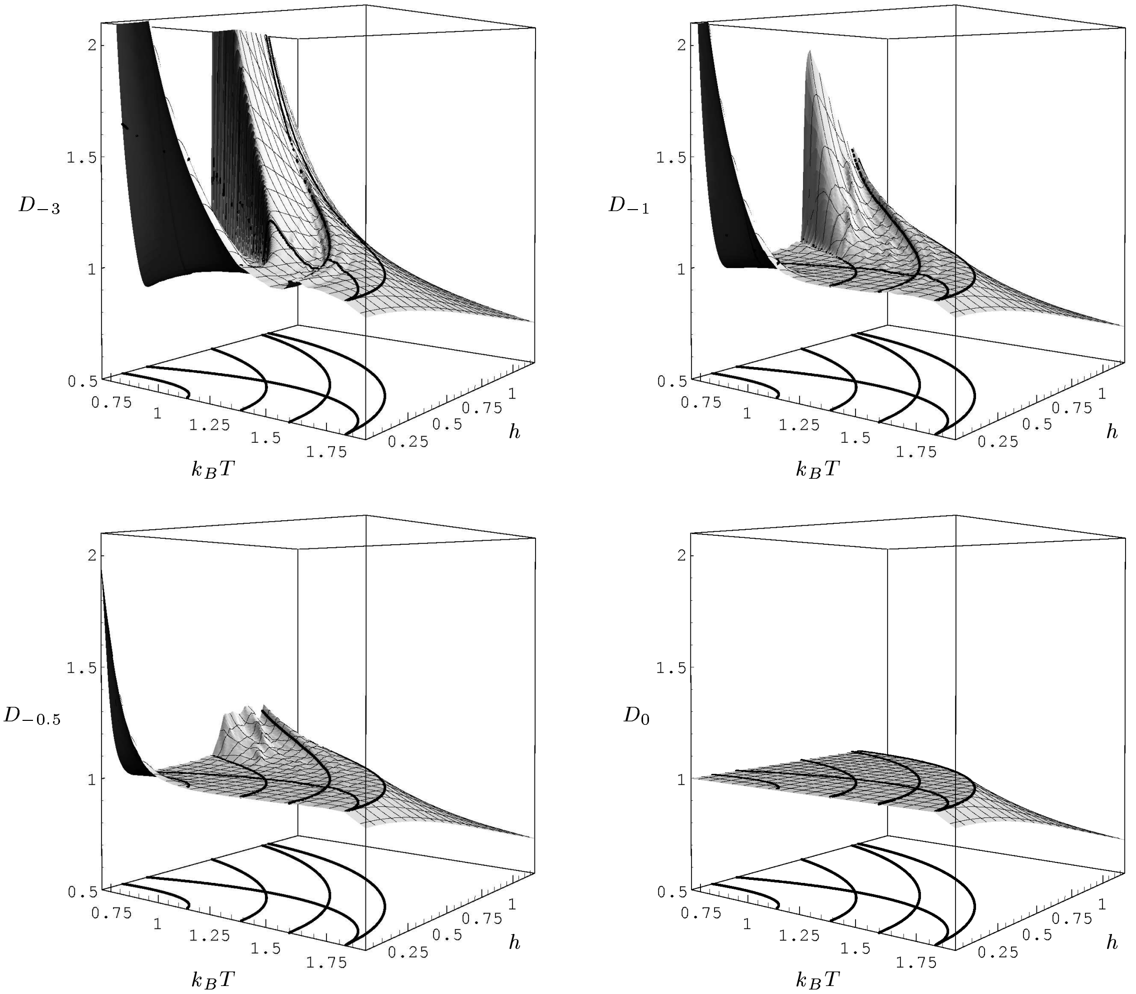

Figure 3.9 Surface plots of D_{-3}, D_{-1}, $D_{-0.5}$ and D_0 as functions of $k_B T$ and h. The lines on the bottom of the graphs are the transitions lines of figure 3.8 and the lines on the surfaces are projetions of these lines. As on can see, the transition lines agree perfectly with the visible transitions (steps, kinks) in the numerical data for all T and h. ($J = 1$)

future. The arguments presented here allow the conjecture that these transitions, if existent, should take place at $h > h_c^{(2a)}$.

3.4.3 Transition diagram

The formulae given for the critical values $h_c^{(n)}$, $n = 1$, 2, $2a$, 3 and 4 allow to draw a phase diagram for the transitions in the D_q-spectrum of the invariant measure, cf figure 3.8. To check the consistency with numerical results for more than the temperature $\beta = 1$ figure 3.9 shows the D_q-spectra as functions of $k_B T$ and h and the phase diagram of figure 3.8 in comparison. It is obvious that the results

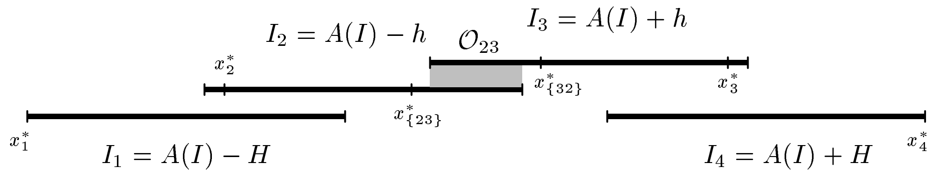

Figure 3.10 Sample situation of first order bands for the random field distribution (3.55) in the vicinity of a transition similar to the one at $h_c^{(2)}$ in the text. If, as shown in the figure, H is large enough, $x_{\{23\}}^*$ and $x_{\{32\}}^*$ are not included in I_1 and I_4 respectively. In this case $x_{\{23\}}^*$ has the unique predecessor $x_{\{32\}}^*$ and vice versa as long as they are not in $\mathcal{O}_{23}$ exactly like $x_{\{-+\}}^*$ and $x_{\{+-\}}^*$ in the dichotomous case. The situation is therefore identical to the situation in the dichotomous case and the transition takes place at $h = h_c^{(2)}$. Of course, szenarios where the overlaps $\mathcal{O}_{12}$ and $\mathcal{O}_{34}$ play important roles are conceivable as well. ($\beta = J = 1$, $h = 0.7$, $H = 1.8$)

match for all T.

All considerations so far were explicitly for the specific choice (3.2) of the distribution of the random field. It is natural to ask whether transitions of the different types discussed also appear in more general situations. This is indeed the case. For illustration consider the random field distribution

$$\rho(h_i) = \tfrac{1}{4}\delta(h_i - H) + \tfrac{1}{4}\delta(h_i - h) + \tfrac{1}{4}\delta(h_i + h) + \tfrac{1}{4}\delta(h_i + H) \tag{3.55}$$

with $h < H$. One can perform a similar analysis as for the dichotomous random field distribution the main difference being that for the random field distribution (3.55) up to three overlaps have to be taken into account. The results roughly are the following.

- For any given temperature β there exists a transition line in the (h,H) parameter plane between a region with $D_0 = 1$ and $D_0 < 1$ which is easily determined from the overlap conditions of the first order bands $I_1, \ldots, I_4$. The conditions for $D_0 = 1$ are $h \leq h_c^{(1)}$ implying the existence of $\mathcal{O}_{23}$ and $f_3(x_4^*) \geq f_4(x_1^*)$ implying the existence of the overlaps $\mathcal{O}_{12}$ and $\mathcal{O}_{34}$. The second inequality is a condition on H as well as h, cf figure 3.10.

- The transitions depending on the scaling at the boundary of the support of μ_∞, i. e. on the scaling at x_1^* and x_4^*, exist in the same way as the transitions at $h_c^{(3)}$ and $h_c^{(4)}$ in the dichotomous case. The transition conditions are $H = h_c^{(3)}$ and $H = h_c^{(4)}$ respectively.

- Even though the orbit structure is more intricate than in the dichotomous case figure 3.10 shows a situation in which a transition of the type of the transition at $h_c^{(2)}$ as discussed in subsection 3.4.1 can take place. The transition occurs at $h = h_c^{(2)}$ provided H is large enough such that the bands

I_1 and I_2 do not include $x^*_{\{23\}}$ or $x^*_{\{32\}}$, i. e. $f_1(x^*_4) < x^*_{\{23\}}$ or equivalently $f_4(x^*_1) > x^*_{\{32\}}$.

In summary, the types of transitions occurring in the D_q-spectrum are the same as in the dichotomous case and it is in principle possible to draw a diagram in the (β, h, H) parameter space similar to the simpler diagram in figure 3.7 which is the $h = H$ slice of this higher dimensional diagram. As there are more than one overlap in this example and the simultanuous overlap of more than two bands can occur there also can be more complicated effects which nevertheless should be amenable to a similar analysis as the transitions discussed in this section.

In the same way, appropriate adaptions of the analytic tools developed in this chapter allow to analyze transitions in the D_q-spectrum of the invariant measure of the effective field for any discrete random field distribution.

3.5 Bounds on the D_q-spectrum

The knowledge of the pointwise dimension of orbits is not only essential for the explanation of the transitions in D_q with $q < 0$ but also very useful to obtain bounds on the D_q-spectrum as well. To see this it is important to understand some general relations between D_q and D_p.

3.5.1 General relations between D_q and D_p

The following considerations are true for any Borel probability measure μ on $\mathbb{R}^n$. They in some sense generalize bounds developed in [Eva87]. Let μ_i be defined as in (2.8) on page 13 for some arbitrary mesh of cubes $\{b^\varepsilon_i\}_{i\in\mathbb{N}}$ and enlarged cubes $\{\overline{b}^\varepsilon_i\}_{i\in\mathbb{N}}$. Naturally one has for any $x \in \mathbb{R}^n$ and $q \in \mathbb{R}$

$$\sum_{i\in\mathbb{N}} \mu_i^q \geq \mu_{i(x)}^q \tag{3.56}$$

where $\mu_{i(x)}$ denotes the measure of the enlarged box $\overline{b}^\varepsilon_{i(x)}$ for which $x \in b^\varepsilon_{i(x)}$. This basic inequality leads to non-trivial bounds on the D_q-spectrum in terms of the pointwise dimension of arbitrary points in the support of μ.

Lemma 3.6 General bounds on D_q *For any $x \in \operatorname{supp}\mu$ the inequalities*

$$\underline{D}_q(\mu) \geq \frac{q}{q-1}\underline{D}_p(x;\mu) \quad \textit{for } q < 1 \tag{3.57}$$

$$\underline{D}_q(\mu) \leq \frac{q}{q-1}\underline{D}_p(x;\mu) \quad \textit{for } q > 1 \tag{3.58}$$

and analogously for the upper dimensions $\overline{D}_q(\mu)$ and $\overline{D}_p(x;\mu)$ hold.

Proof. Let $x \in \operatorname{supp} \mu$. The choice of enlarged boxes of size $\varepsilon(1+\delta)$ implies $B_{\varepsilon(1+\delta)}(x) \supseteq \overline{b}^{\varepsilon}_{i(x)} \supseteq B_{\varepsilon\delta/2}(x)$ such that

$$\mu(B_{\varepsilon(1+\delta)}(x)) \geq \mu_{i(x)} \geq \mu(B_{\varepsilon\delta/2}(x))\,. \tag{3.59}$$

For $q < 0$ inequality (3.56) and the left inequality of (3.59) yield

$$\sum_{i \in N} \mu_i^q \geq \mu(B_{\varepsilon(1+\delta)}(x))^q \tag{3.60}$$

$$\Rightarrow \quad \underline{D}_q(\mu) \geq \frac{q}{q-1} \liminf_{\varepsilon \to 0} \frac{\log \mu(B_{\varepsilon(1+\delta)}(x))}{\log \varepsilon(1+\delta) + \log \frac{\varepsilon}{\varepsilon(1+\delta)}} \tag{3.61}$$

resulting in

$$\underline{D}_q \geq \frac{q}{q-1} \underline{D}_p(x;\mu)\,. \tag{3.62}$$

For $0 < q < 1$ inequality (3.56) and the right inequality of (3.59) yield

$$\sum_{i \in N} \mu_i^q \geq \mu(B_{\varepsilon\delta/2}(x))^q \tag{3.63}$$

$$\Rightarrow \quad \underline{D}_q \geq \frac{q}{q-1} \liminf_{\varepsilon \to 0} \frac{\log \mu(B_{\varepsilon\delta/2}(x))}{\log(\varepsilon\delta/2) - \log(\delta/2)} \tag{3.64}$$

and therefore also

$$\underline{D}_q(\mu) \geq \frac{q}{q-1} \underline{D}_p(x;\mu)\,. \tag{3.65}$$

For $q > 1$ inequality (3.56) and the right inequality of (3.59) yield

$$\sum_{i \in N} \mu_i^q \geq \mu(B_{\varepsilon\delta/2}(x) \tag{3.66}$$

$$\Rightarrow \quad \underline{D}_q(\mu) \leq \frac{q}{q-1} \liminf_{\varepsilon \to 0} \frac{\log \mu(B_{\varepsilon\delta/2}(x))}{\log(\varepsilon\delta/2) - \log(\delta/2)} \tag{3.67}$$

and thus the opposite inequality

$$\underline{D}_q(\mu) \leq \frac{q}{q-1} \underline{D}_p(x;\mu)\,. \tag{3.68}$$

The proof for the upper dimensions $\overline{D}_q$ is analogous with lim inf replaced by lim sup. □

Whenever the measure under consideration has compact support and scales most weakly at some point $x_{\min}$ of its support, i.e. the pointwise dimension at $x_{\min}$ is maximal, the inequality

$$\sum_i \mu_i^q \leq N_\varepsilon \mu^q_{i(x_{\min})} \leq N_\varepsilon \mu(B_{\varepsilon\delta/2}(x_{\min}))^q \tag{3.69}$$

holds for sufficiently small ε and $q < 0$. Here N_ε is the number of boxes with non-vanishing measure. This inequality also implies non-trivial bounds on the D_q-spectrum.

Lemma 3.7 Bounds on D_q in terms of maximal D_p *Let $x_{\min} \in \operatorname{supp} \mu$ such that $D_p(x_{\min}; \mu)$ is maximal. Then*

$$\underline{D}_q(\mu) \le \frac{1}{q-1}(q\underline{D}_p(x_{\min}; \mu) - \underline{D}_0(\mu)) \quad \text{for } q < 0 \tag{3.70}$$

and the same for $\overline{D}_q(\mu)$ and $\overline{D}_p(x_{\min}; \mu)$.

Proof. The inequality (3.69) implies for $q < 0$

$$\underline{D}_q(\mu) \le \frac{1}{q-1} \liminf_{\varepsilon \to 0} \Big(\frac{\log N_\varepsilon}{\log \varepsilon} + \frac{q \log \mu(B_{\varepsilon\delta/2}(x_{\min}))}{\log \varepsilon\delta/2 - \log \delta/2} \Big) \tag{3.71}$$

such that

$$\underline{D}_q(\mu) \le \frac{1}{q-1}(q\underline{D}_p(x_{\min}; \mu) - \underline{D}_0(\mu)) \,. \tag{3.72}$$

The proof for the upper dimensions $\overline{D}_q$ is the same with lim inf replaced by lim sup. □

If on the other hand the measure scales maximal at some point $x_{\max}$, i.e. the pointwise dimension is minimal at $x_{\max}$ then for sufficient small ε and $q > 0$

$$\sum_i \mu_i^q \le N_\varepsilon \mu_{i(x_{\max})}^q \le N_\varepsilon \mu(B_{\varepsilon(1+\delta)}(x_{\max}))^q \,. \tag{3.73}$$

This yields another set of inequalities.

Lemma 3.8 Bounds on D_q in terms of minimal D_p *Let $x_{\max} \in \operatorname{supp} \mu$ such that $D_p(x_{\max}; \mu)$ is minimal. Then*

$$\underline{D}_q(\mu) \le \frac{1}{q-1}(q\underline{D}_p(x_{\max}; \mu) - \underline{D}_0(\mu)) \quad \text{for } 0 < q < 1 \tag{3.74}$$

$$\underline{D}_q(\mu) \ge \frac{1}{q-1}(q\underline{D}_p(x_{\max}; \mu) - \underline{D}_0(\mu)) \quad \text{for } q > 1 \tag{3.75}$$

and accordingly for $\overline{D}_q(\mu)$ and $\overline{D}_p(x_{\max}; \mu)$.

Proof. For $0 < q < 1$ inequality (3.73) implies

$$\underline{D}_q \le \frac{1}{q-1} \liminf_{\varepsilon \to 0} \Big(\frac{\log N_\varepsilon}{\log \varepsilon} + \frac{q \log \mu(B_{\varepsilon(1+\delta)}(x_{\max}))}{\log \varepsilon(1+\delta) - \log(1+\delta)} \Big) \tag{3.76}$$

yielding

$$\underline{D}_q \leq \frac{1}{q-1}\left(q\underline{D}_p(x_{\max};\mu) - \underline{D}_0(\mu)\right). \tag{3.77}$$

For $q > 1$ inequality (3.73) results in

$$\underline{D}_q \geq \frac{1}{q-1} \liminf_{\varepsilon \to 0} \left(\frac{\log N_\varepsilon}{\log \varepsilon} + \frac{q \log \mu(B_{\varepsilon(1+\delta)}(x_{\max}))}{\log \varepsilon(1+\delta) - \log(1+\delta)}\right) \tag{3.78}$$

and therefore

$$\underline{D}_q \geq \frac{1}{q-1}\left(q\underline{D}_p(x_{\max};\mu) - \underline{D}_0(\mu)\right). \tag{3.79}$$

The proof for $\overline{D}_q$ is identical with lim inf replaced by lim sup. □

Note that the inequalities of lemma 3.7 and lemma 3.8 are a little stronger than the ones presented in [NPB01a] as in that work $D_0(\mu) \leq n$ was used as an additional estimate.

Because the right hand sides of (3.57) and (3.70) converge to a common value for $x = x_{\min}$ in the limit $q \to -\infty$ as well as the right hand sides of (3.58) and (3.75) for $x = x_{\max}$ in the limit $q \to \infty$ one can obtain explicit formulae for $D_{-\infty}$ and D_∞.

Corollary 3.9 Explicit formulae for $D_{-\infty}$ and D_∞ *Let $x_{\max}$ and $x_{\min}$ be defined as in lemma 3.7 and lemma 3.8 respectively. Then*

$$D_{-\infty}(\mu) = D_p(x_{\min};\mu) \tag{3.80}$$

$$D_\infty(\mu) = D_p(x_{\max};\mu). \tag{3.81}$$

3.5.2 Application to the measure of the effective field

The inequalities obtained in the preceding subsection can directly be applied to the invariant measure of the effective field as some of the pointwise dimensions are well known, cf section 3.3. Knowing that $D_q(\mu^{(x)})$ and $D_p(x;\mu^{(x)})$ exist for all q and all relevant $x \in \operatorname{supp} \mu^{(x)}$ the inequalities need not be formulated with lower and upper dimensions separately. The pointwise dimension at x_+^* is given by use of (3.18) as

$$D_p(x_+^*;\mu^{(x)}) = \frac{-\log 2}{\log A'(x_+^*)} \tag{3.82}$$

leading via lemma 3.6 to

$$D_q(\mu^{(x)}) \geq \frac{q}{q-1} \frac{-\log 2}{\log A'(x_+^*)} \quad \text{for } q < 1 \tag{3.83}$$

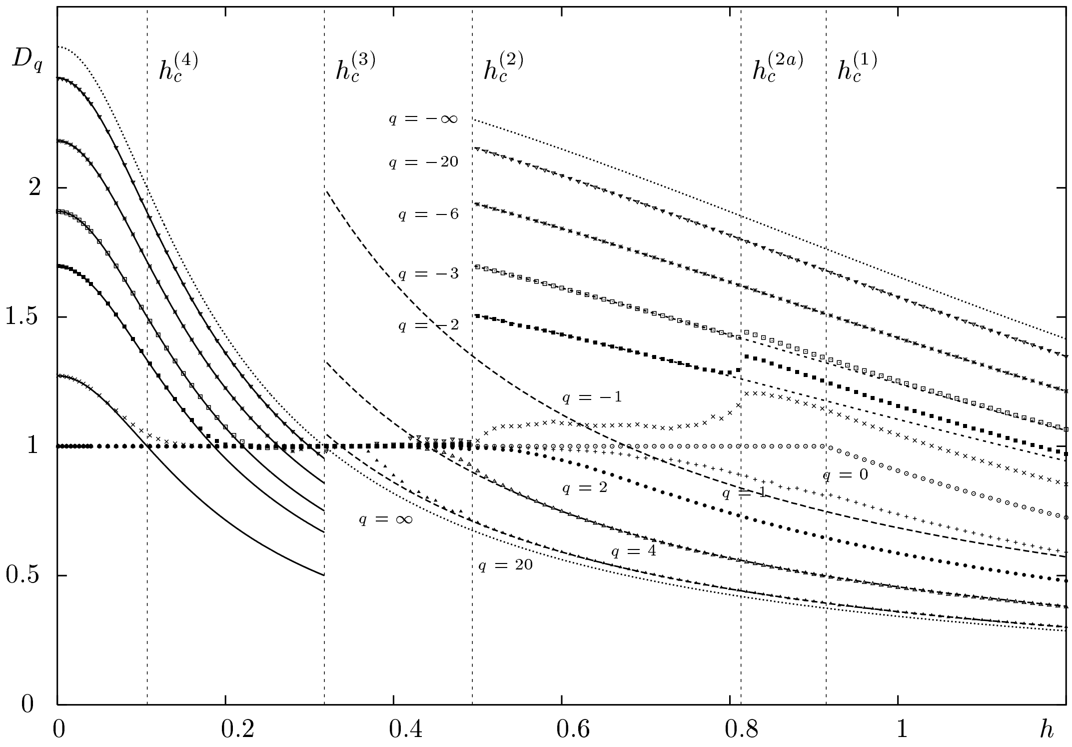

Figure 3.11 D_q-spectrum of the invariant measure of the effective field as a function of h. The solid lines in the region $h < h_c^{(3)}$ are lower bounds on D_q, $q = -20$, -6, -3, -2 and -1 according to (3.83). The short dashed lines in the region $h > h_c^{(2)}$, upper part, are lower bounds on D_q for the same set of q values based on (3.86). The dashed lines in the region $h > h_c^{(2)}$, lower part, are upper bounds on D_q for $q = 2$, 4 and 20 based on (3.84). The dotted lines are the exact values of $D_{-\infty}$ and D_∞ for $h < h_c^{(3)}$, $h > h_c^{(2)}$ and $h > h_c^{(3)}$ respectively. The numerically generated D_q-spectra are taken from figure 3.2 for comparison purposes. ($\beta = J = 1$)

$$D_q(\mu^{(x)}) \leq \frac{q}{q-1} \frac{-\log 2}{\log A'(x_+^*)} \quad \text{for } q > 1. \tag{3.84}$$

The resulting bounds are shown in comparison to numerical results in figure 3.11. The pointwise dimension at $x_{\{+-\}}^*$ is for $h > h_c^{(2)}$ according to (3.18)

$$D_p(x_{\{+-\}}^*; \mu^{(x)}) = \frac{-\log 2}{\log A'(x_{\{+-\}}^*)} \tag{3.85}$$

leading by lemma 3.6 to

$$D_q(\mu^{(x)}) \geq \frac{q}{q-1} \frac{-\log 2}{\log A'(x_{\{+-\}}^*)} \quad \text{for } q < 1 \text{ and } h > h_c^{(2)} \tag{3.86}$$

$$D_q(\mu^{(x)}) \leq \frac{q}{q-1} \frac{-\log 2}{\log A'(x^*_{\{+-\}})} \quad \text{for } q > 1 \text{ and } h > h_c^{(2)}. \tag{3.87}$$

Examples of the resulting bounds for the D_q-spectrum are shown in figure 3.11. Furthermore, for $h < h_c^{(3)}$ the measure scales most weakly at x^*_+ which allows to use lemma 3.7 and equation (3.82) as well as $D_0(\mu^{(x)}) = 1$ in this parameter region to obtain

$$D_q(\mu^{(x)}) \leq \frac{1}{q-1} \Big(\frac{-q \log 2}{\log A'(x^*_+)} - 1 \Big) \quad \text{for } q < 0 \text{ and } h < h_c^{(3)}. \tag{3.88}$$

In the region $h > h_c^{(3)}$ the invariant measure scales most strongly at x^*_+ such that lemma 3.8 and equation (3.82) can be applied. This yields

$$D_q(\mu^{(x)}) \leq \frac{1}{q-1} \Big(\frac{-q \log 2}{\log A'(x^*_+)} - D_0(\mu^{(x)}) \Big) \quad \text{for } 0 < q < 1 \text{ and } h > h_c^{(3)} \tag{3.89}$$

$$D_q(\mu^{(x)}) \geq \frac{1}{q-1} \Big(\frac{-q \log 2}{\log A'(x^*_+)} - D_0(\mu^{(x)}) \Big) \quad \text{for } q > 1 \text{ and } h > h_c^{(3)}. \tag{3.90}$$

As it turns out $D_p(x^*_+; \mu^{(x)}) = -\log(2)/\log A'(x^*_+)$ is so small for typical T and J and the relevant parameter region of h that the right hand side of (3.90) is *increasing* in q. As $D_q \geq D_\infty$ the bound for $q \to \infty$ is therefore always a tighter lower bound for D_q than any of the bounds for finite q, cf also figure 3.12. For $h > h_c^{(2)}$ the invariant measure scales most weakly at $x^*_{\{+-\}}$ if β and J are close to 1, cf [Pat97], such that lemma 3.7 can be applied resulting in

$$D_q(\mu^{(x)}) \leq \frac{1}{q-1} \Big(\frac{-q \log 2}{\log A'(x^*_{\{+-\}})} - D_0(\mu^{(x)}) \Big) \quad \text{for } q < 0 \text{ and } h > h_c^{(2)}. \tag{3.91}$$

The bounds according to inequalities (3.88), (3.90) and (3.91) are shown in figure 3.12. Corollary 3.9 finally yields

$$D_{-\infty} = \begin{cases} \dfrac{-\log 2}{\log(A'(x^*_+))} & \text{for } h < h_c^{(3)} \\[2ex] \dfrac{-\log 2}{\log(A'(x^*_{\{+-\}}))} & \text{for } h > h_c^{(2)} \end{cases} \tag{3.92}$$

and

$$D_\infty = \frac{-\log 2}{\log(A'(x^*_+))} \quad \text{for } h > h_c^3\,. \tag{3.93}$$

The resulting curves for $D_{-\infty}$ and D_∞ are shown in figure 3.11 as well as figure 3.12.

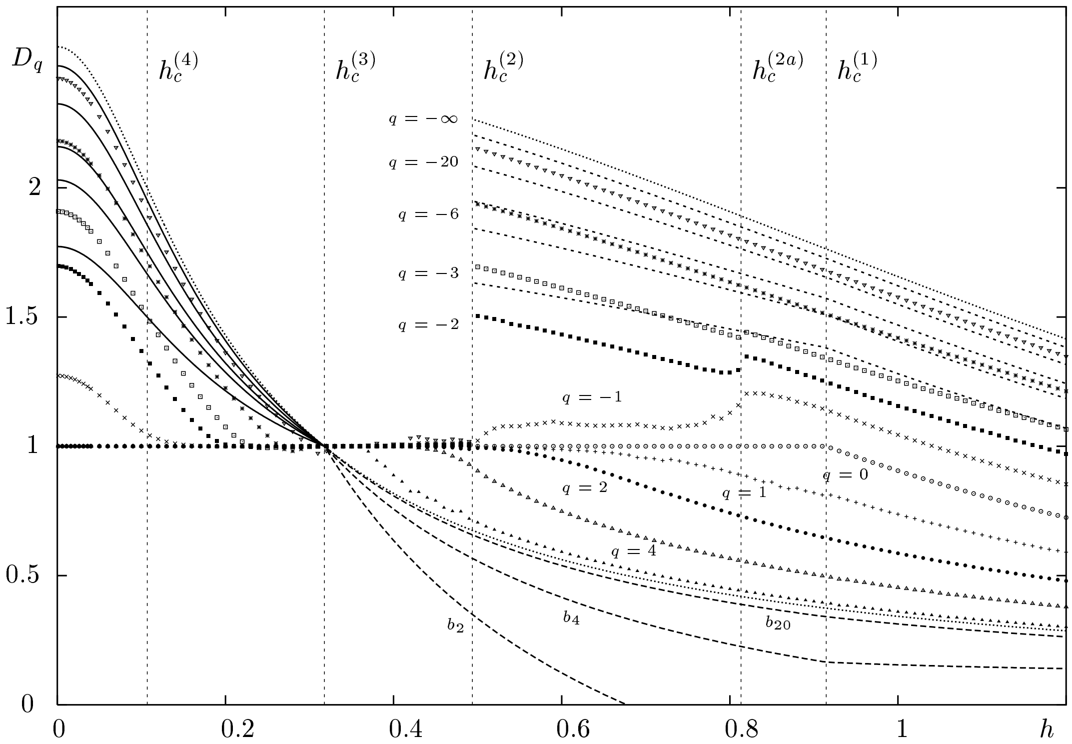

Figure 3.12 D_q-spectrum of the measure of the effective field as a function of h. The solid lines in the region $h < h_c^{(3)}$ are upper bounds on D_q based on (3.88) where $q = -20$, -6, -4, -2 and -1 respectively. The short dashed lines in the region $h > h_c^{(2)}$, upper part, are upper bounds on D_q based on (3.91) for the same q values. The dashed lines in the region $h > h_c^{(2)}$, lower part, are lower bounds on D_q based on (3.90). The labels b_2, b_4 and b_{20} mark the bound for $q = 2$, 4 and 20 respectively. The numerically generated D_q-spectra are taken from figure 3.2 for comparison. It is obvious that these type of bounds are less useful than the ones presented in figure 3.11. Especially the bounds based on (3.90) provide no new information as they are smaller than the exact value of D_∞ and the monotonicity of D_q already implies $D_q \geq D_\infty$ for all q. ($\beta = J = 1$)

Note that whereas the bounds (3.83), (3.84), (3.86) and (3.87) do not need any additional assumptions the bounds (3.88), (3.89), (3.90), (3.91) and the equations (3.93) and (3.92) rest on the assumption of minimal or maximal scaling at x_+^* and $x_{\{+-\}}^*$. Furthermore, as figures 3.11 and 3.12 reveal, the latter bounds are not as tight as the former ones.

The detailed characterization of the D_q-spectrum of the effective field by the various bounds and the description of the transitions in this chapter are necessary prerequisites for the analysis of the local magnetization because the main results for the local magnetization will be relations between the multifractal properties of the measure of the local magnetization and the multifractal properties of the measure of the effective field. This will become clear in the next chapter.

Chapter 4

Convolution of multifractals and the local magnetization of the one-dimensional random field Ising model

In this chapter the multifractal properties of the measure of the local magnetization at an arbitrary site i in the random field Ising chain are investigated. Recall that the model is defined by the Hamiltonian (3.1) and treated in the canonical ensemble. The local magnetization in the bulk is given by $m_{i,N}^{\mathrm{bulk}} = \langle s_i \rangle_N$ at some site $a < i < b$ inside the chain. To obtain its probability distribution with respect to the random field probability space it is helpful to rewrite the partition function of the random field Ising chain with N spins to a partition function with one remaining spin s_i in two effective fields. The reformulation is the same as in chapter 3, cf appendix B.3, except that the procedure is carried out from the right *and* the left boundary. It leads to

$$Z_N = \sum_{s_i=\pm 1} \exp \beta \Big(\big(x_i^{(N)} + A(y_{i-1}^{(N)}) \big) s_i + \sum_{j=a}^{i-1} B(y_j^{(N)}) + \sum_{j=i+1}^{b} B(x_j^{(N)}) \Big) \tag{4.1}$$

with the two effective fields

$$x_j^{(N)} = A(x_{j+1}^{(N)}) + h_j, \quad i \le j \le b, \quad x_{b+1}^{(N)} = 0 \tag{4.2}$$

$$y_j^{(N)} = A(y_{j-1}^{(N)}) + h_j, \quad a \le j < i, \quad y_{a-1}^{(N)} = 0 \tag{4.3}$$

from the right and the left of site i respectively. The local magnetization at i is thus given by [GR84, BZ87a, BZ88b]

$$m_{i,N}^{\mathrm{bulk}} = \langle s_i \rangle_N = \tanh \beta \big(x_i^{(N)} + A(y_{i-1}^{(N)}) \big) \tag{4.4}$$

and its measure is

$$\mu_{l,r}^{(m)} = (\tanh\beta)_{\#}(\mu_r^{(x)} * A_{\#}\mu_l^{(y)}) \tag{4.5}$$

where $l = i - a$ and $r = b - i + 1$. As the effective fields share the same Frobenius-Perron equation (3.7) and the invariant measure of this equation is unique, the measures $\mu^{(x)}$ of the right effective field in the thermodynamic limit $b \to \infty$ and $\mu^{(y)}$ of the left effective field in the thermodynamic limit $a \to -\infty$ are identical. Therefore, as will become clear below, the measure $\mu_{l,r}^{(m)}$ of the local magnetization in the bulk converges to

$$\mu^{(m)} = (\tanh\beta)_{\#}(\mu^{(x)} * A_{\#}\mu^{(x)}) \tag{4.6}$$

in the thermodynamic limit $a \to -\infty$, $b \to \infty$, i.e. the local magnetization $m_{i,N}^{\text{bulk}}$ converges in distribution to a random variable m^{bulk} with measure $\mu^{(m)}$, cf lemma 4.1 below. Note that $\mu^{(m)}$ is independent of the position i because of the uniqueness of the invariant measure of the Frobenius-Perron equation and the continuity of the convolution.

4.1 Convolution of multifractals

To transfer the knowledge of the multifractal properties of the invariant measure $\mu^{(x)}$ to the measure of the local magnetization $\mu^{(m)}$ it is necessary to understand how the multifractal properties of the convolution of two measures are related to the multifractal properties of the two convoluted measures. Such general relations exist and will be developed in this section. As the convolution of two measures consists of the two steps of forming the product measure and projecting it in a given way, this problem is related to the question of the multifractal dimensions of product measures [Ols96] and of projections of multifractal measures [FO99]. But whereas [FO99] considered typical projections the projection leading to the convolution is one special choice which need not have the same properties as the typical ones.

For simplicity the results are all formulated for measures on $\mathbb{R}$ rather than $\mathbb{R}^n$ but most results are easily extendable to the more general case.

Throughout the section $(\mu_n)_{n\in\mathbb{N}}$ and $(\nu_n)_{n\in\mathbb{N}}$ denote sequences of bounded Borel measures on $\mathbb{R}$ which converge to bounded Borel measures μ and ν with respect to the Hutchinson metric d_{Hutch} [Hut81]. As explained above the main interest are the properties of the convolution of bounded Borel measures. The convolution of two bounded Borel measures μ and ν is always well-defined [Bau90] and will in the following be denoted by $\mu * \nu$. As a first step one can show that the convolution is continuous with respect to d_{Hutch}.

Lemma 4.1 Continuity of the convolution *Let $(m_i)_{i\in\mathbb{N}}$ and $(n_i)_{i\in\mathbb{N}}$ be two monotonically increasing and unbounded sequences of natural numbers. Then*

$(\mu_{m_i} * \nu_{n_i})_{i\in\mathbb{N}}$ *converges to a bounded Borel measure in Hutchinson topology and the limit is* $d_{\text{Hutch}}\text{-}\lim_{i\to\infty} \mu_{m_i} * \nu_{n_i} = \mu * \nu$.

Proof. Let $\varepsilon > 0$. The convergence of $(\mu_n)_{n\in\mathbb{N}}$ and $(\nu_n)_{n\in\mathbb{N}}$ implies the existence of numbers $M, N \in \mathbb{N}$ such that for all $i \geq M$ $d_{\text{Hutch}}(\mu_{m_i}, \mu) \leq \varepsilon$ and for all $i \geq N$ $d_{\text{Hutch}}(\nu_{n_i}, \nu) \leq \varepsilon$. Let $\tilde{N} := \max(M, N)$. Then for all $i \geq \tilde{N}$

$$\begin{aligned} &d_{\text{Hutch}}(\mu_{m_i} * \nu_{n_i}, \mu * \nu) \\ &= \sup\left\{ \int f(z)\, \mu_{m_i} * \nu_{n_i}(dz) - \int f(z)\, \mu * \nu(dz) \;:\; \text{Lip}(f) \leq 1 \right\}. \end{aligned} \tag{4.7}$$

The definition of the convolution of two measures implies $\int f(z)\, \mu_{m_i} * \nu_{n_i}(dz) = \iint f(x+y)\, \mu_{m_i}(dx)\, \nu_{n_i}(dy)$ and $\int f(z)\, \mu * \nu(dz) = \iint f(x+y)\, \mu(dx)\, \nu(dy)$. Inserting $0 = -\iint f(x+y)\, \mu(dx)\, \nu_{n_i}(dy) + \iint f(x+y)\, \nu_{n_i}(dy)\, \mu(dx)$ yields

$$\begin{aligned} &d_{\text{Hutch}}(\mu_{m_i} * \nu_{n_i}, \mu * \nu) \\ &= \sup\Big\{ \int \Big(\int f(x+y)\, \mu_{m_i}(dx) - \int f(x+y)\, \mu(dx) \Big)\, \nu_{n_i}(dy) \\ &\qquad + \int \Big(\int f(x+y)\, \nu_{n_i}(dy) - \int f(x+y)\, \nu(dy) \Big)\, \mu(dx) \;\Big|\; \text{Lip}(f) \leq 1 \Big\} \qquad (4.8) \\ &\leq \int \sup\Big\{ \int f(x+y)\, \mu_{m_i}(dx) - \int f(x+y)\, \mu(dx) \;\Big|\; \text{Lip}(f) \leq 1 \Big\}\, \nu_{n_i}(dy) \qquad (4.9) \\ &\quad + \int \sup\Big\{ \int f(x+y)\, \nu_{n_i}(dy) - \int f(x+y)\, \nu(dy) \;\Big|\; \text{Lip}(f) \leq 1 \Big\}\, \mu(dx)\,. \end{aligned}$$

Furthermore, as the condition $\text{Lip}(f) \leq 1$ is translationally invariant,

$$\begin{aligned} &\sup\Big\{ \int f(x+y)\, \mu_{m_i}(dx) - \int f(x+y)\, \mu(dx) \;\Big|\; \text{Lip}(f) \leq 1 \Big\} \\ &= \sup\Big\{ \int f(x)\, \mu_{m_i}(dx) - \int f(x)\, \mu(dx) \;\Big|\; \text{Lip}(f) \leq 1 \Big\} \qquad (4.10) \\ &= d_{\text{Hutch}}(\mu_{m_i}, \mu) \leq \varepsilon. \qquad (4.11) \end{aligned}$$

In the same way

$$\begin{aligned} &\sup\Big\{ \int f(x+y) \nu_{n_i}(dy) - \int f(x+y) \nu(dy) \;:\; \text{Lip}(f) \leq 1 \Big\} \\ &= d_{\text{Hutch}}(\nu_{n_i}, \nu) \leq \varepsilon. \end{aligned} \tag{4.12}$$

This finally yields

$$\begin{aligned} d_{\text{Hutch}}(\mu_{m_i} * \nu_{n_i}, \mu * \nu) &\leq \int \varepsilon\, \nu_{n_i}(dy) + \int \varepsilon\, \mu(dx) \qquad (4.13) \\ &= (\|\nu_{n_i}\| + \|\mu\|)\, \varepsilon \qquad (4.14) \end{aligned}$$

where $\|\nu_{n_i}\| = \nu_{n_i}(\mathbb{R})$ and $\|\mu\| = \mu(\mathbb{R})$ denote the total mass of ν_{n_i} and μ respectively. □

As the metric d_{Hutch} topology and the weak topology coincide on bounded Borel measures with compact support [Hut81] there is an immediate consequence.

Corollary 4.2 *If* supp μ *and* supp ν *are compact,* $\text{w-}\lim_{i\to\infty} \mu_{m_i} * \nu_{n_i} = \mu * \nu$. *Furthermore* supp $\mu * \nu$ *is also compact.*

For the situation of the two-sided random field Ising chain considered here lemma 4.1 implies that the thermodynamic limit $l, r \to \infty$ can be carried out in an arbitrary way and that the result is the same as when first taking the thermodynamic limit of the effective fields and then calculating the measure of the local magnetization. Having detailed knowledge of the properties of the D_q-spectrum and the pointwise dimensions of the invariant measure of the effective field it is now interesting to investigate the relationship of the D_q-spectra and pointwise dimensions of measures μ and ν to the D_q-spectrum and pointwise dimensions of their convolution $\mu * \nu$. It turns out that one can transfer a considerable part of the knowledge about the multifractal properties of the invariant measure of the effective field gathered in chapter 3 to the measure of the local magnetization.

In the following only measures with bounded, i. e. compact, support are discussed. Let $x_- := \min \operatorname{supp} \mu > -\infty$ denote the left and $x_+ := \max \operatorname{supp} \mu < \infty$ the right boundary of supp μ. The boundaries of supp ν are denoted by y_- and y_+. The pointwise dimension at the boundary of the support of $\mu * \nu$ can be obtained from the pointwise dimensions at x_+, x_-, y_+ and y_-.

Lemma 4.3 Pointwise dimension of $\boldsymbol{\mu * \nu}$ at the boundary *Let μ, ν be Borel measures on $\mathbb{R}$ with compact support and such that the pointwise dimensions $D_p(x_\pm; \mu)$ and $D_p(y_\pm; \nu)$ at the boundaries of the support of μ and ν exist. Then, the boundaries of $\mu * \nu$ are $z_\pm = x_\pm + y_\pm$, the pointwise dimension at $z_\pm$ exists and is given by*

$$D_p(z_\pm; \mu * \nu) = D_p(x_\pm; \mu) + D_p(y_\pm; \nu)\,. \tag{4.15}$$

Proof. The pointwise dimension of $\mu * \nu$ at z_- is defined by

$$D_p(z_-; \mu * \nu) = \lim_{\varepsilon \to 0} \frac{\log(\mu * \nu(B_\varepsilon(z_-)))}{\log \varepsilon} \tag{4.16}$$

where $\mu * \nu(B_\varepsilon(z_-))$ is given by

$$\mu * \nu(B_\varepsilon(z_-)) = \iint \mathbf{1}_{B_\varepsilon(z_-)}(x+y)\, \mu(dx)\, \nu(dy). \tag{4.17}$$

The symbol $\mathbf{1}_X$ denotes the characteristic function of a set X, i. e. $\mathbf{1}_X(x) = 1$ if $x \in X$ and $= 0$ otherwise. The area in which $\mathbf{1}_{B_\varepsilon(z_-)}(x+y)$ is non-zero is the diagonal strip in figure 4.1. Neglecting the regions in which either $\mu = 0$ or $\nu = 0$ (or both), the relevant region is the dark gray triangle. As μ and ν are positive measures, integration over the small square gives a lower and integration over the larger square an upper bound

$$\int_{y_-}^{y_-+\frac{\varepsilon}{2}} \nu(dy) \int_{x_-}^{x_-+\frac{\varepsilon}{2}} \mu(dx) \le \mu * \nu(B_\varepsilon(z_-)) \;\le\; \int_{y_-}^{y_-+\varepsilon} \nu(dy) \int_{x_-}^{x_-+\varepsilon} \mu(dx). \tag{4.18}$$

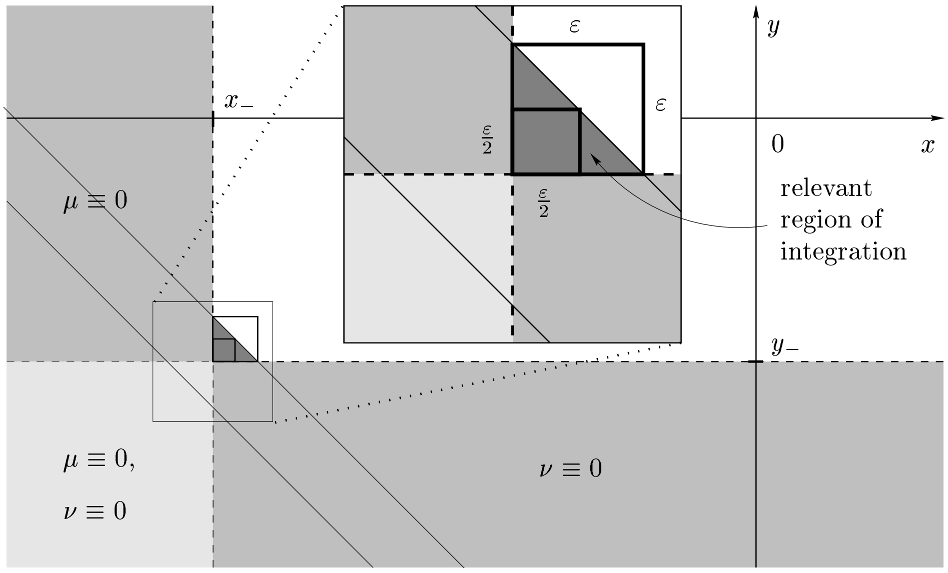

Figure 4.1 Illustration of the proof of lemma 4.3. The diagonal strip is the region in which $\mathbf{1}_{B_\varepsilon(z_-)}(x+y)$ is non-zero. Therefore, the dark grey triangle is the relevant region with non-zero contributions to the integral (4.17). As μ and ν are positive measures, integration over the small square of side length $\frac{\varepsilon}{2}$ provides a lower and integration over the larger square of side length ε an upper bound on the integral.

Taking into account that $\mu = 0$ on $(x_- - \varepsilon, x_-)$ and $\nu = 0$ on $(y_- - \varepsilon, y_-)$ one can write

$$\nu(B_{\frac{\varepsilon}{2}}(y_-))\mu(B_{\frac{\varepsilon}{2}}(x_-)) \leq \mu * \nu(B_\varepsilon(z_-)) \leq \nu(B_\varepsilon(y_-))\mu(B_\varepsilon(x_-)) \tag{4.19}$$

to finally obtain

$$\begin{aligned} \frac{\log \nu(B_{\frac{\varepsilon}{2}}(y_-)) + \log \mu(B_{\frac{\varepsilon}{2}}(x_-))}{\log \frac{\varepsilon}{2} + \log 2} &\geq \frac{\log \mu * \nu(B_\varepsilon(z_-))}{\log \varepsilon} \\ &\geq \frac{\log \nu(B_\varepsilon(y_-)) + \log \mu(B_\varepsilon(x_-))}{\log \varepsilon} \end{aligned} \tag{4.20}$$

which completes the proof as both sides of the inequality converge to $D_p(x_-;\mu) + D_p(y_-;\nu)$ as $\varepsilon \to 0$. The proof for the right boundaries is obtained by applying the same arguments to $\tilde{\mu}(X) := \mu(-X)$ and $\tilde{\nu}(X) := \nu(-X)$. □

As the proof also works with lim inf and lim sup instead of lim the lemma applies to $\overline{D}_p$ and $\underline{D}_p$ seperately if D_p does not exist.

To apply lemma 4.3 to the measure of the local magnetization in the one-dimensional random field Ising model it is important to know how the mappings $A_\#$ and $(\tanh \beta)_\#$ in (4.6) affect the pointwise dimensions of $\mu^{(m)}$. As $A(\cdot)$ and $\tanh \beta(\cdot)$ are bi-Lipschitz on any finite interval lemma 2.6 and lemma 4.3

directly imply $D_p(m_-;\mu^{(m)}) = D_p(m_-;(\tanh\beta)_\#(\mu^{(x)} * A_\#\mu^{(x)})) = D_p(x_-;\mu^{(x)}) + D_p(A(x_-);A_\#\mu^{(x)}) = 2D_p(x_-;\mu^{(x)})$. Thus, the mappings $A_\#$ and $(\tanh\beta)_\#$ in (4.6) do not play a decisive role. In section 3.5 lower (upper) bounds on D_q for $q<0$ ($q>0$) based on the pointwise dimension at arbitrary points in the support of the measure were developed, cf lemma 3.6. These bounds can now directly be applied to the D_q-spectrum of $\mu^{(m)}$ which by use of (3.18) results in

$$D_q(\mu^{(m)}) \geq \frac{q}{q-1} 2D_p(x_-;\mu^{(x)}) = \frac{q}{1-q}\frac{2\log 2}{\log A'(x_-)} \quad (q<1). \tag{4.21}$$

the resulting bounds are shown in figure 4.9 on page 67. They are tight bounds as long as the pointwise dimension at the boundary is large. This is the case as long as $D_p(m_-) > 1$. The critical value $h_c^{(m,3)}$ determined by this condition is

$$\frac{1}{2\beta}\log\left(\frac{R+e^{2\beta J}}{R^{-1}+e^{2\beta J}}\right) \quad \text{with} \tag{4.22}$$

$$R = 3\sinh(2\beta J) - e^{-2\beta J} + \sqrt{\left(3\sinh(2\beta J) - e^{-2\beta J}\right)^2 - 1}. \tag{4.23}$$

The critical value can also be interpreted in terms of the measure density. At this value of h the approximating measure densities $p_{l,r}^{(m)}(m_-)$ at the boundary of the support of the measure of the local magnetization switch from converging to 0 (for $h < h_c^{(m,3)}$) to diverging (for $h > h_c^{(m,3)}$) in the limit $l, r \to \infty$.

For $q>0$ the bound is not of interest for small h as the smoothness of $p^{(x)}$ in the region of small h implies existence and smoothness of $p^{(m)}$ in this region and thus $D_q = 1$ for all $q > 0$. The same applies to the connectedness of the support implying $D_0 = 1$.

The transition of the invariant measure of the effective field where the slope of the approximating measure densities at the boundary of the support switches from converging to 0 to diverging for $n \to \infty$, cf section 3.2, also has an analogue. This effect occurs for the approximating measure densities of the local magnetization at $D_p(m_-) = 2$ corresponding to

$$h_c^{(m,4)} = \frac{1}{\beta}\operatorname{arsinh}\left(2^{-\frac{3}{2}}(1-9e^{-4\beta J})^{\frac{1}{2}}\right) = h_c^{(3)}. \tag{4.24}$$

Note that this transition in the slope of the approximating measure densities of the local magnetization occurs at the same critical value at which the approximating measure densities of the effective field undergo the transition from converging to 0 to diverging at the boundary of the support, cf section 3.2.

For $q>0$ inequality (3.58) of lemma 3.6 applied to $\mu^{(m)}$ results in

$$D_q(\mu^{(m)}) \leq \frac{q}{q-1} D_p(m_\pm;\mu^{(m)}) = \frac{q}{1-q}\frac{2\log 2}{\log A'(x_-^*)} \tag{4.25}$$

in full analogy to the lower bounds (4.21) for $q < 0$. The resulting upper bounds are shown in figure 4.9 on page 67.

Apart from the relation between the pointwise dimensions of the convolution at its boundaries and the pointwise dimension at the boundaries of the convoluted measures discussed so far there also exists a general relation between the D_q-spectra.

Theorem 4.4 Upper bound on $D_q(\mu * \nu)$ *The D_q-spectrum of the convolution is bounded from above by the sum of the D_q-spectra of the convoluted measures,*

$$D_q(\mu * \nu) \leq D_q(\mu) + D_q(\nu) \tag{4.26}$$

provided $D_q(\mu)$ and $D_q(\nu)$ exist.

Proof. It is necessary to distinguish three cases, $q > 1$, $0 < q < 1$ and $q < 0$. For the first two cases the improved multifractal formalism with enlarged boxes coincides with the usual one and for simplicity the latter will be used in these cases. Let $\varepsilon > 0$ and denote $x_i := \frac{\varepsilon}{2} i$, $i \in \mathbb{Z}$.
Let $q > 1$. For any $i \in \mathbb{Z}$

$$(\mu * \nu)_i := \mu * \nu(B_{\frac{\varepsilon}{2}}(x_{2i})) = \int\!\!\int \mathbf{1}_{B_{\frac{\varepsilon}{2}}(x_{2i})}(x+y)\, \mu(dx)\, \nu(dy) \tag{4.27}$$

is the integral over the diagonal strip in the (x, y) plane shown in figure 4.2a. Integration over the dark gray squares provides a lower bound on this integral,

$$(\mu * \nu)_i \geq \sum_j \mu(B_{\frac{\varepsilon}{4}}(x_{2i+j}))\, \nu(B_{\frac{\varepsilon}{4}}(x_{2i-j})). \tag{4.28}$$

Taking the qth power of both sides and using $(\sum_i x_i)^q \geq \sum_i x_i^q$ for $q > 1$ and any positive numbers x_i yields

$$(\mu * \nu)_i^q \geq \sum_j \mu(B_{\frac{\varepsilon}{4}}(x_{2i+j}))^q\, \nu(B_{\frac{\varepsilon}{4}}(x_{2i-j}))^q. \tag{4.29}$$

For $(\mu * \nu)_i'^q := \mu * \nu(B_{\frac{\varepsilon}{2}}(x_{2i+1}))^q$ one has in the same way

$$(\mu * \nu)_i'^q \geq \sum_j \mu(B_{\frac{\varepsilon}{4}}(x_{2i+j+1}))^q\, \nu(B_{\frac{\varepsilon}{4}}(x_{2i-j}))^q. \tag{4.30}$$

Denote $\mu_i := \mu(B_{\frac{\varepsilon}{4}}(x_i))$ and $\nu_j := \nu(B_{\frac{\varepsilon}{4}}(x_j))$. When summing (4.29) and (4.30) and over all i the right hand side is $\sum_i \sum_j \mu_i^q\, \nu_j^q$. It is straightforward to show that $\sum_i (\mu * \nu)_i'^q \leq 2^{q+1} \sum_i (\mu * \nu)_i^q$, cf appendix B.10, such that the left hand side of the sum of (4.29) and (4.30) summed over all i is less or equal $(2^{q+1}+1) \sum_i (\mu * \nu)_i^q$.

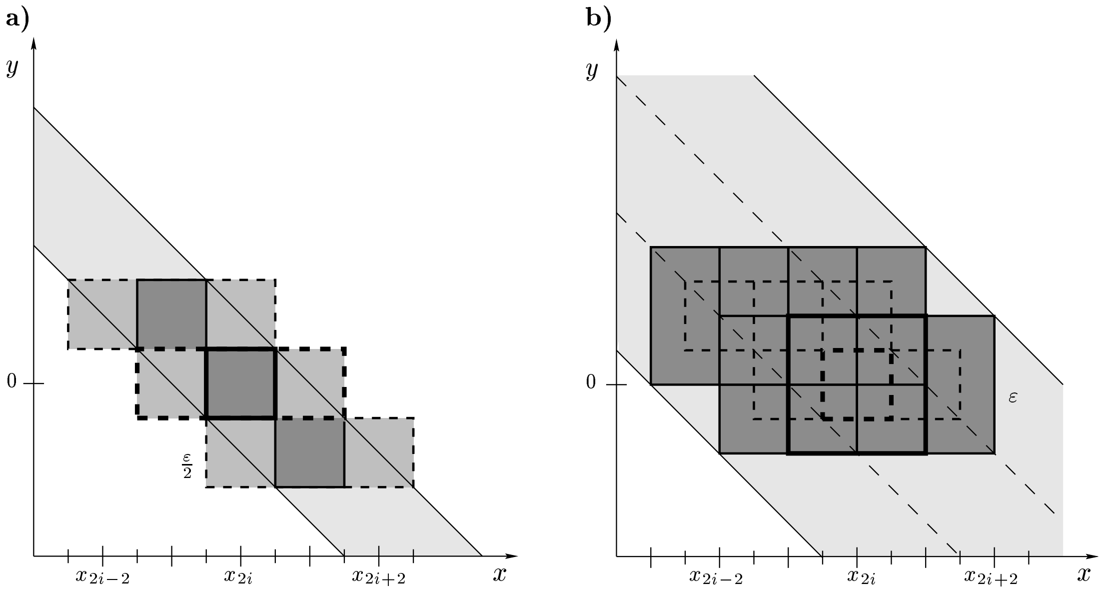

Figure 4.2 Illustration of the main ideas of the proof of theorem 4.4. Figure a) applies to $q > 0$ and figure b) to $q < 0$. The diagonal strip in a) represents the region of integration for $(\mu * \nu)_i$, the measure of one of the disjoint intervals of length ε covering supp $\mu * \nu$. The integral over the dark grey squares (and diagonally translated disjoint copies) provides a lower bound on $(\mu * \nu)_i$ used in the case $q > 1$. Considering additionally the integral over the dashed squares gives an upper bound on $(\mu * \nu)_i$ needed in the case $0 < q < 1$. The wide diagonal strip in b) is the region of integration for $(\mu * \nu)_i$, the measure of one of the (intersecting) enlarged intervals of length $3\,\varepsilon$ covering supp $\mu * \nu$. The narrow dashed strip is the region of integration for the corresponding inner interval of size ε. Integration over each of the six overlapping large squares of side length ε (solid lines) and their disjoint by $(-n\varepsilon, n\varepsilon)$ diagonally translated copies gives a lower bound on $(\mu * \nu)_i$ such that the sum of the six integrals gives a lower bound on $6(\mu * \nu)_i$. The narrow strip is contained in the union of all the interior small squares of side length $\frac{\varepsilon}{2}$ (dashed lines) assuring that the lower bound obtained is non-zero whenever the integral over the narrow strip is. This is an important point in the proof. The details are given in the text.

After taking the logarithm, dividing by $\log \varepsilon$ and multiplying with $1/(q-1)$ this results in

$$\frac{1}{q-1} \frac{\log \sum_i (\mu * \nu)_i^q + \log 2^{q+1}}{\log \varepsilon} \leq \frac{1}{q-1} \frac{\log \sum_i \mu_i^q + \log \sum_j \nu_j^q}{\log \frac{\varepsilon}{2} + \log 2} \tag{4.31}$$

which completes the proof for $q > 1$ as the left hand side converges to $D_q(\mu * \nu)$ and the right hand side to $D_q(\mu) + D_q(\nu)$ as $\varepsilon \to 0$.
Let $0 < q < 1$ and $i \in \mathbb{Z}$ and again denote $(\mu * \nu)_i := \mu * \nu(B_{\frac{\varepsilon}{2}}(x_{2i}))$, $\mu_i := \mu(B_{\frac{\varepsilon}{4}}(x_i))$ and $\nu_j := \nu(B_{\frac{\varepsilon}{4}}(x_j))$. The solid and dashed squares in figure 4.2a and by $(n\varepsilon, -n\varepsilon)$ diagonally translated disjoint copies cover the diagonal strip over

which one needs to integrate to obtain $(\mu * \nu)_i$. Therefore,

$$(\mu * \nu)_i \leq \sum_j \sum_{k=-1}^{1} \mu_{2i+j+k} \nu_{2i-j}. \tag{4.32}$$

Taking the q-th power and using $(\sum_i x_i)^q \leq \sum_i x_i^q$ for $q < 1$ and arbitrary positive numbers x_i yields

$$(\mu * \nu)_i^q \leq \sum_j \sum_{k=-1}^{1} \mu_{2i+j+k}^q \, \nu_{2i-j}^q. \tag{4.33}$$

When summing over all i each combination $\mu_i \nu_j$ appears at most twice in the sum on the right hand side such that

$$\sum_i (\mu * \nu)_i^q \leq 2 \sum_i \sum_j \mu_i^q \nu_j^q. \tag{4.34}$$

Taking the logarithm, dividing by $\log \varepsilon$ and multiplying with $1/(q-1)$ results in

$$\frac{1}{q-1} \frac{\log \sum_i (\mu * \nu)_i^q}{\log \varepsilon} \leq \frac{1}{q-1} \frac{\log \sum_i \mu_i^q + \log \sum_j \nu_j^q + \log 2}{\log \frac{\varepsilon}{2} + \log 2}. \tag{4.35}$$

The limit $\varepsilon \to 0$ then yields $D_q(\mu * \nu) \leq D_q(\mu) + D_q(\nu)$.
Let $q < 0$. In this case it is necessary to use the improved multifractal formalism with enlarged intervals. In the following the notation

$$(\mu * \nu)_i := \begin{cases} \mu(B_{\frac{3}{2}\varepsilon}(x_{2i})) & (\mu * \nu(B_{\frac{\varepsilon}{2}}(x_{2i})) > 0) \\ 0 & (\text{otherwise}) \end{cases} \tag{4.36}$$

will be used. By this choice the ε-intervals are enlarged by ε on both sides corresponding to $\delta = 2$, cf definition 2.2. Furthermore denote

$$\mu_i := \begin{cases} \mu(B_{\frac{\varepsilon}{2}}(x_i)) & (\mu(B_{\frac{\varepsilon}{4}}(x_i)) \geq 0) \\ 0 & (\text{otherwise}) \end{cases} \tag{4.37}$$

$$\nu_i := \begin{cases} \nu(B_{\frac{\varepsilon}{2}}(x_i)) & (\nu(B_{\frac{\varepsilon}{4}}(x_i)) \geq 0) \\ 0 & (\text{otherwise}) \end{cases} \tag{4.38}$$

i.e. the $\frac{\varepsilon}{2}$-intervals of μ and ν are enlarged by $\frac{\varepsilon}{4}$ corresponding to $\delta = 1$. This choice facilitates the proof and has no influence on the resulting D_q [Rie95]. Let $i \in \mathbb{Z}$ with $(\mu * \nu)_i > 0$, i.e. the integral over the i-th interior interval is non-zero. When calculating $(\mu * \nu)_i$ one has to integrate over the wide diagonal strip in figure 4.2b. The large squares $B_{\frac{\varepsilon}{2}}(x_{2i+2j}) \times B_{\frac{\varepsilon}{2}}(x_{2i-2j})$, $j \in \mathbb{Z}$, are disjoint and are all contained in the strip. Therefore,

$$(\mu * \nu)_i \geq \sum_j \mu_{2i+2j} \, \nu_{2i-2j}. \tag{4.39}$$

This applies analogously to the other shown five squares and their by $(n\varepsilon, -n\varepsilon)$ diagonally translated disjoint copies such that

$$6(\mu * \nu)_i \geq \sum_j \sum_{k=-1}^{1} \mu_{2i+j+k}\, \nu_{2i-j}. \tag{4.40}$$

The integral over the narrow diagonal strip determines that $(\mu*\nu)_i$ is greater than zero. In the same way the integral over the small squares determines whether the terms on the right hand side are greater than zero. As the narrow strip is contained in the union of the small squares, the right hand side *is* greater than zero because $(\mu * \nu)_i$ is by assumption. One therefore can take the q-th power on both sides and (omitting all terms being zero) use $(\sum_i x_i)^q \leq \sum_i x_i^q$ for $q < 1$ and arbitrary positive numbers x_i to obtain

$$6^q(\mu * \nu)_i^q \leq \sum_j \sum_{k=-1}^{1} \mu_{2i+j+k}^q\, \nu_{2i-j}^q. \tag{4.41}$$

When summing over all i with $(\mu * \nu)_i > 0$, each combination $\mu_i^q\, \nu_j^q$ appears at most twice. Furthermore, adding terms which do not already appear only enlarges the right hand side. Therefore,

$$6^q \sum_i (\mu * \nu)_i^q \leq 2 \sum_i \mu_i^q \sum_j \nu_j^q. \tag{4.42}$$

From this one immediately obtains

$$\frac{1}{q-1} \frac{\log \sum_i (\mu * \nu)_i^q + \log 6^q}{\log \varepsilon} \leq \frac{1}{q-1} \frac{\log \sum_i \mu_i^q + \log \sum_j \nu_j^q + \log 2}{\log \frac{\varepsilon}{2} + \log 2} \tag{4.43}$$

which implies $D_q(\mu * \nu) \leq D_q(\mu) + D_q(\nu)$ in the limit $\varepsilon \to 0$. □

Note that this proof easily generalizes to measures on $\mathbb{R}^n$. Furthermore, it also applies to $\underline{D}_q$ and $\overline{D}_q$ separately if D_q does not exist.

The invariance of the D_q-spectrum with respect to bi-Lipschitz maps, cf lemma 2.4, and theorem 4.4 immediately imply

$$\begin{aligned} D_q(\mu^{(m)}) &= D_q(\mu^{(x)} * A_\# \mu^{(x)}) \\ &\leq D_q(\mu^{(x)}) + D_q(A_\# \mu^{(x)}) = 2 D_q(\mu^{(x)}). \end{aligned} \tag{4.44}$$

As the D_q-spectrum of the invariant measure of the effective field is — at least on a numerical level — very well known this provides interesting insights for the D_q-spectrum of the measure of the local magnetization, cf figure 4.9 on page 67. Prior to the comprehensive discussion of the consequences of the results of this section on the D_q-spectrum of the measure of the local magnetization in section 4.3 the following section provides more insight into the relevant mechanisms in the convolution of multifractal measures.

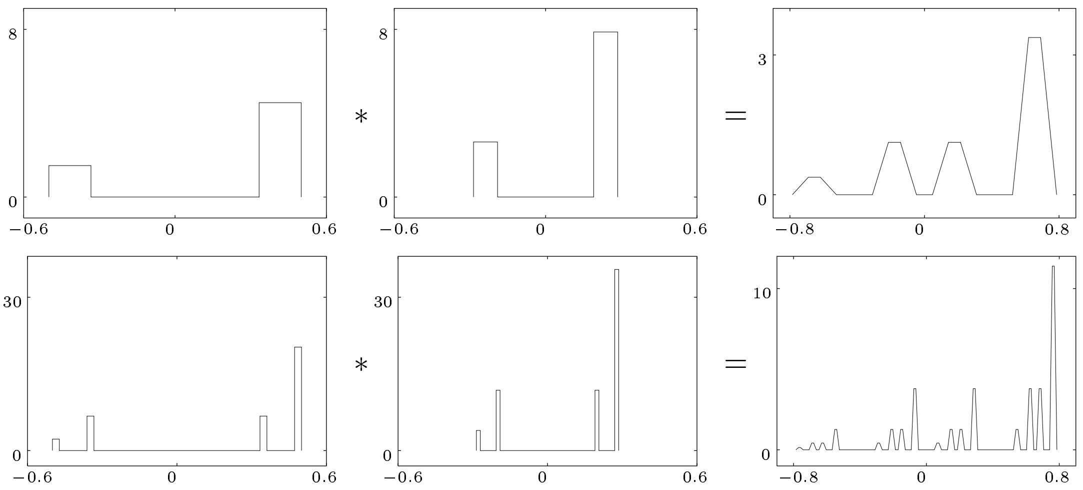

Figure 4.3 Illustration of the convolution of $\mu_{a,p}^{(1)}$ with $\lambda_{\#}\mu_{a,p}^{(1)}$ and $\mu_{a,p}^{(2)}$ with $\lambda_{\#}\mu_{a,p}^{(2)}$ for $a=\frac{1}{6}$, $p=\frac{3}{4}$ and $\lambda=\frac{4}{7}$. The condition for the disjointness of the trapezoids, $a/(1-2a)\le\lambda\le(1-2a)$ is clearly fulfilled for this choice of parameters such that in the limit $n\to\infty$ example 4.1 applies.

4.2 Convolution of Cantor sets with weights

In many examples in fractal and multifractal theory Cantor sets and measures on Cantor sets are the first examples accessible to rigorous analysis. For the convolution of multifractals this also turns out to be the case. It is possible to calculate the D_q-spectrum for Cantor sets with weights analytically in certain situations. In this section two examples are given which provide some insight into the mechanisms which are important in the convolution of multifractal measures.

Let $\mathcal{C}_a^{(0)}=[-\frac{1}{2},\frac{1}{2}]$ and $\mathcal{C}_a^{(n)}$ be defined inductively by $\mathcal{C}_a^{(n)}:=f_{a+}(\mathcal{C}_a^{(n-1)})\cup f_{a-}(\mathcal{C}_a^{(n-1)})$ with $f_{a+}(x)=ax+\frac{1-a}{2}$ and $f_{a-}=ax-\frac{1-a}{2}$. The infinite intersection $\mathcal{C}_a:=\bigcap_{n=0}^{\infty}\mathcal{C}_a^{(n)}$ is the a-Cantor set. On the approximating sets $\mathcal{C}_a^{(n)}$ define the probability densities

$$p_{a,p}^{(n)}(x)=\frac{p}{a}p_{a,p}^{(n-1)}(f_{a+}^{-1}(x))+\frac{1-p}{a}p_{a,p}^{(n-1)}(f_{a-}^{-1}(x)). \tag{4.45}$$

The corresponding measures are denoted by $\mu_{a,p}^{(n)}(X)=\int_X p_{a,p}^{(n)}\,dx$ for any Borel set $X\subset\mathbb{R}$. The measures $\mu_{a,p}^{(n)}$ converge to a limit measure $\mu_{a,p}$ which is often referred to as an a-Cantor set with weights p and $1-p$. For a generic choice of a and p the measure $\mu_{a,p}$ is a multifractal. For an illustration cf figure 4.3 and 4.4. In the following two examples the D_q-spectrum of the convolution of $\mu_{a,p}$ with $\lambda_{\#}\mu_{a,p}$, a 'compressed' version of it, is calculated ($\lambda\le 1$). In full generality this is a hard problem. The examples give the solution for certain parameter combinations of a and λ.

Example 4.1 Let $0 < p < 1$ and $a/(1-2a) \leq \lambda \leq (1-2a)$. This is meaningful for $a \leq \frac{1}{4}$. Then, the two intervals of supp $\mu_{a,p}^{(1)}$ fit into the gap of supp $\lambda_{\#}\mu_{a,p}^{(1)}$ and on the other hand the complete supp $\lambda_{\#}\mu_{a,p}^{(1)}$ fits into the gap of supp $\mu_{a,p}^{(1)}$. Self-similarity of $\mathcal{C}_a$ and $\lambda_{\#}\mathcal{C}_a$ implies that for any given n and $y \in \mathbb{R}$ at most one pair of bars in $p_{a,p}^{(n)}(x)$ and $\lambda_{\#}p_{a,p}^{(n)}(y-x)$ can overlap in the process of the convolution. The convolution is therefore a collection of trapezoids as shown in figure 4.3. Denoting the intervals of supp $\mu_{a,p}^{(n)} * \lambda_{\#}\mu_{a,p}^{(n)}$ (the bases of the trapezoids) by $T_j^{(n)}$, $j = 1, \ldots, 2^n$, only the structure of the measure within the trapezoids but not their total measure changes, i.e. $\mu_{a,p} * \lambda_{\#}\mu_{a,p}(T_j^{(n)}) = \mu_{a,p}^{(n)} * \lambda_{\#}\mu_{a,p}^{(n)}(T_j^{(n)})$. Therefore, $\mu_{a,p} * \lambda_{\#}\mu_{a,p}$ and $\mu_{a,p}^{(n)} * \lambda_{\#}\mu_{a,p}^{(n)}$ can be used interchangeably on the set of intervals $T_j^{(n)}$. This fortunate circumstance is due to the fact that the self-similarity of the Cantor sets induces a direct iteration for the convolution rendering it self-similar itself. The analytical treatment of the D_q-spectrum in this example is essentially based on this fact. If choosing $\varepsilon_n := a^n + \lambda a^n$, which is the width of the trapezoids at level n, boxes $B_{\frac{3}{2}\varepsilon_n}(x_i)$, $x_i = i\varepsilon_n$, $i \in \mathbb{Z}$ with $\mu_{a,p}(B_{\frac{\varepsilon_n}{2}}(x_i)) > 0$ contain at least one whole trapezoid of level n and intersect at most four. Thus, denoting

$$\mu_i := \begin{cases} \mu_{a,p} * \lambda_{\#}\mu_{a,p}(B_{\frac{3}{2}\varepsilon_n}(x_i)) & (\mu_{a,p} * \lambda_{\#}\mu_{a,p}(B_{\frac{\varepsilon_n}{2}}(x_i)) > 0) \\ 0 & (\text{otherwise}) \end{cases} \tag{4.46}$$

one obtains for $q > 0$, $q \neq 1$

$$\mu_{a,p} * \lambda_{\#}\mu_{a,p}\big(T_{j(i)}^{(n)}\big)^q \leq \mu_i^q \leq \big(4 \max_{j \in J(i)} \mu_{a,p} * \lambda_{\#}\mu_{a,p}(T_j^{(n)})\big)^q \tag{4.47}$$

where $j(i)$ is the index of a trapezoid completely contained in $B_{\frac{3}{2}\varepsilon_n}(x_i)$ and $J(i)$ is the set of the indices of all trapezoids intersecting $B_{\frac{3}{2}\varepsilon_n}(x_i)$. As any trapezoid can appear at most four times on the right hand side when summing over i and any trapezoid appears at least once on the left hand side this implies

$$\sum_j \mu_{a,p} * \lambda_{\#}\mu_{a,p}\big(T_j^{(n)}\big)^q \leq \sum_i \mu_i^q \leq 4\sum_j \big(4\mu_{a,p} * \lambda_{\#}\mu_{a,p}(T_j^{(n)})\big)^q. \tag{4.48}$$

The measures of the trapezoids can explicitly be calculated such that

$$\sum_j \mu_{a,p} * \lambda_{\#}\mu_{a,p}(T_j^{(n)})^q = \sum_{k,l=0}^{n} \binom{n}{k}\binom{n}{l}\big(p^k(1-p)^{n-k}p^l(1-p)^{n-l}\big)^q. \tag{4.49}$$

Applying $\sum_k \binom{n}{k}(p^q)^k((1-p)^q)^{n-k} = (p^q + (1-p)^q)^n$ then results in

$$((p^q + (1-p)^q)^{2n} \leq \sum_i \mu_i^q \leq 4^{q+1}((p^q + (1-p)^q)^{2n} \tag{4.50}$$

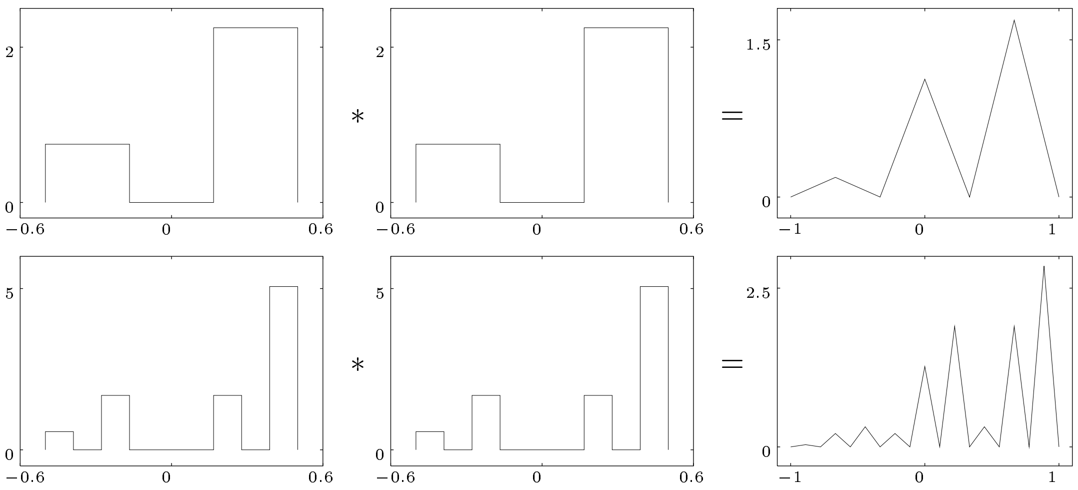

Figure 4.4 Illustration of the convolution of $\mu_{a,p}^{(1)}$ with itself and $\mu_{a,p}^{(2)}$ with itself for $a = \frac{1}{3}$ and $p = \frac{3}{4}$. For this choice of parameters example 4.2 applies in the limit $n \to \infty$.

and therefore

$$D_q(\mu_{a,p} * \lambda_{\#}\mu_{a,p}) = \frac{1}{q-1}\frac{2\log(p^q + (1-p)^q)}{\log a}. \tag{4.51}$$

For $q < 0$ the argument is the same with reversed inequality signs which leads to an identical result. For $q = 1$ the limit $q \to 1$ of (4.51) yields

$$\begin{aligned} D_1(\mu_{a,p} * \lambda_{\#}\mu_{a,p}) &= \lim_{q\to 1}\frac{1}{q-1}\frac{2\log(p^q + (1-p)^q)}{\log a} \\ &= 2(p\log p + (1-p)\log(1-p))/\log a. \end{aligned} \tag{4.52}$$

For any $\lambda \in [a^{k+1}/(1-2a), a^k(1-2a)]$, $k \in \mathbb{N}$, the arguments above apply to $\mu_{a,p}^{(n+k)} * \lambda_{\#}\mu_{a,p}^{(n)}$ which according to lemma 2.4 also converges to $\mu_{a,p} * \lambda_{\#}\mu_{a,p}$. Therefore, (4.51) and (4.52) apply to all λ taken from these intervals. For an example cf figure 4.5.

Example 4.2 Let $0 < p < 1$, $a \leq \frac{1}{3}$ and $\lambda = 1$. Then choose $\varepsilon_n := 2a^n$ and boxes of length ε_n in such a way that each box covers one of the spikes of $\mu_{a,p}^{(n)} * \mu_{a,p}^{(n)}$. This leads to an admissible sequence $\{\varepsilon_n\}_{n\in\mathbb{N}}$ and avoids any complications with $q < 0$ such that enlarged boxes are not necessary here. The situation is like shown in figure 4.4. For $n = 1$ one obtains $(\mu_{a,p}^{(1)} * \mu_{a,p}^{(1)})_i = (1-p)^2$, $2p(1-p)$ and p^2 for $i = 1$, 2 and 3 respectively. As in example 4.1 self-similarity implies for the specific choice of boxes made that $\mu_{a,p}^{(n)} * \mu_{a,p}^{(n)}$ and $\mu_{a,p} * \mu_{a,p}$ can be used interchangeably as they coincide on all boxes of level n. Furthermore, the result of the convolution of the next iteration, $n = 2$, can be constructed by replacing each triangle in figure 4.4 by the complete figure and choosing the corresponding weight. Therefore, the $(\mu_{a,p}^{(2)} * \mu_{a,p}^{(2)})_i$ are the nine terms of the sum

$$\begin{aligned}&\sum_{k=0}^{2}\sum_{l=0}^{n-k}\binom{2}{k}\binom{2-k}{l}(1-p)^{2k}(2p(1-p))^{2-k}p^{2(2-k-l)}\\&=\big((1-p)^2+2p(1-p)+p^2\big)^2 .\end{aligned} \tag{4.53}$$

This continues for larger n such that

$$\begin{aligned}\sum_i(\mu_{a,p}^{(n)} * \mu_{a,p}^{(n)})_i^q &= \sum_{k=0}^{n}\sum_{l=0}^{n-k}\binom{n}{k}\binom{n-k}{l}\big((1-p)^{2k}(2p(1-p))^{n-k}p^{2(n-k-l)}\big)^q\\&=\big((1-p)^{2q}+2^qp^q(1-p)^q+p^{2q}\big)^n.\end{aligned} \tag{4.54}$$

For $q \neq 1$ this yields

$$D_q(\mu_{a,p} * \lambda_{\#}\mu_{a,p}) = \frac{1}{q-1}\lim_{n\to\infty}\frac{n\log\big((1-p)^{2q}+2^qp^q(1-p)^q+p^{2q}\big)}{n\log a+\log 2} \tag{4.55}$$

$$= \frac{1}{q-1}\frac{\log\big((1-p)^{2q}+2^qp^q(1-p)^q+p^{2q}\big)}{\log a}. \tag{4.56}$$

The limit $q \to 1$ results in

$$\begin{aligned}D_1(\mu_{a,p} * \lambda_{\#}\mu_{a,p}) &= \lim_{q\to 1}\frac{1}{q-1}\frac{\log\big((1-p)^{2q}+2^qp^q(1-p)^q+p^{2q}\big)}{\log a}\\&= 2\big(p\log p+p(1-p)\log 2+(1-p)\log(1-p)\big)/\log a.\end{aligned} \tag{4.57}$$

As in example 4.1 the arguments can be repeated for the a^n-fold value of λ such that (4.56) and (4.57) are also correct for all $\lambda = a^n$, $n \in \mathbb{N}$. This means that the D_q-spectrum can be calculated at specific points between the intervals where it is given by (4.51) and (4.52). The results are illustrated in figure 4.5.

In the case of the random field Ising model one is interested in the dependence of the D_q-spectrum on the strength h of the random field which rather corresponds to varying a in the convolution of Cantor sets. Viewing (4.51) and (4.52) in this light it is possible to choose $\lambda = \frac{1}{2}$ such that for all $a < \frac{1}{4}$ example 4.1 applies. This results in the right part of the D_q-spectrum shown in figure 4.6. For the left part with a close to one the usual lower bounds for $q < 0$ based on the pointwise dimension at the boundary of the support apply. For $q \geq 1$ all D_q are 1 in this region because of the regularity of $\mu_{a,p}$.

The convolution of two-scale Cantor sets shows a far richer behaviour than the two examples above. It turns out that the lacking strict self-similarity does not allow the kind of analytical treatment used here. Numerical investigations show that the D_q-spectrum strongly depends on the two scales of the Cantor sets.

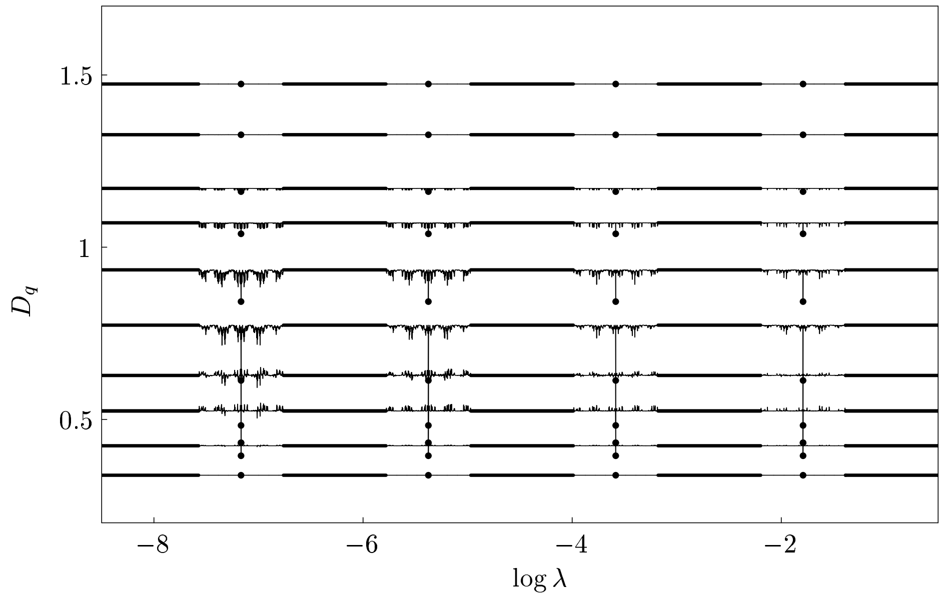

Figure 4.5 D_q spectrum of $\mu_{a,p} * \lambda_{\#}\mu_{a,p}$ as a function of $\log\lambda$ for $q = -20$, -6, -3, -2, -1, 0, 1, 2, 4 and 20. The thick lines are the exact D_q obtained in example 4.1 and the points the D_q obtained in example 4.2. The thin lines are numerical results obtained from iteration depths $l = r = 8$ compared to $l = r = 7$ in the new natural partition method of the convolution, cf appendix A.2.1.

Furthermore, in a large parameter regime the obtained numerical estimates are extremely sensitive to the iteration depth to which the Cantor sets are generated. The situation is of similar complexity as for the measure of the local magnetization in the one-dimensional random field Ising model discussed in the next section.

4.3 The D_q-spectrum of the local magnetization

4.3.1 The approximating measure densities

Before discussing the D_q-spectrum of the measure of the local magnetization one should first have a look at the approximating densities of this measure to get an impression of its general form and its dependence on the strength h of the random field. In figure 4.7 the measure densities of the effective field and of the local magnetization are shown in comparison for various values of h. The measure densities of the effective field were obtained on their new natural partition by the third method described in appendix A.1.1. The iteration depths were $n = 20$ for $h = 0.02$ and $n = 16$ for all other values. The measure densities of the local magnetization were obtained on the natural partition at $l = r = 8$ from the measure of the effective field at iteration depths $l = r = 8$ with the convolution algorithm described in appendix A.2.1. In figure 4.8 the same measure densities

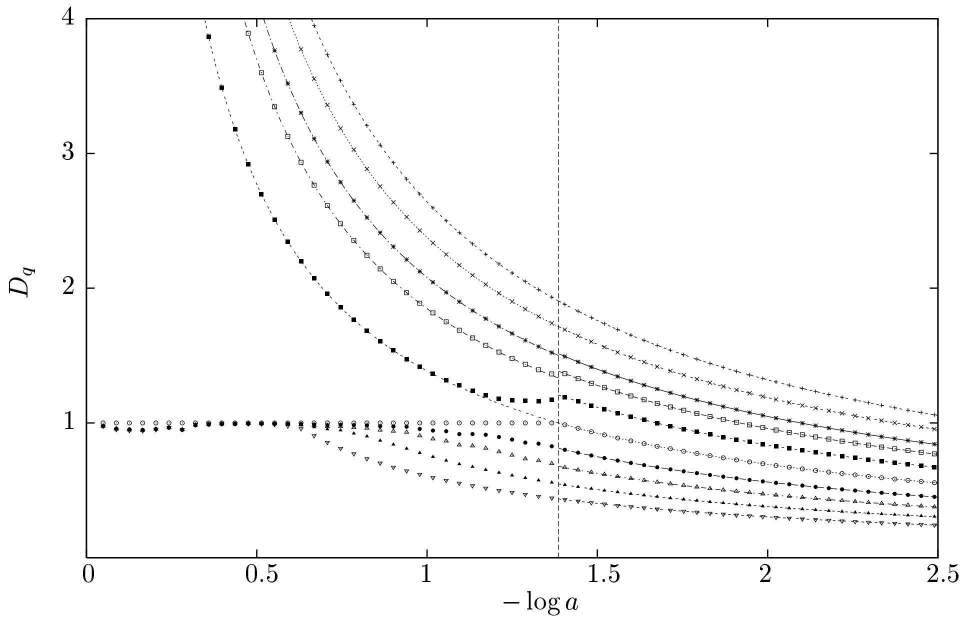

Figure 4.6 D_q-spectrum of $\mu_{a,p} * \lambda_\# \mu_{a,p}$ as a function of $-\log a$ with $p = \frac{3}{4}$, $\lambda = \frac{1}{2}$ and $q = -20, -6, -3, -2, -1, 0, 1, 2, 4$ and 20. The lines to the left of $-\log a = \log 4$ are the usual lower bounds based on the pointwise dimension at the left boundary of $\mathcal{C}_{a,p}$. The lines on the right are the calculated exact values of D_q according to (4.51) and (4.52). The points are numerical results for iteration depths $l = r = 6$ compared to $l = r = 5$ in the new natural partition method for the convolution, cf appendix A.2.1.

are shown in a logarithmic plot in order to reveal the structure of the measure of the local magnetization for large h.

As one can see, the measure of the local magnetization is much smoother than the measure of the effective field in agreement with the general belief. For $h = 0.02$ both measures are smooth and the slope at the boundary is zero. For $h = 0.2 > h_c^{(4)}$ the slope of $p_n^{(x)}$ already diverges whereas the slope of $p_{l,r}^{(m)}$ converges zero. For $h = 0.4 > h_c^{(3)} = h_c^{(m,4)}$ the density of the measure of the effective field diverges at the boundary whereas $p_{l,r}^{(m)}$ converges to zero but has diverging slope. For $h = 0.7 > h_c^{(m,3)}$ the density $p_{l,r}^{(m)}$ also diverges at the boundary. The fractality of the support is in the same way 'delayed' for $\mu^{(m)}$. For $h = 1.0 > h_c^{(1)}$ the support of $\mu^{(x)}$ is already fractal but the support of $\mu^{(m)}$ is still connected.

Overall, there is a gradual transition of the measure of the local magnetization from a strongly peaked monomodal distribution for small random field to an even more strongly peaked bimodal distribution for large random field. The local magnetization (which is a thermodynamic average but still a random variable with respect to the probability space of the random field) shows a transition from a paramagnetic situation where the most probable value is zero to a ferromagnetic

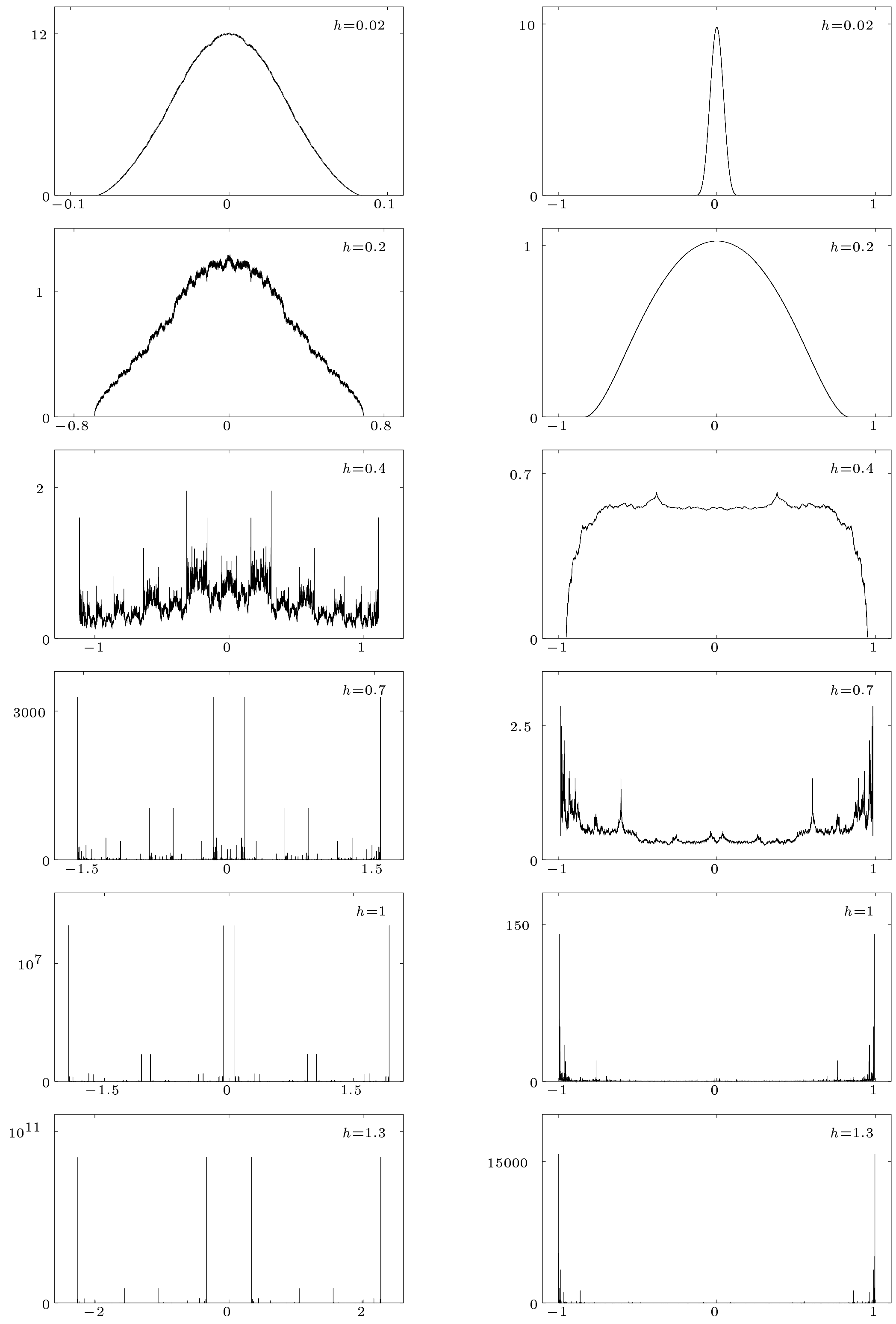

Figure 4.7 Measure densities of the effective field $p_n^{(x)}(x)$ versus x (left column) for $n = 20$ ($h = 0.02$) and $n = 16$ (otherwise) and of the local magnetization $p_{l,r}^{(m)}(m)$ versus m (right column) for $l = r = 8$. The details are explained in the text. ($\beta = J = 1$)

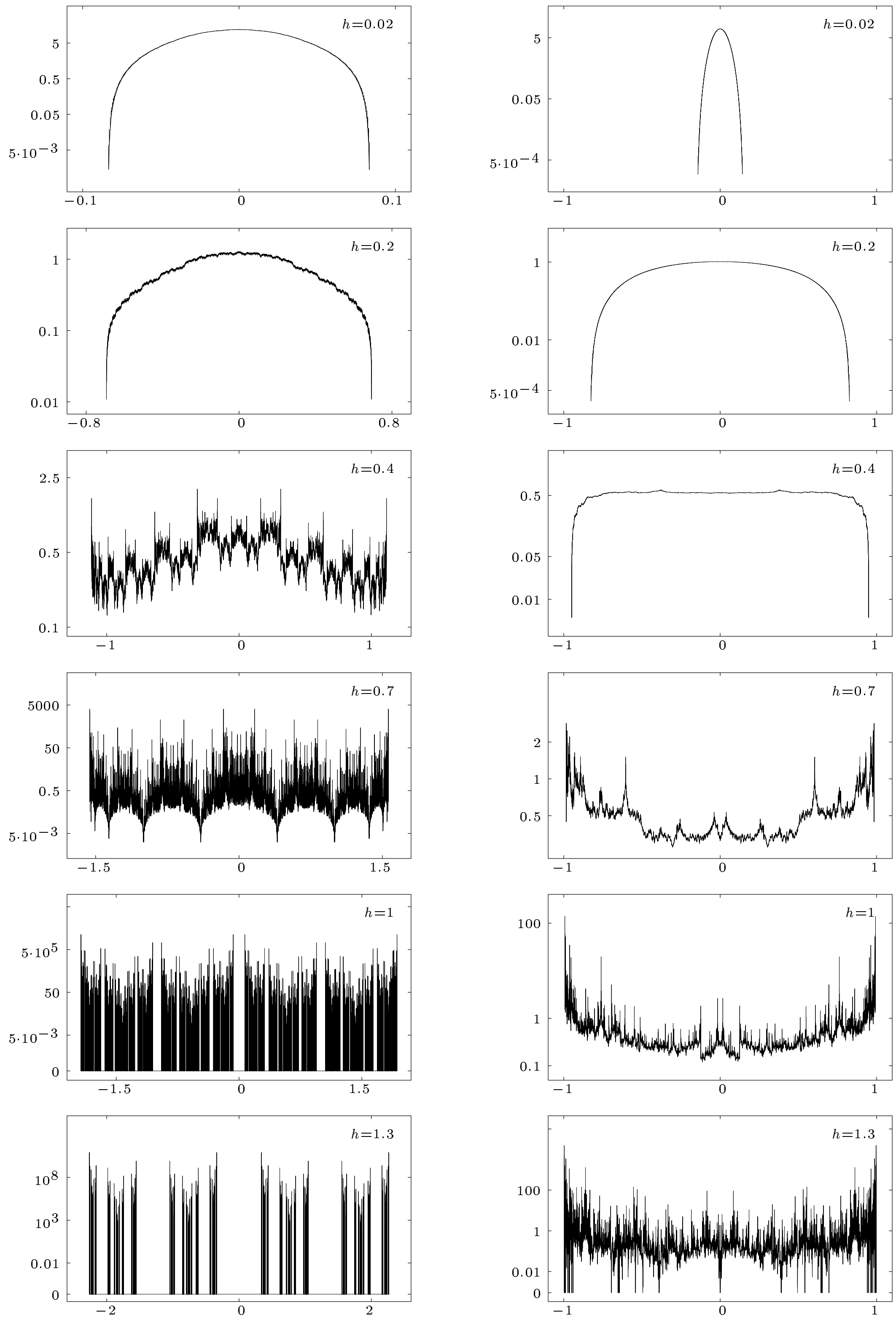

Figure 4.8 Measure densities $p_n^{(x)}(x)$ versus x (left column) and $p_{l,r}^{(m)}(m)$ versus m (right column) as in figure 4.7 but in a logarithmic plot. The details are explained in the text. $(\beta = J = 1)$

situation where the most probable value is ± 1. Between these extremal situations is the regime where multifractality is most obvious. The distribution always remains symmetric however such that this is not a phase transition. There is no symmetry breaking even if an infinitesimal homogeneous field is applied.

4.3.2 The D_q-spectrum

The D_q-spectrum of the measure of the local magnetization was numerically approximated by two methods. For rather small h and rather large h the method based on the new natural partition of the local magnetization, cf appendix A.2.3, yields excellent results. The alternative method is a box method based directly on definition 2.2, cf appendix A.2.2. The results of both methods are shown in figure 4.9. The points with error bars in region a) and b) are the results of the natural partition method obtained from comparing the partition functions (A.17) for all three combinations of $l = r \in \{9, 10\}$ and $l' = r' \in \{8, 9\}$ where $l \neq l'$. The calculation was carried out with C++ long doubles. The error bars are the standard deviation of the average of the 3 obtained values. In region c) the same calculation was performed for $l = r \in \{6, 7\}$ and $l' = r' \in \{5, 6\}$ using CLN high precision numbers with guaranteed 50 decimal digits. All points with a standard deviation greater than 0.05 were omitted in the figure as it must be assumed that these were not properly determined. The reason for this 'failure' of the natural partition method occurring for some values of h will be discussed in more detail below.

The variously dashed lines above $D_q = 1$ in regions b) and c) of figure 4.9 are results of the box method. The steps in h for these lines were chosen as $\Delta h = 0.005$ for $0.56 \leq h \leq 0.66$ and $\Delta h = 0.02$ everywhere else. The measure was generated with iteration depths $l = r = 12$ and the support was divided into at least 5 and at most 1500 boxes. As one can see the results are in reasonable agreement with the results of the method of the new natural partition in all regions where both results could be obtained. In region a) the box results are known to systematically underestimate D_q with $q < 0$ as they depend more or less exclusively on the two boxes at the boundary. The same applies to D_q with $q > 0$ in regions b) and c). Therefore, the box results are not shown for these values of q in these regions.

The dashed lines in region a) of figure 4.9 are lower bounds on D_q with $q < 0$ based on (4.21) for $q = -20$, -6, -3, -2, and -1. The upper bounds for $q > 0$ based on inequality (4.25) are shown as short dashed lines in regions b) and c) of figure 4.9 for $q = 4$ and $q = 20$. Finally, the dotted lines are the twofold D_q-spectra of $\mu^{(x)}$ which are upper bounds on $D_q(\mu^{(m)})$ according to theorem 4.4. As one can see immediately, all numerical results are in good agreement with the exact bounds.

In region b) all D_q for $q < 0$ are 1 close to $h = h_c^{(m,3)}$. At some $h > h_c^{(m,3)}$ they are again greater than 1. In this region the method based on the new natural

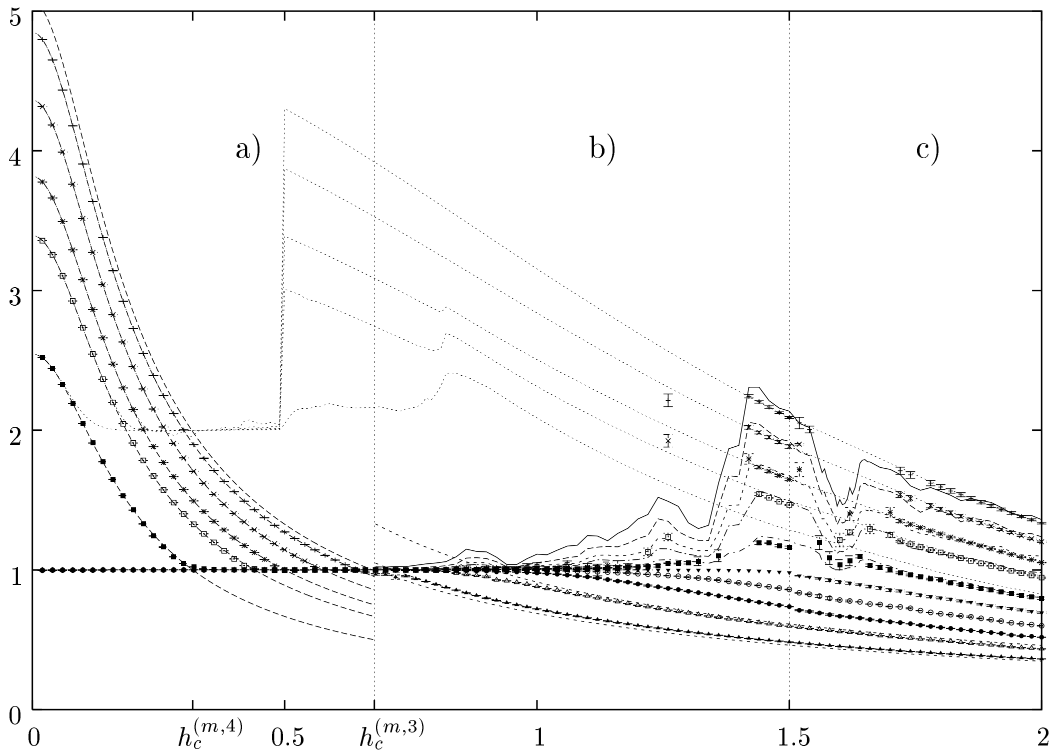

Figure 4.9 Numerical results for the D_q-spectrum of the measure of the local magnetization in the bulk. The results are shown for $q = -20, -6, -3, -2, -1, 0, 1, 2, 4$ and 20. All points with errorbars were obtained by the method based on the new natural partition. In regions a) and b) and $q \neq 0$ the results of all combinations of iteration depths $l = r \in \{9, 10\}$ and $l' = r' \in \{8, 9\}$ where $l \neq l'$ were used and the number representation was C++ long doubles. In region c) and also $q \neq 0$ all combinations of iteration depths $l = r \in \{6, 7\}$ and $l' = r' \in \{5, 6\}$ with $l \neq l'$ were used with numbers of the arbitrary precision library CLN with guaranteed 50 decimal digits. The errorbars are obtained from the standard deviations of the averages of the results of the three possible combinations of iteration depths. All points with standard deviation greater than 0.05 are not shown. For $q = 0$ iteration depths up to $l = r = 13$ were used. The long dashed lines in a) are lower bounds on D_q with $q < 0$ and the short dashed lines in b) and c) are upper bounds on D_q with $q > 1$ both based on the pointwise dimension at the boundary of the support of $\mu^{(m)}$. The dotted lines are the twofold numerical results for the D_q ($q < 0$) of the effective field, cf figure 3.2, and are upper bounds on the D_q with $q < 0$ according to theorem 4.4. Finally, the other lines in b) and c) are the results for D_q with $q < 0$ obtained by the box scaling approach, cf appendix A.2.2. The usual spacing in h for all data points is 0.02 except for the region between $h = 0.56$ and $h = 0.66$ where a spacing of $\Delta h = 0.005$ was used in the box method. ($\beta = J = 1$)

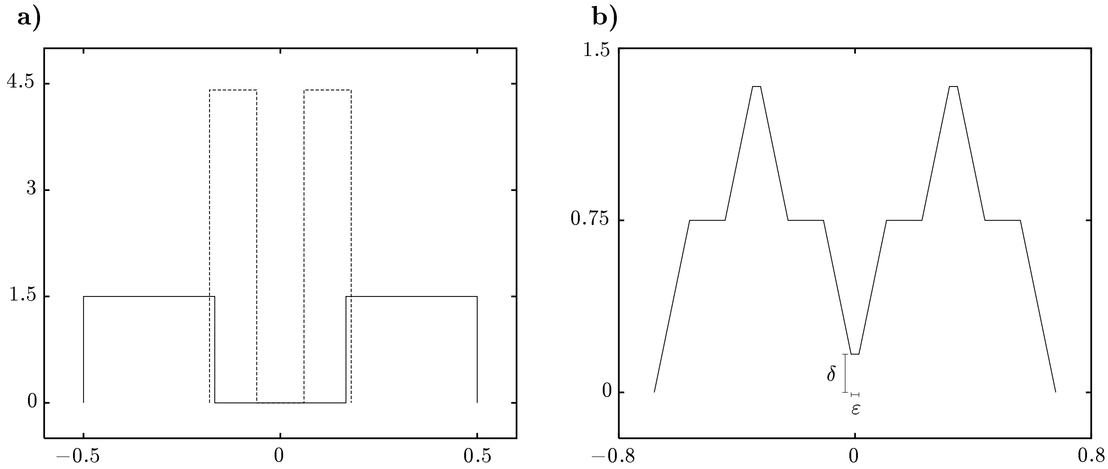

Figure 4.10 Example of the convolution of two Cantor sets with weights where arbitrarily small intervals appear in the new natural partition of the convolution. a) The two Cantor sets with weights which are convoluted. One is the usual mid-third Cantor set (solid lines) and the other is the mid-third Cantor set compressed with a factor $\lambda = 0.36$ (dashed lines). b) The resulting convolution. The interval at the origin has length $\varepsilon = \lambda - \frac{1}{3}$ and the measure density of the convolution is $\delta = \frac{9}{4\lambda}(\lambda - \frac{1}{3})$. Therefore, the measure of this interval is $\delta \cdot \varepsilon = \frac{(3\lambda-1)^2}{4\lambda}$ and thus can get arbitrarily small for λ close to $\frac{1}{3}$.

partition yields completely different results for different iteration depths. It is therefore not possible to deduce the asymptotic behaviour from the scaling in the accessible finite iteration depth. Most data points had to be left out for this reason. Provided h is large enough ($h \gtrsim 1.7$) the numerical results of the new natural partition method are again stable for all iteration depths considered which leads to small error bars in figure 4.9. For $q > 0$ there is perfect agreement with the upper bounds in regions b) and c) and no problems arise.

The difficulties in obtaining the asymptotic scaling for $q < 0$ in the region $1 \lesssim h \lesssim 1.7$ are of the same type as encountered in the convolution of two-scale Cantor sets. This shows that this is an effect of more than one relevant scale present (infinitely many in this case). As the asymptotic scaling seems not to be attainable in this region the physicists point of view is to ask what an experimentalist would observe. In any experiment the scale of resolution is bounded from below. This corresponds to the box method where the scale is bounded by the size of the smallest box whereas the scale in the new natural partition can get more or less arbitrarily small already for finite iteration depths, cf figure 4.10 for an example. Therefore, the estimates of D_q based on the box method are the physical results in this region.

The results of the box method are robust against changes in the iteration depth whereas they depend on an appropriate choice of box sizes. As a rule of thumb the smallest box size should be chosen of the order of the length of the longest band of the new natural partition.

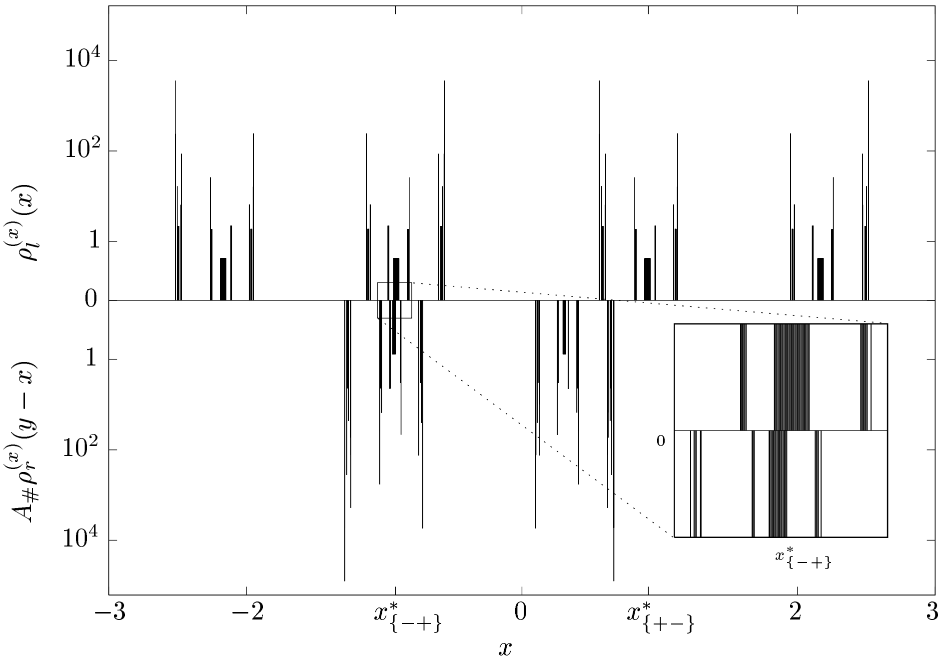

Figure 4.11 Illustration of the situation leading to the weakest band in the convolution of $\mu_l^{(x)}$ and $A_{\#}\mu_r^{(x)}$ at $h = 1.54$ and $l = r = 6$. The integration over the product of $\rho_l^{(x)}$ (the density of $\mu_l^{(x)}(x)$, upper part) and $A_{\#}\rho_r^{(x)}(y-x)$ (the density of $A_{\#}\mu_r^{(x)}$, lower part) yields the density of the convolution at y. In this figure $y = 0.309965$ which is the position of the weakest band. Only for the weak band around $x^*_{\{-+\}}$ the two densities are simultaneously non-zero (see inlay). This leads to a very small value for the density of the convolution at y. Note that even though the two convoluted measures are already rather sparse, the convolution still has non-fractal support at this h. ($\beta = J = 1$)

The local minimum of the D_q, $q < 0$ at $h \approx 1.6$ can be understood as a change in the overlap structure of the bands of the two convoluted measures for different h. For $h \approx 1.5$ there is a relative position for $\mu_l^{(x)}$ and $A_{\#}\mu_r^{(x)}$ for which only the two very weak bands around $x^*_{\{-+\}}$ and $A(x^*_{\{+-\}})$ overlap which leads to a very weak band in the convolution, cf figure 4.11 for an example. This results in the large values of D_q observed numerically. For $h \approx 1.6$ the band structure is such that no position of this type can be found in the iteration depths under consideration. For any relative position of $\mu_l^{(x)}$ and $A_{\#}(\mu_r^{(x)})$ more than one pair of bands or considerably stronger ones overlap. This results in the considerably smaller values of D_q. For larger h the formation of a very weak band in the convolution reappears and again large values of D_q with $q < 0$ are obtained. For other iteration depths the situation can again change as there is no strict self-similarity of the measure $\mu^{(m)}$.

From another point of view the values of D_q for negative q strongly depend on the random field strength h for given iteration depth due to the changes in the overlap structure described above. This mechanism is to be expected at any iteration depth such that there is a sensitive dependence of the D_q-spectrum with $q < 0$ on the random field strength h.

It is now clear that the convolution of two multifractal measures can lead to difficulties in determining the D_q-spectrum for negative q. It will become clear at the end of the next chapter that the continued convolution encountered for the effective field on the Bethe lattice can even lead to so-called left-sided multifractal measures where the D_q for $q < 0$ are not defined. Another effect of the different form of the iteration for the effective field on the Bethe lattice is the possible loss of contractivity leading to the existence of physical phase transitions for non-zero temeperature. This subject will be addressed in the first part of the next chapter.

Chapter 5

Random field Ising model on the Bethe lattice

In this chapter the random field Ising model on a Bethe lattice is considered. The Bethe lattice of degree k is uniquely characterized by the two properties that it is an infinite Graph with constant vertex degree $k+1$ and that it contains no closed paths. The formulation of the random field Ising model on a Bethe lattice requires some notations for the underlying lattice. V denotes the set of vertices of the Bethe lattice and $d(y,z)$ is the natural metric on the lattice given by the length of the unique path connecting y and z. Furthermore, $V_R := \{y \in V : d(y, y_0) \leq R\}$ denotes the ball of radius R around some arbitrarily chosen central vertex y_0 and $\partial V_R := \{y \in V : d(y, y_0) = R\}$ its boundary, the sphere of radius R. In the following it will be useful to decompose V into two subtrees V^+ and V^- with roots y_0 and z_0 in the way illustrated in figure 5.1.

Introducing the notation $\mathcal{S}(y) := \{z \in \partial V_{R+1} : d(y,z) = 1\}$ for the successors of $y \in \partial V_R$ the Hamiltonian of the random field Ising model on the Bethe lattice reads

$$H_R(\{s_y\}_{y\in V_R}) = -\sum_{\substack{y\in V_{R-1}\\ z\in\mathcal{S}(y)}} J s_y s_z - \sum_{y\in V_{R-1}} h_y s_y - \sum_{y\in\partial V_R} x_y^b s_y \tag{5.1}$$

where s_y denotes the classical spin at vertex y taking values ± 1, J is the coupling strength, h_y is the random field at site y and x_y^b the field at the boundary encoding the chosen boundary conditions. In the following the considerations are restricted to independent, identically distributed, symmetric dichotomous random fields, i. e. $h_y = \pm h$ with probability $\frac{1}{2}$ for all $y \in V$. The canonical partition function

$$Z_R := \sum_{\{s_y\}_{y\in V_R}} \exp(-\beta H_R(\{s_y\})) \tag{5.2}$$

where $\beta = (k_B T)^{-1}$ is the inverse temperature can be reformulated by a method first introduced by Ruján [Ruj78] for the one dimensional random field Ising

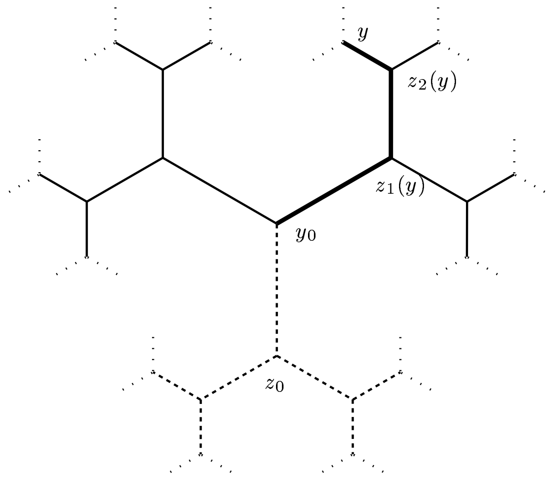

Figure 5.1 Bethe lattice of degree $k = 2$. The solid lines mark the part of the lattice denoted by V^+ and the dashed lines the part denoted by V^-. The roots of the two subtrees are denoted by y_0 and z_0 respectively. The thick line shows the unique path from a vertex $y \in \partial V_3$ at the boundary to the central vertex y_0 to illustrate the labeling along the path used in section 5.1.

model resulting in

$$Z_R = \sum_{s_{y_0}=\pm 1} \exp \beta \Big((x_{y_0}^{(R)} + A(x_{z_0}^{(R)})) s_{y_0} + \sum_{y \in V_R \setminus \{y_0\}} B(x_y^{(R)}) \Big) \tag{5.3}$$

where the effective fields $x_z^{(R)}$ are determined by the generalized random iterated function system

$$x_y^{(R)} = \sum_{z \in \mathcal{S}(y)} A(x_z^{(R)}) + h_y \tag{5.4}$$

with boundary conditions $x_y^{(R)} = x_y^b$ for $y \in \partial V_R$. The functions A and B are given by

$$A(x) = (2\beta)^{-1} \log(\cosh \beta(x+J) / \cosh \beta(x-J)) \tag{5.5}$$

$$B(x) = (2\beta)^{-1} \log(4 \cosh \beta(x+J) \cosh \beta(x-J)) \tag{5.6}$$

cf appendix B.4 for more details. Note that the upper index $^{(R)}$ of the effective field refers to the radius of the sphere where the boundary conditions are fixed. The partition function in the form (5.3) is a partition function of one spin s_{y_0} in two effective fields $x_{y_0}^{(R)}$ and $A(x_{z_0}^{(R)})$ which are both determined through the random iterated function system (5.4). The sum in (5.4) implies that although $|A'| < 1$ for non-zero temperature T, the random iterated function system is not necessarily contractive in contrast to the one-dimensional case. A loss of contractivity indicates a phase transition as is explained in more detail below.

Being functions of the random fields h_y the effective fields are random variables on the random field probability space and the iteration (5.4) induces a Frobenius-Perron or Chapman-Kolmogorov equation for their probability measure

$$\nu_y^{(R)}(X) = \sum_{h_y=\pm h} \frac{1}{2}\Big({\prod_{z\in\mathcal{S}(y)}}^{*} A_{\#}\nu_z^{(R)}\Big)(X - h_y) \tag{5.7}$$

where $\prod^*$ denotes the convolution product of measures, X is some measurable set, $X - h_y := \{x - h_y \mid x \in X\}$ and $A_\#$ is the induced mapping of A cf definition 2.3. The measures of the effective fields at the boundary are fixed by boundary conditions e. g. as $\nu_y^{(R)} = \delta(x - x_y^b)$, the Dirac measure at x_y^b. Any other choice of the random variables x_y^b is also possible of course.

It was proved in [BRZ98] that the existence of limiting Gibbs measures with finite restrictions compatible with (5.1) and (5.2), cf [Geo88], implies the weak convergence of the random variables $x_y^{(R)}$, i. e. the weak convergence of the measures $\nu_y^{(R)}$ to invariant measures ν_y in the limit $R \to \infty$. For homogeneous boundary conditions $x_y^b \equiv x^b$ for all $y \in V$, the measures ν_y are all identical and will be denoted by ν.

Before the results on phase transitions in the random field Ising model on the Bethe lattice are presented some more properties of the random iterated function system (5.4) and the function A are necessary. $A(x)$ is a monotonic function in x. For a given random field configuration $\{h_y\}_{y\in V_R^+} = \{\sigma_y h\}_{y\in V_R^+}$, $\sigma_y = \pm$, the composite function mapping the effective fields in ∂V_{R+1}^+ to the effective field at y_0 are denoted by $f_{\{\sigma\}_R}$. Here, $\{\sigma\}_R$ is the tree of $k^{R+1}-1$ symbols $\pm$ characterizing the configuration of the random field and k is the degree of the Bethe lattice. These composite functions are monotonic in the sense that if $x_y^b \geq {x'}_y^b$ for all $y \in \partial V_{R+1}^+$ then $f_{\{\sigma\}_R}(\{x_y^b\}) \geq f_{\{\sigma\}_R}(\{{x'}_y^b\})$. In the same way they are monotonic with respect to the random field, $f_{\{\sigma\}_R}(\{x_y^b\}) \geq f_{\{\sigma'\}_R}(\{x_y^b\})$ if $\sigma_y \geq \sigma'_y$ for all $y \in V_R^+$. Furthermore, there exists an invariant interval $I = [x_-^*, x_+^*]$ with the property that if $x_y \in I$ for all $y \in \partial V_{R+1}^+$ then also $f_{\{\sigma\}_R}(\{x_y\}) \in I$ for any random field configuration $\{\sigma\}_R$. Here, x_-^* and x_+^* are the fixed points of the composite functions for homogeneous $\{-\}$ and homogeneous $\{+\}$ configuration of the random field respectively. As $A(x) = -A(-x)$, these fixed points are symmetric, $x_-^* = -x_+^*$.

5.1 Upper bounds for the existence of a unique paramagnetic phase

In this section an exact upper bound for the existence of a unique paramagnetic phase in terms of the random field strength h is developed. This bound improves earlier results in [BRZ98].

Throughout this section the effective fields $g_y := A(x_y)$ instead of the fields x_y will be used in close analogy to the notation in [BRZ98]. This has some advantages in the calculation which will become clear below. The iteration (5.4) for g_y reads

$$g_y^{(R)} = \begin{cases} g_y^b & \text{(for } y \in \partial V_R\text{)} \\ A\big(\sum_{z\in\mathcal{S}(y)} A(g_z^{(R)}) + h_y\big) & \text{(otherwise)} \end{cases} \tag{5.8}$$

and the composite functions mapping the effective fields $\{g_y\}_{y\in\partial V_{R+1}^+}$ to g_{y_0} will be denoted by $\tilde{f}_{\{\sigma\}_R}$. They have the same monotonicity properties as the composite functions $f_{\{\sigma\}_R}$.

In order to prove the existence of a unique paramagnetic phase it is sufficient to show that the random variables g_y do not depend on the boundary conditions $\{g_y^b\}$ in the limit $R \to \infty$ for any choice of the boundary conditions. Let g_y^+ denote the effective field at $y \in V$ for homogeneous boundary conditions $g_y^b \equiv g_+^*$ in the limit $R \to \infty$ and g_y^- the effective field resulting from the corresponding negative boundary conditions $g_y^b \equiv g_-^*$ where $g_+^* = A(x_+^*)$ and $g_-^* = A(x_-^*)$. For $g_{y_0}^+$ and $g_{y_0}^-$ the shorthand notations g^+ and g^- will be used. Note that the dependence of the effective fields on the random field configurations is suppressed in this notation.

Inspired by the proof for the existence of a unique paramagnetic phase for the random field Ising model on the Bethe lattice of degree 2 for almost all random field configurations and $2 < h < 3$ in [BRZ98], the expectation value

$$\mathbb{E}_{\{\sigma\}}(|g^+ - g^-|) \tag{5.9}$$

is considered. The monotonicity of the composite functions $\tilde{f}_{\{\sigma\}_R}$ implies that if this expectation value is zero for the two extremal boundary conditions chosen above then it is zero for any two sets of boundary conditions. This then implies that the random variable g_{y_0} is independent of the boundary conditions for almost all random field configurations. The goal of this section is therefore to find a criterion for the random field strength h which implies that the expectation value (5.9) is zero. Because of the monotonicity of the composite functions $\tilde{f}_{\{\sigma\}_R}$ one has $g^+ \geq g^-$ and thus $|g^+ - g^-| = g^+ - g^-$. Therefore, it is sufficient to consider

$$\begin{aligned} \mathbb{E}_{\{\sigma\}}\big(g^+ - g^-\big) &= \int d\eta(\{\sigma\})\,(g^+ - g^-) \\ &= \sum_{\{\sigma\}_R} \int_{\{\tilde\sigma\}_R = \{\sigma\}_R} d\eta(\{\tilde\sigma\})\,\big(g^+(\{\tilde\sigma\}) - g^-(\{\tilde\sigma\})\big) \end{aligned} \tag{5.10}$$

where η is the product measure of the probability measures of the random fields $h_y = \sigma_y h$. In the second step the integration was split up into a sum of a finite number of integrals over sets of configurations with fixed symbols $\{\sigma\}_R$ in V_R and arbitrary $\{\tilde{\sigma}\} \in V\backslash V_R$. Using the recursion relation (5.4) the integrand can be expressed as a function of the effective fields $\{g_y^+\}_{y\in\partial V_R}$ on the boundary of V_R,

$$\begin{aligned} g^+(\{\tilde{\sigma}\}) - g^-(\{\tilde{\sigma}\}) &= \tilde{f}_{\{\tilde{\sigma}\}_{R-1}}(\{g_y^+\}_{y\in\partial V_R}) - \tilde{f}_{\{\tilde{\sigma}\}_{R-1}}(\{g_y^-\}_{y\in\partial V_R}) \\ &= \sum_{y\in\partial V_R} \partial_{g_y}\tilde{f}_{\{\tilde{\sigma}\}_{R-1}}(\{\delta_z\}_{z\in\partial V_R}\}) \cdot (g_y^+ - g_y^-). \end{aligned} \tag{5.11}$$

In the second step the mean value theorem has been used for $\tilde{f}_{\{\tilde{\sigma}\}_R}$ and $\delta_z \in [g_z^-, g_z^+]$ are appropriately chosen. The partial derivatives in (5.11) are given by

$$\partial_{g_y}\tilde{f}_{\{\tilde{\sigma}\}_{R-1}}(\{\delta_z\}_{z\in\partial V_R}\}) = \prod_{l=0}^{R-1} A'\big(f_{\{\tilde{\sigma}\}_{R-1-l}(z_l(y))}(\{\varepsilon_z\}_{z\in\partial V_R})\big) \tag{5.12}$$

where $\varepsilon_z = A^{-1}(\delta_z)$, $z_l(y) \in \partial V_l$ are the vertices along the unique path from y to y_0, cf also figure 5.1, and $\{\tilde{\sigma}\}_{R-1-l}(z_l(y))$ are the signs of the random field configuration on the subtree of depth $R-1-l$ with root $z_l(y)$. The terms $f_{\{\tilde{\sigma}\}_{R-1-l}(z_l(y))}(\{\varepsilon_z\}_{z\in\partial V_R})$ are effective fields $x^{(R)}_{z_l(y)}$ corresponding to boundary conditions $\{x_z^b = \varepsilon_z\}_{z\in\partial V_R}$. These fields are denoted by $x_z^{(R)}(\epsilon)$ and the corresponding effective fields with boundary conditions $x_z^b = x_z^+$ and $x_z^b = x_z^-$ by $x_z^{(R)}(x^+)$ and $x_z^{(R)}(x^-)$. Then one can estimate

$$\begin{aligned} A'\big(x^{(R)}_{z_l(y)}(\epsilon)\big) &\le \max\big\{A'\big(x^{(R)}_{z_l(y)}(\epsilon')\big) \bigm| \varepsilon'_z \in [x_z^-, x_z^+], z \in \partial V_R\big\} \\ &= \max\big\{A'(x) \bigm| x \in [x^{(R)}_{z_l(y)}(x^-), x^{(R)}_{z_l(y)}(x^+)]\big\} \\ &= \min\big\{A'(\max\{x^{(R)}_{z_l(y)}(x^-), 0\}), A'(\min\{x^{(R)}_{z_l(y)}(x^+), 0\})\big\}. \end{aligned} \tag{5.13}$$

The last step uses that the maximum of A' in an interval $[a, b]$ is at a if $a \ge 0$, at b if $b \le 0$ and at zero in all other cases. As the effective fields can never be larger than x_+^* and never smaller than x_-^* one can estimate $x_z^- \ge h_z + kA(x_-^*) = x_z^{(R+1)}(x_-^*)$ and $x_z^+ \le h_z + kA(x_+^*) = x_z^{(R+1)}(x_+^*)$ for $z \in \partial V_R$. This allows to replace x^+ and x^- in the argument of $x^{(R)}_{z_l(y)}$ in (5.13) and with $x^{(R)}_{z_l(y)}(x_y^{(R+1)}(x_\pm^*)) = x^{(R+1)}_{z_l(y)}(x_\pm^*)$ this yields

$$\begin{aligned} A'\big(x^{(R)}_{z_l(y)}(\epsilon)\big) &\le \min\big\{A'(\max\{x^{(R+1)}_{z_l(y)}(x_-^*), 0\}), A'(\min\{x^{(R+1)}_{z_l(y)}(x_+^*), 0\})\big\} \\ &=: A'^{(R+1)}_{z_l(y)\,\max}. \end{aligned} \tag{5.14}$$

Inserting (5.14) into (5.12) then results in

$$\partial_{g_y}\tilde{f}_{\{\tilde{\sigma}\}_{R-1}}(\{\delta_z\}_{z\in\partial V_R}\}) \le \prod_{l=0}^{R-1} A'^{(R+1)}_{z_l(y)\,\max} \tag{5.15}$$

which only depends on $\{\tilde{\sigma}\}_R = \{\sigma\}_R$ and therefore is independent of the integration. Therefore,

$$\mathbb{E}_{\{\sigma\}}(g^+ - g^-) \le \sum_{\{\sigma\}_R}\sum_{y\in\partial V_R}\prod_{l=0}^{R-1} A'^{(R+1)}_{z_l(y)\,\max} \int_{\{\tilde{\sigma}\}_R=\{\sigma\}_R} d\eta(\{\tilde{\sigma}\})\,(g_y^+ - g_y^-). \tag{5.16}$$

The remaining integral for each y is

$$\int_{\{\tilde\sigma\}_R=\{\sigma\}_R} d\eta(\{\tilde\sigma\})\,(g_y^+ - g_y^-) = 2^{-|V_R|+1}\int_{\tilde\sigma_y=\sigma_y} d\eta(\{\tilde\sigma\})\,(g_y^+ - g_y^-)$$
$$= 2^{-|V_R|}\,\mathbb{E}_{\{\sigma\}}(g_y^+ - g_y^- \mid \tilde\sigma_y = \sigma_y). \tag{5.17}$$

Here, the first step uses the independence of the random variables g_y of the signs $\{\sigma_z\}_{z\in V_R\setminus\{y\}}$ and $|V_R|$ denotes the number of vertices in V_R, i.e. $|V_R| = (k^{R+1} - 1)/(k-1)$. The function A is antisymmetric which implies $g_y^+(\{-\sigma\}) = -g_y^-(\{\sigma\})$ and therefore

$$\mathbb{E}(g_y^+ - g_y^- \mid \sigma_y = +) = \mathbb{E}(g_y^+ - g_y^- \mid \sigma_y = -) \tag{5.18}$$

implying

$$\begin{aligned}\mathbb{E}(g_y^+ - g_y^-) &= \tfrac{1}{2}\mathbb{E}(g_y^+ - g_y^- \mid \sigma_y = +) + \tfrac{1}{2}\mathbb{E}(g_y^+ - g_y^- \mid \sigma_y = -)\\ &= \mathbb{E}(g_y^+ - g_y^- \mid \sigma_y = \sigma)\end{aligned} \tag{5.19}$$

for any $\sigma \in \{-,+\}$. Setting

$$\mathbb{E}_R := \max_{y\in\partial V_R} \mathbb{E}_{\{\sigma\}}(g_y^+ - g_y^- \mid \tilde\sigma_y = \sigma_y) = \max_{y\in\partial V_R} \mathbb{E}_{\{\sigma\}}(g_y^+ - g_y^-) \tag{5.20}$$

leads to

$$\mathbb{E}_0 = \mathbb{E}_{\{\sigma\}}(g^+ - g^-) \le \sum_{\{\sigma\}_R} 2^{-|V_R|} \sum_{y\in\partial V_R} \prod_{l=0}^{R-1} {A'}^{(R+1)}_{z_l(y)\ \max}\,\mathbb{E}_R. \tag{5.21}$$

The finite sums commute and as ${A'}^{(R+1)}_{z_l(y)\ \max}$ is obtained with homogeneous boundary conditions the sums $\sum_{\{\sigma\}_R}$ are identical for all $y \in \partial V_R$ such that the sum over y can be replaced by a factor $|\partial V_R| = k^R$ yielding

$$\mathbb{E}_0 \le K\,\mathbb{E}_R \tag{5.22}$$

where

$$K := \sum_{\{\sigma\}_R} 2^{-|V_R|}\,k^R \prod_{l=0}^{R-1} {A'}^{(R+1)}_{z_l(y)\ \max}. \tag{5.23}$$

Because of the translation invariance of the Bethe lattice the considerations are not restricted to y_0 such that the estimate can be applied recursively. This implies $\mathbb{E}_0 \le K^r\mathbb{E}_{r\cdot R}$. If the factor K is less than 1 for any parameters $(T,\,h)$ then $\mathbb{E}_0 = \mathbb{E}_{\{\sigma\}}(|g^+ - g^-|) = 0$ as $\mathbb{E}_{r\cdot R}$ is uniformly bounded by $2g_+^*$ for all $r \in \mathbb{N}$ and therefore $K^r\mathbb{E}_{r\cdot R} \to 0$ for $r \to \infty$. By translation symmetry this result holds

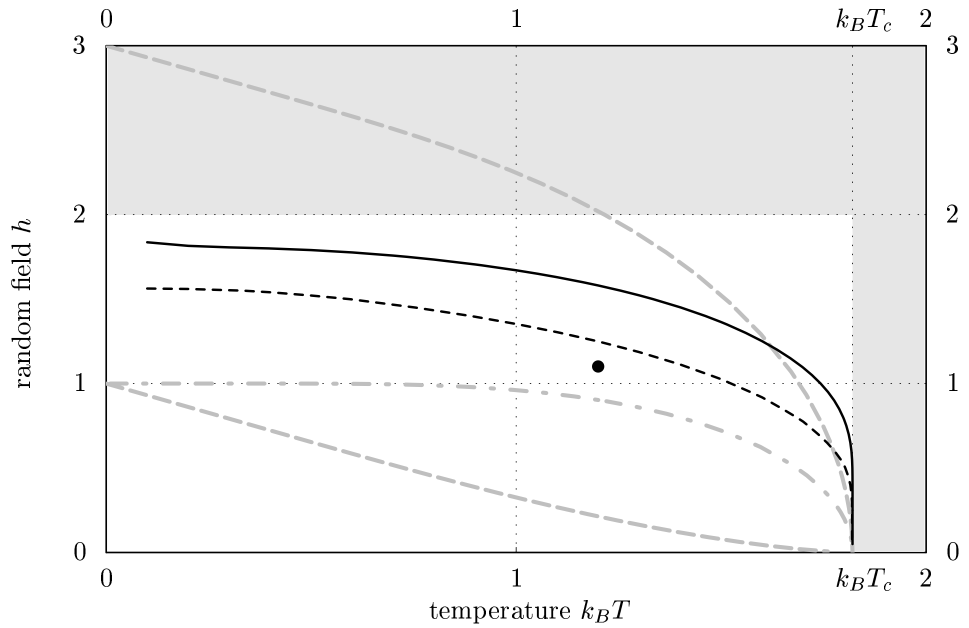

Figure 5.2 Exact upper bound for the existence of a stable paramagnetic phase on the Bethe lattice of degree $k = 2$ (solid line). The bound was obtained as described in the text with all random field configurations at $R = 4$. The dashed line is a similar upper bound obtained by considering a sample of 10^4 realizations of the random field at $R = 11$ using the complete sum (5.21). Close to $T = 0$ the problem is numerically unstable; results are presented only for $T \geq 0.1$. The large dot was obtained for $R = 20$ using (5.23) and 10^5 random field configurations. In the shaded region the result of [BRZ98] for the existence of a unique paramagnetic phase applies. The grey dashed lines are the ferromagnetic and the antiferromagnetic lines [Bru84], cf also [BRZ98] and the grey dash-dotted line is Bruinsma's lower bound for the existence of a stable ferromagnetic phase [Bru84], cf also subsection 5.2.4. ($J = 1$)

for all g_y with $y \in V$. As $|g^+ - g^-| \geq 0$ the vanishing expectation even implies $|g^+ - g^-| = 0$ for almost all realizations $\{\sigma\}$ of the random field.

The reason for using g_y instead of x_y is now easily explained. If the effective fields x_y were used instead of g_y the product over derivatives of A would be from $l = 1$ up to R. This gives a less precise estimate because x_y with $y \in \partial V_R$ is less restricted than x_{y_0} and therefore the bound for $A'(x_y)$ with $y \in \partial V_R$ is greater than the one for $A'(x_{y_0})$.

To apply the criterion obtained above K was evaluated on a computer. The calculation time is proportional to the number of random field configurations on V_R and thus asymptotically grows for e. g. $k = 2$ as 2^{2^R}. Therefore, the calculation was restricted to $R \leq 4$ (for $R = 5$ each data point in an array of 20×40 points would take about 3 days on a Pentium II 350MHz). The solid line in figure 5.2 shows the upper bound for the existence of a unique paramagnetic phase obtained for $R = 4$.

To estimate the results for $R > 4$ the field configurations were randomly sampled instead of considering all possible configurations. When doing so it is saving time not to exploit the symmetry and use (5.21) instead of (5.23). The resulting bound for $R = 11$ and a sample of 10^4 random field configurations is the dashed line in figure 5.2.

5.2 Approximations of the transition line

Even though the bounds presented in the preceding section considerably improve former analytical results they are still far away from the region where the phase transition from paramagnetic to ferromagnetic behaviour is suspected. In [Bru84] Bruinsma claimed to have found a lower bound in h for the existence of a ferromagnetic phase which is in the relevant parameter region, cf figure 5.2. To check this bound and to get a good numerical approximation of the transition line several numerical criteria for the existence of a ferromagnetic phase or the existence of a stable paramagnetic phase were developed. These criteria are discussed in the following subsections.

5.2.1 Direct calculation of the magnetization

The most obvious criterion for the existence of a ferromagnetic phase is a non-vanishing expectation value for the magnetization for small but non-zero boundary conditions. The expectation value for the local magnetization at the spin in the center is given by

$$\begin{aligned} m := \mathbb{E}_{\{\sigma\}}\langle s_{y_0}\rangle &= \int d\nu(x)\, d\nu(y)\, \frac{\sum_{s=\pm 1} s \exp\big(\beta s\, x + \beta s\, A(y)\big)}{\sum_{s=\pm 1} \exp\big(\beta s\, x + \beta s\, A(y)\big)} \\ &= \int d\nu(x)\, d\nu(y)\, \tanh\big(\beta(x + g(y))\big) \end{aligned} \tag{5.24}$$

where $\langle\cdot\rangle$ denotes the thermodynamic average, $\mathbb{E}_{\{\sigma\}}$ the expectation value with respect to all random field configurations and ν is the limit measure of the effective field for homogeneous boundary conditions $x_y^b \equiv x^b$ for all $y \in V$ in the limit $R \to \infty$. To approximate ν a large number of random field configurations on a finite region V_R was generated and the corresponding effective field $x_{y_0}^{(R)}$ was calculated. The obtained values were then sorted into small boxes of length ϵ. The resulting histogram was used as an approximation of $\nu_{y_0}(b_i) =: \nu_i$ where b_i is the i-th box. Explicitly this yields for the magnetization

$$\begin{aligned} m &\approx \int d\nu_{y_0}^{(R)}(x)\, d\nu_{y_0}^{(R)}(y)\, \tanh\big(\beta(x + g(y))\big) \\ &\approx \sum_i \sum_j \nu_i \nu_j\, \tanh \beta(x_i + g(y_j)) \end{aligned} \tag{5.25}$$

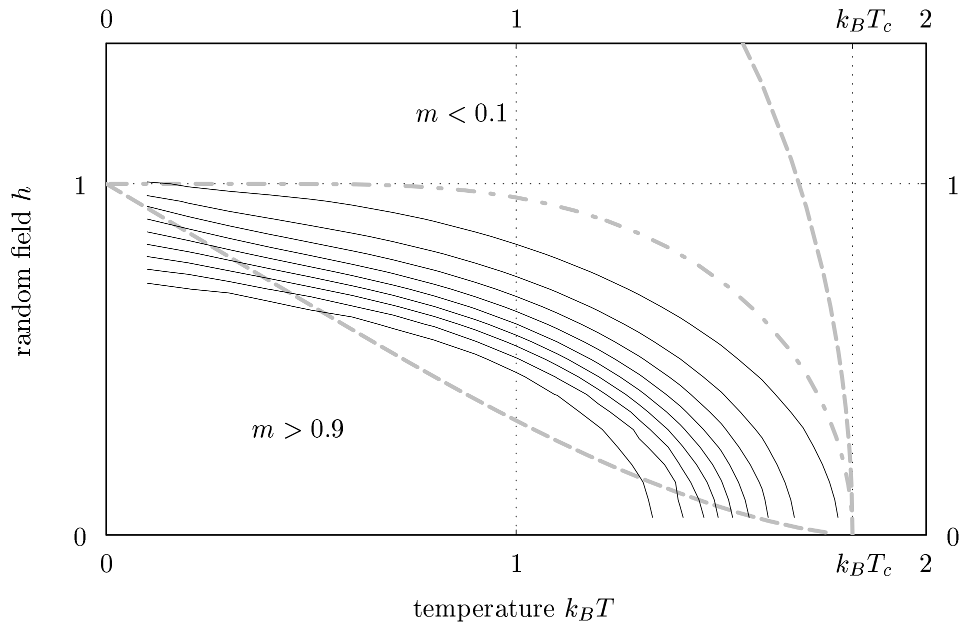

Figure 5.3 Contour plot of the magnetization m at y_0 for $R = 13$ obtained from sampling (5.25) with $4 \cdot 10^5$ random field configurations and $x^b = 0.1$. The lowest contour is $m = 0.9$ the upmost is $m = 0.1$. The grey lines are as in figure 5.2. ($J = 1$)

where the points x_i and y_j were chosen as the center of box i and j respectively. The resulting magnetization m is shown as a contour plot in figure 5.3 for $R = 13$, $x^b = 0.1$, $\epsilon = 10^{-3}$ and $4 \cdot 10^5$ random field configurations.

Assuming that the magnetization in the center varies monotonically with the radius R of the finite volume V_R one would expect to observe a monotonically increasing magnetization in the ferromagnetic regime and a monotonically decreasing magnetization in the paramagnetic regime for increasing R. Therefore, the contours in figure 5.4 which divide the two regions in which the numerical estimate of the magnetization is increasing or decreasing with increasing R are good estimates for the transition line. As one can see the estimates only depend slightly on the boundary condition and disagree significantly with Bruinsma's bound.

In contrast to this qualitative behaviour the absolute value of the magnetization for a given system size depends essentially on the chosen boundary condition. Figure 5.5 compares the numerical results for finite system size and zero random field to the analytical result in the thermodynamic limit given below.

For $h = 0$ the iteration (5.4) degenerates to $x_n = kg(x_{n+1})$ with the non-trivial fixed points ($k = 2$)

$$x^* = \frac{1}{\beta} \log \left(\tfrac{e^{2\beta J} - 1}{2} \pm \sqrt{\left(\tfrac{e^{2\beta J} - 1}{2}\right)^2 - 1} \right) \tag{5.26}$$

which are real for $T < T_c = 2J/k_B \log 3$. Inserting $d\nu(x) = \delta(x - x^*)dx$ into

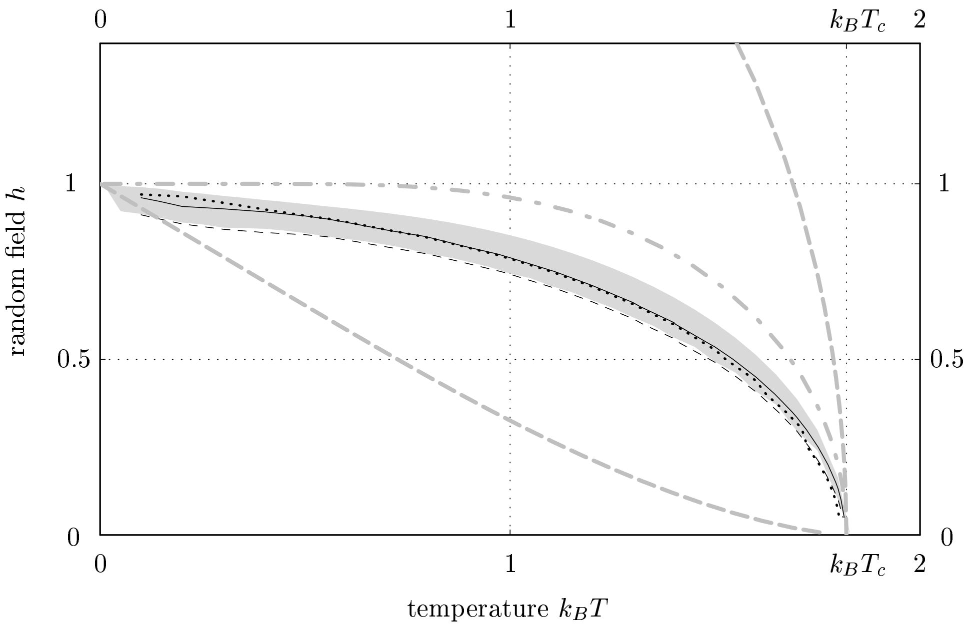

Figure 5.4 Contours separating regions where the average magnetization decreases or increases with the distance from the boundary for homogeneous boundary conditions $x^b = 0.3$ (dotted line), 0.1 (solid line), and 0.01 (dashed line). The configurational averages over $4 \cdot 10^5$ up to $64 \cdot 10^5$ samples at distances 9 and 13 from the boundary were compared. The grey lines are as in figure 5.2. The grey shaded region marks the region all our numerical results are contained in, compare figures 5.6 and 5.7. ($k = 2$, $J = 1$)

(5.24) results in

$$m = \tanh \beta(x^* + A(x^*)). \tag{5.27}$$

The finite size result is good far from the critical point and less good close to it. This was to be expected because the finite size effects are most prominent near T_c as usual.

5.2.2 Average contractivity of the random iterated function system

For zero boundary conditions there is a paramagnetic state for any temperature T and random field strength h. The stability of this paramagnetic state is tied to the average contractivity of the random iterated function system (5.4). If it is globally contracting the paramagnetic state is stable and unique. If it is at least contracting on the average for some interval around zero, the paramagnetic phase is stable but the existence of other stable phases is not a priori excluded. The investigation of the contractivity of the random iterated function system was first proposed in [Pat97].

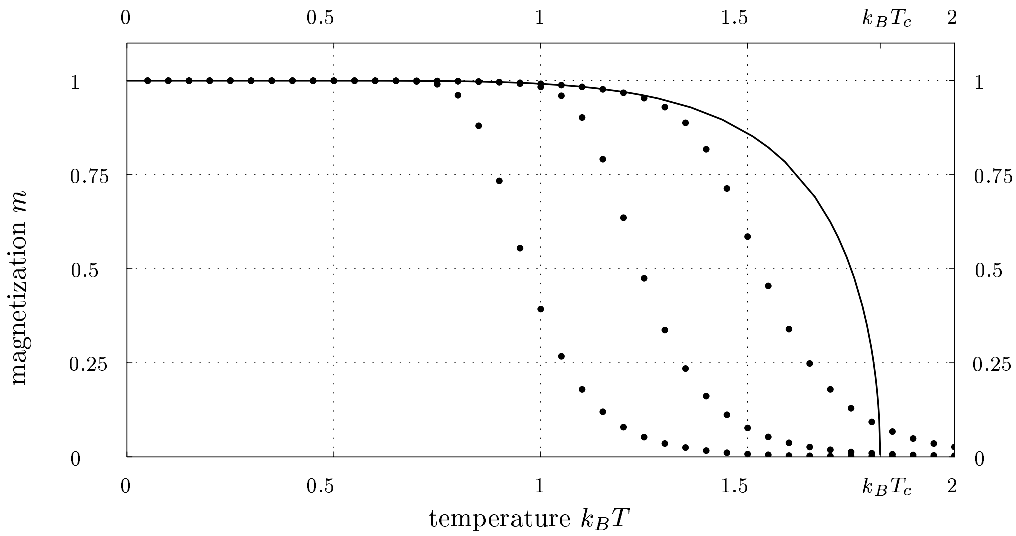

Figure 5.5 Comparison of the exact total magnetization per spin to the numerical result for $R = 13$ at $h = 0$ for several boundary conditions. The lowest points correspond to $x^b = 0.001$ the middle to $x^b = 0.01$ and the upmost to $x^b = 0.1$. As to be expected for the finite system the phase transition is smeared out. ($k = 2$, $J = 1$)

To estimate the average contractivity of the iteration (5.4) a set Σ_R of random field configurations $\{\sigma\}_R$ on a finite ball V_R was generated and the image of a small initial interval $I^b = [-x^b, x^b]$ was calculated. Because of the monotonicity of $f_{\{\sigma\}_R}$ the image of this interval at vertex y is $I_y = [x_y^{(R)}(-x^b), x_y^{(R)}(x^b)]$. To estimate the average contractivity of the random iterated function system the average length $1/k^{R_1} \sum_{y \in \partial V_{R_1}} |I_y|$ at the vertices $y \in \partial V_{R_1}$ is compared to the length $|I_{y_0}|$ at the central vertex y_0. As the effective fields at all $y \in \partial V_{R_1}$ contribute to the effective field at y_0 by iteration (5.4) it is necessary to consider the average interval lengths at vertices in ∂V_{R_1} and not individual values. To minimize the influence of the somewhat arbitrary choice of the initial interval the comparison was performed for $R_1 \ll R$.

There are essentially two ways of performing the comparison. Either one first averages over the lengths $|I_y|$ at all vertices $y \in \partial V_{R_1}$ then calculates the quotient of $|I_{y_0}|$ and the obtained average length in ∂V_{R_1} and averages over the sample Σ_R of random field configurations at the end,

$$\left\langle \frac{|I_{y_0}|}{\frac{1}{k^{R_1}} \sum_{y \in \partial V_{R_1}} |I_y|} \right\rangle_{\Sigma_R}. \tag{5.28}$$

Or one first averages $|I_y|$ over all $y \in \partial V_{R_1}$ and all random field configurations as well as $|I_{y_0}|$ over the same random field configurations and calculates the quotient

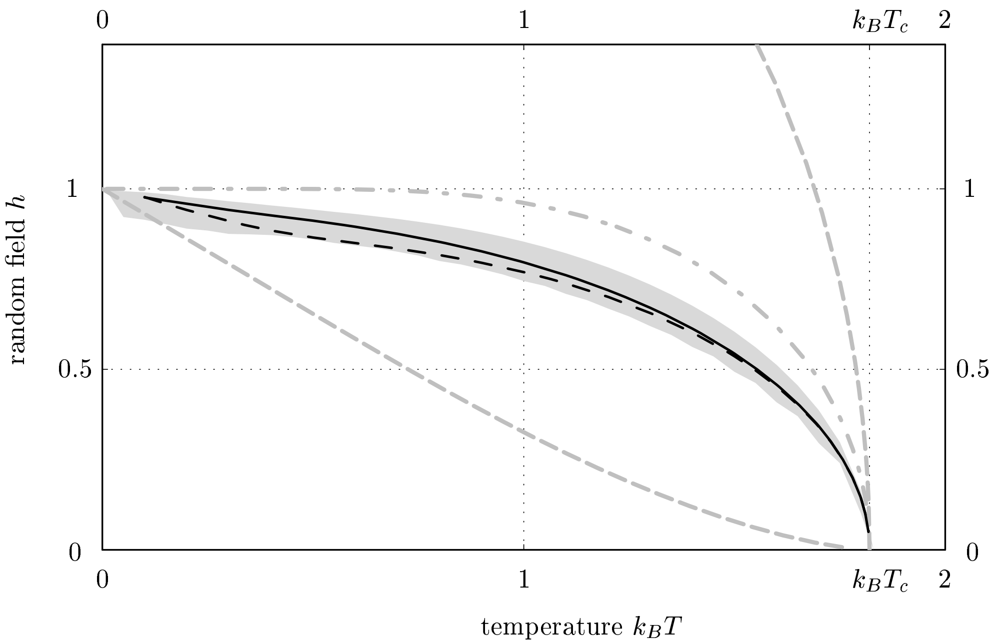

Figure 5.6 (a) Upper bound for the emergence of a stable paramagnetic phase obtained by calculating the average contractivity of the random iterated function system (5.4) for a small initial interval $I^b = [-0.01, 0.01]$. The solid line was obtained by generating 10^5 random field configurations on a Bethe lattice of degree $k = 2$ with radius $R = 13$ and comparing the length of the image of the interval at y_0 to the average length at $R_1 = 4$. Above the solid line the quotient of the interval lengths is less than 1 and below it is greater than 1. The dashed line was obtained in the same way with $R = 11$ by comparing the interval lengths at y_0 and $R_1 = 2$. The grey lines are as in figure 5.2 and the shaded region as in figure 5.4. ($J = 1$)

at the end,

$$\frac{\left\langle |I_{y_0}| \right\rangle_{\Sigma_R}}{\left\langle \frac{1}{k^{R_1}} \sum_{y \in \partial V_{R_1}} |I_y| \right\rangle_{\Sigma_R}}. \tag{5.29}$$

The two averaging procedures (5.28) and (5.29) yield identical results and thus obviously are equivalent.

To extract a criterion for the emergence of a stable paramagnetic phase the reasoning is the following. If the images of the initial interval contract on the average for a finite iteration of (5.4) they will do so for all further iterations as well and thus are likely to completely contract to length zero for infinite iteration. The complete contraction corresponds to a stable paramagnetic phase. Therefore, the contour in the (T, h) parameter plane at which the average quotient of band lengths switches from greater than 1 below to less than 1 above is an estimate for the position of the emergence of a stable paramagnetic phase.

The resulting estimated transition line for the emergence of a stable paramagnetic phase is shown for $R = 13$, $R_1 = 4$, the initial interval $I^b = [-0.01, 0.01]$ and 10^5 random field configurations as the solid line and for $R = 11$, $R_1 = 2$, $I^b = [-0.01, 0.01]$ and also 10^5 random field configurations as the dashed line in figure 5.6. The agreement of both results is satisfactory but there is again a large deviation from Bruinsma's line which is shown for comparison.

5.2.3 Independence of the effective fields from boundary conditions

Another somewhat related criterion for the existence of a stable paramagnetic phase is the independence of the effective field from boundary conditions. As in section 5.1 it is advantageous to use the effective fields $g_y^{(R)}$ rather than $x_y^{(R)}$. Consider boundary conditions $\{g_y^b\}_{y\in\partial V_R}$ taking values in a small interval $[-g^b, g^b]$. By means of the iteration with (5.4) the effective fields $g_y^{(R)}$ are functions of the boundary conditions

$$g_y^{(R)} = \tilde{f}_{\{\sigma\}_{R-n-1}(y)}(\{g_z^b\}) \tag{5.30}$$

where the function $\tilde{f}_{\{\sigma\}_{R-n-1}(y)}$ has k^{R-n} arguments for $y \in \partial V_n$ and it is the identity if $R = n$. For simplicity and without loss of generality the following discussion is restricted to $g_{y_0}^{(R)}$. The boundary conditions can be written as $g_y^b = g^b\,\hat{g}_y^b$ where $\hat{g}_y^b$ takes values in $[-1, 1]$. To investigate how the effective fields depends on the boundary conditions consider the expectation value of the derivative of $g_{y_0}^{(R)}$ with respect to g^b, the *strength* of the applied boundary condition

$$\begin{aligned}\mathbb{E}_{\{\sigma\}_{R-1}}\left|\frac{d}{dg^b}g_{y_0}^{(R)}\right| &\le \mathbb{E}_{\{\sigma\}_{R-1}}\sum_{y\in\partial V_R}\partial_{g_y}\tilde{f}_{\{\sigma\}_{R-1}}(\{g_z^b\}_{z\in\partial V_R})\,|\hat{g}_y^b| \\ &\le \sum_{y\in\partial V_R}\mathbb{E}_{\{\sigma\}_{R-1}}\prod_{l=0}^{R-1}A'\big(x_{z_l(y)}^{(R)}(x^b)\big)\end{aligned} \tag{5.31}$$

where $x_{z_l(y)}^{(R)}(x^b)$ denotes the effective fields along the unique path from y to y_0 with homogeneous boundary conditions $x_y^b \equiv g^{-1}(g^b)$. One can estimate as in section 5.1

$$\begin{aligned}A'(x_{z_l(y)}^{(R)}(x^b)) &\le \min\{A'(\max\{x_{z_l(y)}^{(R)}(x^b), 0\}, A'(\min\{x_{z_l(y)}^{(R)}(-x^b), 0\}\} \\ &=: {A'}_{z_l(y)\,\max}^{(R+1)}(x^b).\end{aligned} \tag{5.32}$$

As the boundary conditions are homogeneous this implies

$$\mathbb{E}_{\{\sigma\}_{R-1}}\left|\frac{d}{dg^b}g_{y_0}^{(R)}\right| \le k^R\mathbb{E}_{\{\sigma\}_{R-1}}\prod_{l=0}^{R-1}{A'}_{z_l(y)\,\max}^{(R+1)}(x^b). \tag{5.33}$$

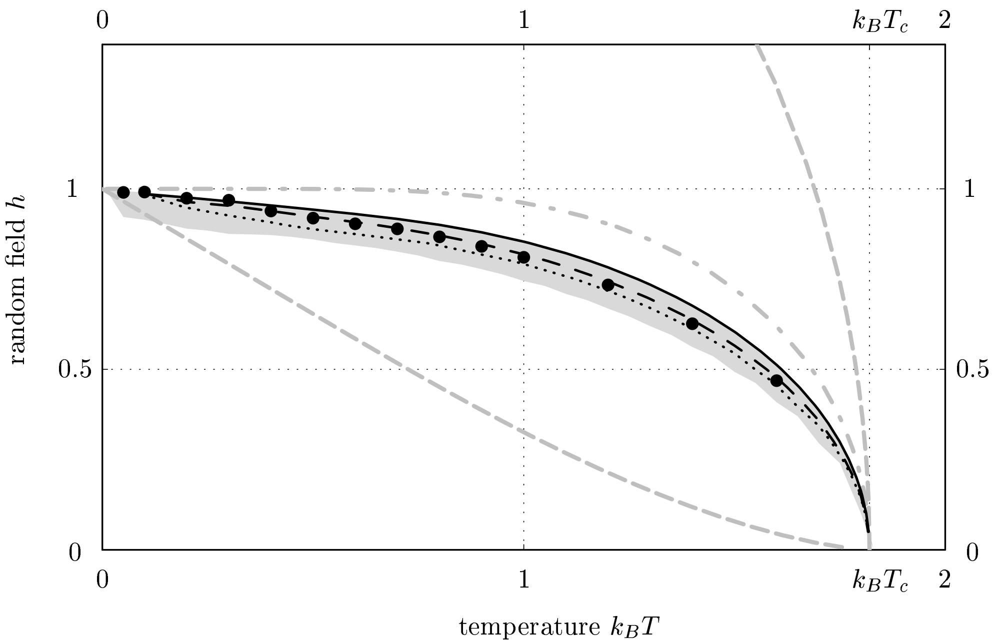

Figure 5.7 Estimated upper bound for a stable paramagnetic phase based on the dependence of the effective fields on the boundary conditions. For the solid line the expectation value (5.33) was estimated by generation of all random field configurations on a Bethe lattice of radius $R = 4$. For the dashed line 10^4 random field configurations on a Bethe lattice of radius $R = 11$, homogeneous boundary conditions $x^b = 0.01$ and (5.34) were used. The large dots were obtained from calculating (5.37) for $R = 20$, between 10^5 and $2.4 \cdot 10^6$ random field configurations and selected temperatures T. For all these lines and the large dot the caculated expectation value is less than 1 above and greater than 1 below. The dotted contour results from comparing (5.34) at $R_1 = 2$ and at y_0 for $R = 11$ and 10^4 random field configurations. The expectation value is decreasing with the distance from the boundary above the dotted line and increasing below. The grey lines are as in figure 5.2 and the shaded region as in figure 5.4. ($k = 2$, $J = 1$)

If the right hand side vanishes for $R \to \infty$ the effective field g_{y_0} is on the average independent from boundary conditions taking values in $[-g^b, g^b]$. By determining the parameter region in which the right hand side of (5.33) vanishes for $R \to \infty$ one therefore gets an upper bound on the emergence of a stable paramagnetic phase.

As the calculations on a computer are limited to finite R, convergence to zero of the right hand side of (5.33) is assumed whenever the obtained values for radius $R > 0$ are smaller than 1 which is the value for $R = 0$.

For the Bethe lattice of degree $k = 2$, radius $R = 4$ and homogeneous boundary conditions $g^b = 0.01$ the right hand side of (5.33) was evaluated. The contour between values smaller than 1 above and greater than 1 below is shown as the solid line in figure 5.7.

For $R > 4$ a calculation of all random field realizations is very costly as the calculation time scales like $2^{2^{R}-1}$. Therefore, again a statistical sample of random field configurations was used instead. In this case it is time saving not to exploit the symmetry of the system but to calculate the complete sum

$$\Big\langle \sum_{j=0}^{k^R-1} \prod_{l=0}^{R-1} {A'}^{(R+1)}_{z_l(y)\,\max}(x^b) \Big\rangle_{\Sigma_{R-1}}. \tag{5.34}$$

where $\langle\cdot\rangle_{\Sigma_{R-1}}$ denotes the average over the sample Σ_{R-1}. The resulting contour for $R = 11$ with a sample of 10^4 random field configurations is the dashed line in figure 5.7. The dotted line in figure 5.7 was obtained by analyzing whether the value is decreasing (above the line) or increasing (below the line) with increasing distance to the boundary. The values at $y \in \partial V_2$ were compared to the value at y_0 for $R = 11$ and 10^4 random field configurations to obtain this line.

If one considers the derivative of the effective field at y_0 in the case of boundary conditions $g^b \equiv 0$ one obtains

$$\mathbb{E}_{\{\sigma\}_{R-1}} \frac{dg^{(R)}_{y_0}}{dg^b}(\{0\}) = \mathbb{E}_{\{\sigma\}_{R-1}} \sum_{y\in\partial V_R} \prod_{l=0}^{R-1} A'(x^{(R)}_{z_l(y)}) \tag{5.35}$$

$$= k^R \mathbb{E}_{\{\sigma\}_{R-1}} \prod_{l=0}^{R-1} A'(x^{(R)}_{z_l(y)}) \tag{5.36}$$

for any $y \in \partial V_R$ because of the symmetry and the homogeneous boundary conditions. If this derivative does not tend to zero for some parameters (T, h) and $R \to \infty$ there is no stable paramagnetic phase. By determination of the parameter region in which this is the case a lower bound on the emergence of a stable paramagnetic phase is obtained. The numerical results obtained by evaluation of

$$\Big\langle \sum_{y\in\partial V_R} \prod_{l=0}^{R-1} A'(x^{(R)}_{z_l(y)}) \Big\rangle_{\Sigma_{R-1}} \tag{5.37}$$

for a sample Σ_{R-1} of random field configurations are the large dots in figure 5.7.

5.2.4 Discussion

In order to interpret the discrepancies between Bruinsma's bound for the onset of ferromagnetism and the numerical results it is necessary to briefly review Bruinsma's argument [Bru84].

The probability measures ν_y of the effective fields x_y are fixed points of the Frobenius-Perron equation (5.7). They can be approximated by finite iterations of some initial probability densities (boundary conditions) ν^b_y for $y \in \partial V_R$. Requiring that the support of the boundary conditions ν^b_y is a subset of the invariant interval I, the support of the resulting measure ν_{y_0} is a subset of the images of I by a)

```
- - - - - - - -    + + + + + + + +    + + + + + + + +    - - - - - - - -
 -   -   -   -      +   +   +   +      -   -   -   -      +   +   +   +
   -       -          +       +          +       +          -       -
       -                  +                  -                  +
```

b)

```
+ - + - + - + -    + - - + + - + -    + - + - + - + -    + - + - + - + -
 +   -   +   -      +   -   +   -      -   +   +   -      +   -   +   -
   +       -          +       -          +       -          -       +
       +                  +                  +                  +
```

Figure 5.8 a) The two ferromagnetic and the two antiferromagnetic configurations at $R = 4$ corresponding to the ferromagnetic and the antiferromagnetic line in the phase diagrams respectively. b) Four equivalent chessboard configurations at $R = 4$. The second configuration is obtained from the first by permutation of two subtrees of a vertex in the sphere ∂V_2, the third one by permutation of two subtrees of a vertex in the sphere ∂V_1 and the last one by permutation of the two subtrees of the root itself.

functions $f_{\{\sigma\}_R}$. These images of I are called *bands*. The left and right boundary of the bands are the effective fields corresponding to homogeneous boundary conditions $x^b_y \equiv x^*_+$ and $x^b_y \equiv x^*_-$ for $y \in \partial V_R$ respectively. The investigation of the structure of the set of bands has proved to be a powerful tool in the treatment of the one-dimensional random field Ising model, cf chapter 3.

In contrast to the one-dimensional case the bands are highly degenerate here, i. e. different configurations of the random field result in the same band. This is due to the invariance of the model with respect to permutations of subtrees for homogeneous boundary conditions. The most degenerate bands correspond to the two *chess-board* configurations, cf figure 5.8b, of the random field with $+h$ or $-h$ at y_0 respectively. There are $2^{2^{R-1}-1}$ equivalent random field configurations in the case of the Bethe lattice of degree $k = 2$ and radius R. As the total number of configurations is $N = 2^{2^R-1}$ the most degenerate bands have a weight of $2^{2^{R-1}-1}/2^{2^R-1} = 2^{-2^{R-1}} \sim 1/\sqrt{N}$. The bands with the least weight are the bands corresponding to homogeneous $+h$ or $-h$ random field configurations, cf figure 5.8a. They have the weight $1/N$. The weights of all other bands are distributed between these values.

Bruinsma started with boundary conditions $\nu^b_y \equiv \delta_{x^b}$ for some $x^b \in \mathbb{R}$ and iterated with (5.7). He only considered the lowest and highest weight terms corresponding to the least and the most degenerate bands. The highest weight term obeys a recursion relation. The fixed points of this recursion can be calculated. They correspond to the position of the highest weight term after infinite iteration of the Frobenius-Perron equation (5.7). It is straightforward to determine for which temperatures T and random field strengths h these highest weight contributions are symmetric to the origin. Proving differentiability of the density ρ of the invariant measure ν in a neighbourhood of $T = T_c$ and $h = 0$, Bruinsma concluded that an asymmetric position of the highest weight terms corresponds to asymmetric maxima of ρ of non-zero weight and therefore to the existence of a ferromagnetic phase. Note that because the contribution of the highest weight term by itself converges to zero in the limit of infinite iteration the property of differentiability of the invariant measure density is crucial for the argument.

The symmetric position of the highest weight terms corresponds to the complete contraction of the most degenerate bands such that the asymmetric boundary condition has no effect in the limit of infinite iteration. The asymmetric position of the highest weight terms on the other hand occurs if the most degenerate bands do not completely contract such that the asymmetry of the boundary condition remains visible throughout the infinite iteration. Seen in this light the argument above is similar to the criterion of average contractivity of the random iterated function system discussed in section 5.2.2 except that it considers the contractivity of one specific band, the most degenerate band, instead of the average contractivity.

There are two problematic points in the reasoning above. Firstly, it is not clear whether the fact that the most degenerate bands have the greatest weight in finite iterations of the Frobenius-Perron equation necessarily allows the conclusion that their position determines the location of local maxima provided the measure density is differentiable. For small h this actually seems not to be the case, cf figure 5.9. Unfortunately the maxima are at $\pm h$ and therefore close to zero for small h such that it is difficult to argue on the base of numerical data. Figure 5.9 also shows however that the maxima are clearly present for sufficiently large random field amplitude h.

Secondly, the differentiability of the resulting measure density has been proved only for small random field strength and in a neighbourhood of the critical tmeperature of the model without random field. The lower bound for the onset of ferromagnetism was given for all temperatures $0 \leq T \leq T_c$ though. For sufficiently large h or sufficiently small T, the measure density ρ is clearly *not* differentiable such that the argument does not apply. It is unclear whether it is differentiable in the region of Bruinsma's lower bound for the onset of ferromagnetism, cf figure 5.9.

The disagreement of the numerical results with Bruinsma's lower bound therefore allows two interpretations. Either Bruinsma's bound is not true outside the proven region of validity because the most degenerate bands are not a sufficient indicator for the symmetry of ρ when the measure density is not differentiable. Or a stable paramagnetic phase coexists with the — also stable — ferromagnetic phases in the region between the upper bounds for the existence of a stable paramagnetic phase found in this work and Bruinsma's lower bound for the onset of ferromagnetism. This would imply the existence of a first order phase transition and of hysteresis loops depending on the strength of the random field in con-

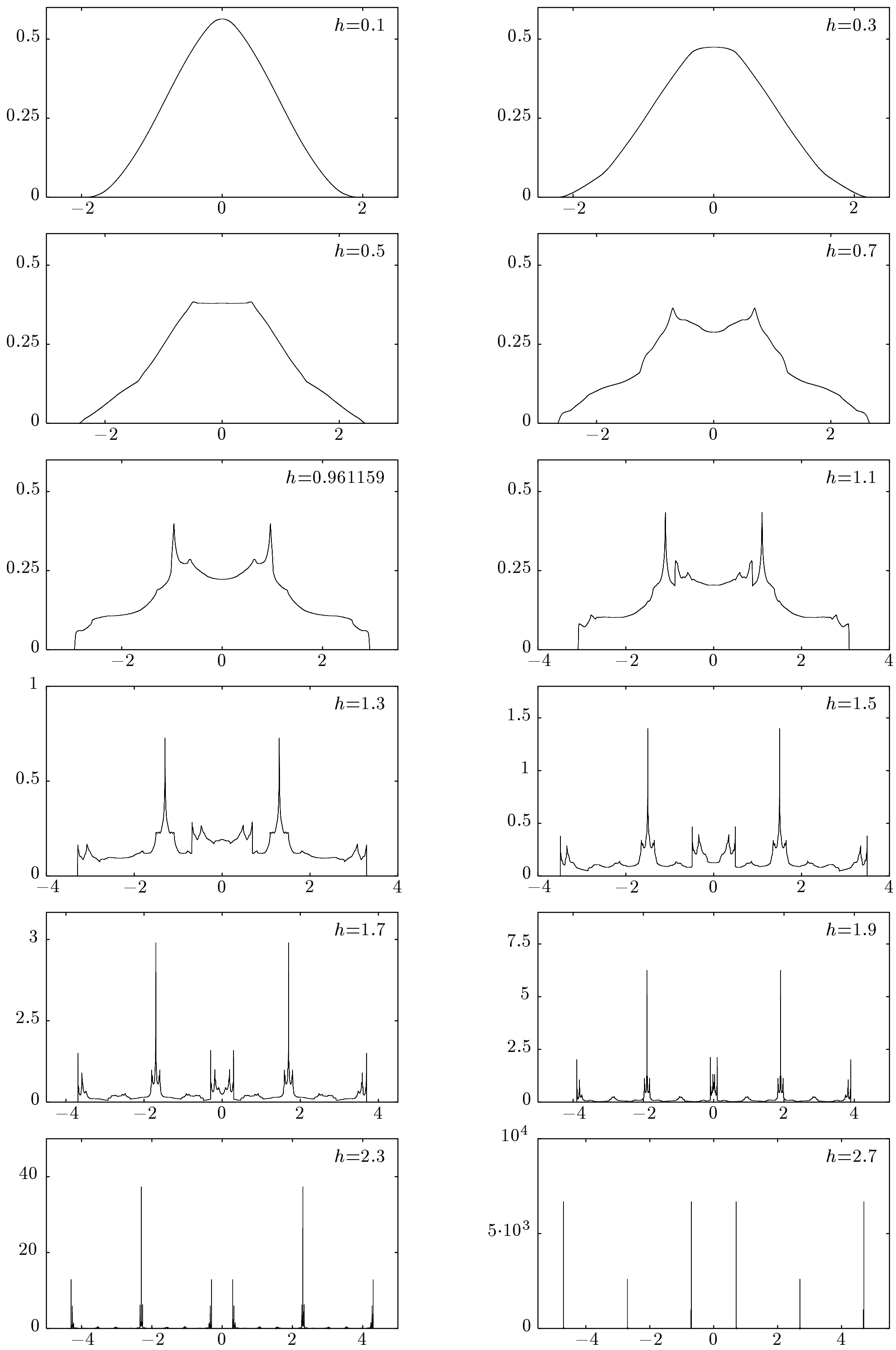

Figure 5.9 Approximations of the invariant measure density ρ obtained from four-fold application of (3.7) to the equipartition on the invariant interval I. The value $h = 0.961159$ is very close to Bruinsma's bound. ($\beta = J = 1$)

trast to the hysteresis at $T = 0$ [DSS97, Shu00, SRR00] which depends on the homogeneous offset of the random field.

5.3 Multifractal properties of the effective field

5.3.1 Left-sidedness of the invariant measure

After the D_q-spectrum of the invariant measure $\mu^{(x)}$ of the effective field and the measure $\mu^{(m)}$ of the local magnetization in the one-dimensional random field Ising model could be characterized very precisely and interesting transitions were found for $q < 0$ it seems natural to try to analyze the invariant measure ν of the effective field in the random field Ising model on the Bethe lattice in the same way.

However, lemma 4.3 and the fact that ν is a fixed point of the Frobenius-Perron equation (5.7) imply that the pointwise dimension of ν at the boundary x^*_- of its support obeys the relation

$$D_p(x^*_-;\nu) = 2D_p(x^*_-;\nu)\,. \tag{5.38}$$

The only solutions to this are $D_p(x^*_-;\nu) = 0$ or $D_p(x^*_-;\nu) = \infty$. As a direct calculation reveals the latter is the only possible solution, cf appendix B.11. By lemma 3.6 this implies that all D_q with $q < 0$ are undefined. In terms of the $f(\alpha)$-spectrum this corresponds to the situation that the $f(\alpha)$-spectrum does not terminate at some $\alpha_{\max}$ but is non-zero on the whole positive real axis. Measures of this type have been called *left-sided multifractals* and have attracted some interest recently [HGH00, RM95, ME91, MEH90]. They also seem to be relevant in fully developed turbulence and in diffusion limited aggregation [Man90]. That this effect appears naturally in the context of physical models shows that it is not an artificially constructed counterexample to the commonly assumed properties of the $f(\alpha)$-spectrum.

The appearance of this effect can also be understood in terms of the degeneracy of bands. As the homogeneous $\{+\}$ and $\{-\}$ bands are non-degenerate whereas the most degenerate bands are $2^{2^{R-1}-1}$ fold degenerate these bands which contribute to the measure at the boundary of its support are exponentially suppressed in the iteration. The maxima at the positions of the bands corresponding to the chess-board configurations are exponentially stronger than the measure at the boundary. It also becomes clear that the weight of bands is much more determined by the degeneracy than by the local contractivity of the iteration in contrast to the one-dimensional model. On the other hand even the most degenerate band has with increasing iteration depth an exponentially decreasing weight such that single bands are never sufficient for the calculation of e. g. pointwise dimensions also in clear contrast to the one-dimensional case.

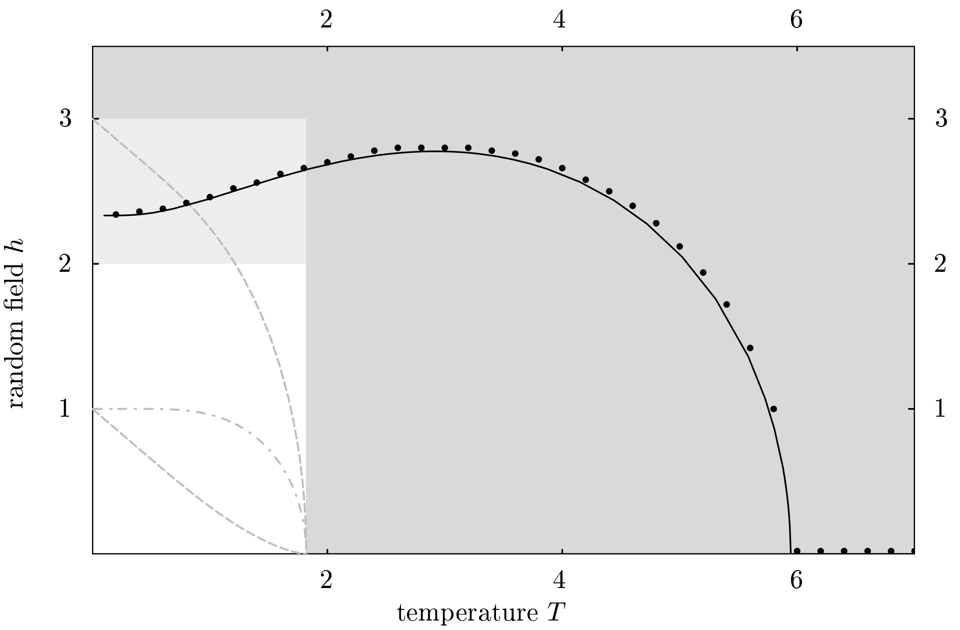

Figure 5.10 Lower bound for the transition from Euclidean to fractal support of the invariant measure of the effective field in the random field Ising model on the Bethe lattice (solid line). The bound was obtained from evaluating condition (5.39). The points are estimates for the transition obtained from the condition $D_0 < 0.999$ for all h above the points. D_0 was obtained with the method for the new natural partition on measure generated through fourfold application of the convolution algorithm to a constant initial measure. The grey lines are as in figure 5.2 and the shaded regions are the regions of a unique paramagnetic phases for almost all (light grey) and all (dark grey) random field configurations. Note that the transition in D_0 takes place in a region far away from the physical phase transitions.

For the analysis of the D_q-spectrum the left-sidedness of the invariant measure implies that the only remaining transition of those discussed for the D_q-spectrum of the effective field of the one-dimensional model is the transition in D_0 which will be treated in the next subsection.

5.3.2 Transition in D_0

In the one-dimensional random field Ising model the approximate self-similarity of the support of the invariant measure of the effective field implied that as soon as the first order bands do not overlap the support is a fractal set with $D_0 < 1$. For the measure of the local magnetization this reasoning was not possible because of lack of self-similarity and one had to rely on numerical methods. The situation of the invariant measure of the effective field of the random field Ising model on the Bethe lattice is somewhere in between. One can give a lower bound in h for the transition to a fractal support by investigating for which h the support first

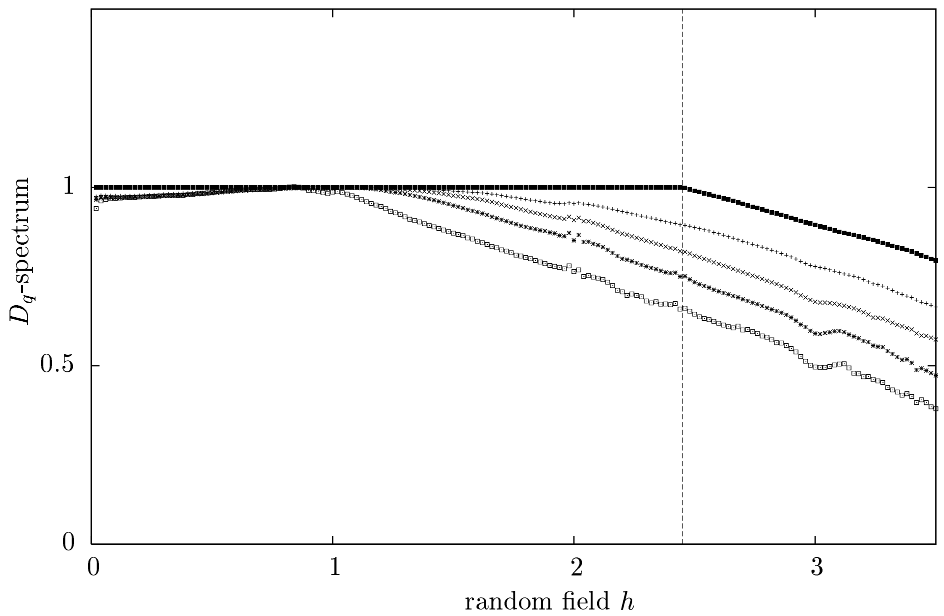

Figure 5.11 D_q-spectrum of the measure of effective field of the random field Ising model on the Bethe lattice with degree $k = 2$ for $q = 0,\ 1,\ 2,\ 4$ and 20. It was obtained by the method of the new natural partition on measure approximations obtained from up to fourfold application of the convolution algorithm on a constant initial measure corresponding to fourfold iteration of the Frobenius-Perron equation (5.7). The dashed line marks the position of the transition in D_0 obtained from (5.39). ($\beta = J = 1$)

becomes disconnected. As it turns out this lower bound is in good agreement with the numerically determined transition in D_0.

The first order bands $[2A(x^*_-) - h,\ 2A(x^*_+) - h]$ and $[2A(x^*_-) + h,\ 2A(x^*_+) + h]$ corresponding to radius $R = 1$ always intersect. Therefore, the transition to fractal support can not be detected on this level. For $R = 2$ there are 6 distinct bands. The first gaps in the support of ν appear if the right boundary of the band ${}^{-}{}_{+}{}^{+}$ begins to be less than the left boundary of the ${}^{+}{}_{+}{}^{+}$ band. This leads to the condition

$$A(2A(x^*_+) - h) + A(x^*_+) + h = 2A(2A(x^*_-) + h) + h\,. \tag{5.39}$$

The condition can be evaluated numerically and leads to the lower bound of the transition in D_0 shown as the solid line in figure 5.10. The points in the figure are numerical estimates for the transition determined from the condition that $D_0 < 0.999$ above the points. D_0 was determined with the algorithm of the new natural partition and has a sharp edge where it becomes less than 1. The necessary approximations for the invariant measure were obtained by fourfold application of the Frobenius-Perron equation (5.7) to a constant initial measure on I. Obviously the lower bound is a good approximation of the real transition line.

Finally, the generalized box dimensions D_q with $q > 0$ are rather unspectacular like in the one-dimensional model. Figure 5.11 shows the numerically generated D_q-spectrum.

There has been some hope that there might be some connection between the transitions in the multifractal D_q-spectrum of the effective field and the physical phase transitions from paramagnetic to ferromagnetic behaviour. As of now no such relations have been found. To the contrary the transition in D_0 for example is in a completely different region and the transition line also has a somewhat different shape.

This concludes the investigations of the random field Ising model on the Bethe lattice in the scope of this work. The results are discussed in comparison and an outlook is given in the conclusions below.

Chapter 6

Conclusions

In this work several aspects of random field Ising models with quenched random field were considered. The models under consideration allow to reformulate the canonical partition function for N spins to a partition function for one spin in effective fields which are characterized by random iterated function systems. The essential requirement for this reformulation is that the underlying lattice contains no loops. This requirement is met by the Bethe lattice and the one-dimensional chain which is a Bethe lattice of degree $k = 1$.

The random iterated function system for the effective field of the one-dimensional model is contractive and therefore defines a unique invariant measure of the corresponding Frobenius-Perron equation. The multifractal properties of this invariant measure were investigated in chapter 3. The random iterated function system allows the introduction of a symbolic dynamic in a way that each point in the support of the invariant measure is the fixed point of a suitably defined infinite iteration which corresponds to an infinite symbol sequence. To investigate the multifractal properties of the invariant measure the concept of orbits was introduced. An orbit to a given symbol sequence was defined as the set of predecessors of the fixed point with respect to a given symbol sequence generalizing the notion of periodic orbits in [Pat97] to arbitrary, generically non-periodic, symbol sequences. This conceptual step allowed some remarkable progress on the pointwise dimension at the points of orbits.

In section 3.3 it could be proven that the points of periodic orbits which do not touch the overlap have a well-defined pointwise dimension and an explicit formula for this pointwise dimension was established in lemma 3.3. This is a considerable improvement of earlier results for which the existence of the pointwise dimension and even strong scaling at the points of the periodic orbit under consideration had to be *assumed*. Furthermore, the result is not specific for the random iterated function system considered in this work but applies to any contractive random iterated function system for which periodic orbits with unique predecessors in the

Frobenius-Perron equation can be identified.

The generalized notion of orbits allowed to identify a special class of orbits named *offshoots* in this work. These are orbits with a symbolic sequence which has an infinite periodic tail but an arbitrary head. It was shown that the invariant measure has the same pointwise dimension at all points of an orbit provided it does not get into the overlap. This implied for the offshoots that they have the same pointwise dimension as the periodic tail which is known. This observation revealed the interesting roles played by the head and the tail of a symbol sequence. Whereas the infinite tail determines the local properties, i. e., the pointwise dimension, the head determines the position of the fixed point of the orbit.

In the case of empty overlap it was possible to generalize the expression for the pointwise dimension at points of periodic orbits to non-periodic orbits as well leading to lemma 3.4. Whereas the pointwise dimension at the points of periodic orbits is determined by the slope of the function A at the finitely many points of the periodic orbit, the pointwise dimension at the points of a non-periodic orbit depends on this slope at all infinitely many points of the orbit. Provided the average of the logarithm of the slope of A at the points of an orbit exists, the pointwise dimension at the points of that orbit also exists and is given by the generalized formula. By use of general results of ergodic theory [Elt87] this provided a formula for the pointwise dimension of $\mu^{(x)}$-almost all points of the support of the invariant measure $\mu^{(x)}$ of the effective field. The result again applies to other random iterated function systems without overlap and therefore is of interest in its own right.

The knowledge of the pointwise dimension at the points of periodic orbits furthermore allowed to explain transitions in the D_q-spectrum of the invariant measure for $q < 0$ in section 3.4 and to obtain the critical values $h_c^{(2)}$ and $h_c^{(2a)}$ at which they take place. The transition at $h_c^{(2a)}$ was discovered in improved numerical D_q-spectra generated as part of this work. The transitions are caused by the superseding of pointwise dimensions of orbits which have points in the overlap. The investigation for which values of the random field strength certain orbits have points in the overlap or not provided an equation for the critical field strength of each of the two transitions. The mechanism was understood in detail rendering the earlier results [Pat97] more precisely. In particular the obtained exact results on the pointwise dimension of periodic *and* non-periodic orbits improve the argument. In addition, the critical value $h_c^{(2)}$ was also calculated explicitly. Note, that the change in the pointwise dimension of an orbit which is a local effect has grave consequences for the D_q-spectrum which characterizes a measure globally. The transitions at $h_c^{(2)}$ and $h_c^{(2a)}$ are thus an interesting example of relations between local and global multifractal properties.

The excellent agreement with numerical results confirmed the validity of the analytical arguments for the transitions, the explicit value for $h_c^{(2)}$ and the criterion for $h_c^{(2a)}$ as well as the numerical techniques.

The transitions in the D_q-spectrum are also not specific for the random iterated function system considered here. Similar effects have already been found in the context of learning in neural networks [BvHK+93]. Any random iterated function system with an overlap structure similar to the one encountered here can display such transitions [BvHK+94] and the explanation patterns developed in [Pat97, NPB01a] and this work apply.

In section 3.5 general inequalities between D_q and D_p based on basic inequalities between sums of positive numbers and the individual summands were established. They are of very general nature applying to any measure which allow to define D_q and D_p. For the invariant measure of the effective field the application of these inequalities and the knowledge of the pointwise dimension of the points of periodic orbits led to explicit lower and upper bounds on the D_q-spectrum and explicit formula for D_∞ and $D_{-\infty}$. In many regions of the (T, h) parameter plane the bounds almost coincide with the D_q-spectrum. This is a hint that in these regions the local dimension at the points of a single orbit (and its offshoots) more or less solely determines the D_q-spectrum.

Together with the results of earlier work a comprehensive understanding of the D_q-spectrum of the effective field has been achieved. One interesting further question would yet be whether other transitions of the type $h_c^{(2a)}$ exist. This is commonly expected and can be investigated numerically when higher iteration depths become realizable. Another related question is how to quantify the height of the step in the D_q-spectrum at $h_c^{(2a)}$. To this end it would be necessary to understand in which sense the countably infinitely many periodic orbits with their countably infinitely many offshoots each constitute a non-negligible fraction of all orbits with large pointwise dimension at the critical point $h = h_c^{(2a)}$. Understanding this would allow to decide whether and which other orbits or families of orbits can also trigger transitions in the D_q-spectrum.

The results on multifractal properties of the one-dimensional Ising model so far mainly had been concentrated on the effective field which is not a quantity amenable to direct physical measurement. The local magnetization investigated in chapter 4 however is in principle experimentally observable by neutron scattering. Its investigation brings the theoretical work closer to the experimental realizations.

The probability measure of the local magnetization is essentially the convolution of the invariant measure of the effective field with a deformed version of itself. Therefore, the investigation of the multifractal properties of the local magnetization led in a natural way to the question how the multifractal properties of the convolution of two measures are related to the multifractal properties of the two convoluted measures which was investigated in section 4.1. There were three main results in this general investigation.

The first was the continuity of the convolution of Borel measures with respect to the Hutchinson metric established in lemma 4.1 which implies that the thermodynamic limit for the measure of the local magnetization can be performed in an arbitrary way.

Secondly, the pointwise dimension at the boundary of the support of the convolution was proved to be the sum of the pointwise dimensions at the boundaries of the support of the convoluted measures as formulated in lemma 4.3. This result applies to any pair of bounded Borel measures with compact support. As the pointwise dimension at any point of the support can reveal a lot about the D_q-spectrum by means of the general inequalities between D_q and D_p derived in section 3.5 this is an important result for the characterization of the D_q-spectrum of the local magnetization.

The third main result was that the D_q-spectrum of the convolution of two measures is bounded from above by the sum of the D_q of the convoluted measures. It was stated in theorem 4.4 and applies to any pair of bounded Borel measures. For the local magnetization this provided a non-trivial bound on the D_q-spectrum in terms of the D_q-spectrum of the effective field.

As all three results apply to arbitrary bounded Borel measures (with compact support in the second case) they are of general interest beyond the example of the measure of the local magnetization in the one-dimensional random field Ising model. This is the more so as sums of independent random variables leading to the convolution of the corresponding probability measures appear quite naturally in a wide variety of applications.

The convolution of Cantor sets with weights in section 4.2 provided some non-trivial examples in which the multifractal D_q-spectrum can be obtained analytically. This allowed further insight into the mechanism of the convolution of multifractals. The comparison of the numerical methods to the exact analytical results showed excellent agreement thus verifying the numerical methods.

For the measure of the local magnetization the general results for the pointwise dimension and the D_q-spectrum of the convolution of two measures together with the covariance and invariance of D_p and D_q with respect to bi-Lipschitz maps allowed a characterization of the D_q-spectrum by various bounds in section 4.3. The numerically obtained D_q-spectrum is in good agreement with the analytical results. Numerical instabilities in some parameter regions hinted to more complex mechanisms in the convolution. Some important steps towards an understanding of these effects have been taken by the analysis of the overlap structure of bands in the process of the convolution of the measures at finite iteration depth. This led to the realization that variations in the iteration depth or, equivalently, in the random field strength or the temperature can lead to a qualitative change in the overlap structure in the process of the convolution. This can qualitatively change the obtained value of D_q for arbitrarily small changes in T and h and at all iteration depths.

The more pragmatic approach was to ask for the possible observation in experiments which led to the consideration of box methods for the numerical determination of the D_q-spectrum. In these methods the scale of resolution is bounded from below by the smallest considered box in contrast to the situation of the new natural partition where the scale can get arbitrarily small already at finite iteration depths. Choosing the smallest box size according to the iteration depth led to meaningful results for the D_q-spectrum.

Nevertheless, the parameter regions where the numerical method based on the new natural partition becomes unstable is open to further investigations of numerical and analytical nature. It would be interesting to find out if and for which T and h the pointwise dimension exists in a strict mathematical sense and how it can be caluclated. As the general impression is that the inpredictability of the usual numerical methods on small scales is present for any scale below some lower critical length scale there might even be need for other multifractal concepts to characterize this measure.

The random field Ising model on the Bethe lattice of degree $k \geq 2$ exhibits a phase transition from ferro- to paramagnetic behaviour in dependence on the temperature T and the random field strength h. This phase transition was investigated in detail in chapter 5. It is an example of a phase transition where the ordered phase is suppressed by the disorder at large random field amplitudes.

The improved exact upper bound for the existence of a unique paramagnetic phase in section 5.1 is a further step towards the exact determination of the phase diagram of the random field Ising model on the Bethe lattice. Even though it is a considerable improvement of earlier results [BRZ98] it is still far from the region where the real transition line is expected.

The estimates for the transition line in section 5.2 are while all being slightly different in method and interpretation nevertheless in very good agreement with each other and all disagree with an earlier result by Bruinsma [Bru84].

The direct calculation of the expectation value of the local magnetization in subsection 5.2.1 provided an estimate for the extent of the ferromagnetic region. In the way it was exploited this estimate for the transition line was based on determining the instability of the paramagnetic phase. The investigation of the average contractivity of the random iterated function system (5.4) at large iteration depths in subsection 5.2.2 provided a reliable estimate for the stability region of the paramagnetic phase and the numerical calculation of the derivative of the effective field with respect to the strength of the boundary condition in section 5.2.3 led to a compatible result. A closer look at the different methods reveals that they all measure the average contractivity of the random iterated function system in one way or the other. This seems to be the important quantity indicating the phase transition. A contractive random iterated function system leads to a paramagnetic and a non-contracting one to a ferromagnetic situation. If the contractivity of the random iterated function system depends on the type of the applied boundary conditions more complicated phase diagram structures are conceivable.

The relation between the contractivity of the generalized random iterated function system and the phase transition in the random field Ising model on the Bethe lattice is a prominent example where methods and notions of one field of physics are useful in describing effects encountered in a model usually described within a different context.

The obvious disagreement of the obtained transition lines with the earlier result of Bruinsma [Bru84] motivates further investigations into whether the bound for the onset of ferromagnetism given in [Bru84] needs to be reconsidered or whether there might be a coexistence region for stable ferromagnetic phases with a stable paramagnetic phase. This would correspond to the situation that the random iterated function system is contractive for boundary conditions with small amplitude and non-contractive for large boundary conditions which seems somewhat improbable as the function A is more contractive for large arguments than for small ones.

The last topic were the multifractal properties of invariant measures of the effective field on the Bethe lattice were investigated in section 5.3. It was shown that invariance with respect to the Frobenius-Perron equation implies that the invariant measures must be left-sided multifractals and therefore all D_q with $q < 0$ are not defined. As a consequence, transitions in these D_q can not be observed. The only remaining transition of those investigated for the effective field of the one-dimensional model is the transition in D_0. It was obtained numerically and explained by an overlap condition which is while being somewhat more complicated still similar to the overlap condition for the transition in the one-dimensional case. It is noteworthy that the transition in D_0 is located in parameter regions far inside the paramagnetic regime. This also implies that the transition does not depend on the boundary conditions.

The D_q for $q > 0$ were obtained numerically and exhibit the expected monotonically decreasing behaviour. The much used bounds between pointwise dimensions and generalized box dimensions are not useful for the measure of the effective field on the Bethe lattice because the pointwise dimensions are not known. This results from the strong degenaracy of the bands which dominates the scaling of the measure in contrast to the situation for the one-dimensional model where the contractivity of the iterated function system was the decisive influence. A comprehensive understanding of the distribution of degeneracies and the resulting consequences for the D_q- or $f(\alpha)$-spectrum has yet to be obtained.

Appendix A

Numerical methods

All numerical work was carried out on the Linux PC cluster of the Institute for Theoretical Physics of the University of Leipzig. The cluster comprises about 70 processors ranging from Pentium Pro 200 MHz up to Pentium III 866 MHz. The programs were written in C++ and compiled with a GNU g++ compiler. Some more demanding calculations were distributed over the whole cluster using the Condor queueing system. The calculation of D_0 of the measure of the local magnetization up to iteration depths $l = r = 13$, cf figure 4.9, was extremely memory consuming and thus was parallelized using the PVM functionality of the Condor program to be able to use about 3 GB of RAM simultaneously.

In the following sections the numerical methods used in this work are briefly discussed. The explicit C++ code is not shown because the total source code is far to bulky and the programming too modular to extract the specific core pieces of the algorithms in an understandable way. Nevertheless, the descriptions below should be precise enough to allow anyone capable of some computer language to reproduce the numerical results without further information.

All methods were realized for three different number types. The fastest version is implemented with C++ long doubles. This version was always used if not stated otherwise. At parameter values with problematic numerical stability the arbitrary precision numbers of the CLN library based on the GNU GMP algorithms were used. The precision was usually set to 50 guaranteed decimal digits. The third version uses an interval arithmetic tracing the exact lower and upper bound of the calculation in a worst case scenario for all rounding errors. With the third version the problematic parameter regions for numeric stability could be identified.

A.1 Effective field

There are basically two numerical techniques to obtain the D_q-spectrum of the invariant measure of the effective field. One is based on definition 2.2 and is called box method in the following. The other uses a partition function like in definition 2.9. It is called method of the new natural partition for reasons which will become clear later.

A.1.1 Box method

In this method the invariant measure is represented as an array of numbers $\mu_i^{\varepsilon_n} \approx \mu^{(x)}(b_i^{\varepsilon_n})$ which are approximations of the measure of boxes $b_i^{\varepsilon_n}$ of size $\varepsilon_n := k^n \varepsilon_0$. Here, $0 < k < 1$ is a scaling parameter which can be chosen arbitrarily. The number of boxes for each ε_n is $N(\varepsilon_n) = \lceil |I|/\varepsilon_n \rceil$.

Generation of the measure

There are three methods to obtain approximations of the measure of the boxes. In the first method the ergodicity of the invariant measure is exploited. A trajectory $x_j = A(x_{j-1}) + h_j$ is calculated for $j = 1, \dots M$. The number of points M is typically of the order $10^6 \dots 10^8$ and h_j is chosen by a random number generator for each j independently. Then, a histogram for the number of points x_j falling into each box $b_i^{\varepsilon_n}$ is generated and the values of the normalized histogram are used as the approximations $\mu_i^{\varepsilon_n}$ of $\mu^{(x)}(b_i^{\varepsilon_n})$.

In the second method the left and right boundary of the bands $I_{\{\sigma\}_n}$ are calculated. The weight $\frac{1}{2^n}$ is associated to each band and it is assumed that this weight is in approximation evenly distributed within the band. Then the measure of a box is calculated as

$$\mu_i^{\varepsilon_n} := \sum_{\{\sigma\}_n} \frac{1}{2^n} \frac{|I_{\{\sigma\}_n} \cap b_i^{\varepsilon_n}|}{|I_{\{\sigma\}_n}|}. \tag{A.1}$$

The sum only needs to extend over all $\{\sigma\}_n$ for which $I_{\{\sigma\}_n}$ has non-void intersection with $b_i^{\varepsilon_n}$, of course.

The third method is the most precise but also the most costly one in terms of memory and calculation time. In this method the Frobenius-Perron equation for the measure density $p_n^{(x)}$ is used to calculate $\mu_n^{(x)}(b_i^{\varepsilon_n})$ without any additional approximation. The n-fold Frobenius-Perron equation for the measure density $p_n^{(x)}$ reads

$$p_n^{(x)}(x) = \sum_{\{\sigma\}_n} \frac{1}{2^n} \frac{p_0^{(x)}\left(f_{\{\sigma\}_n}^{-1}(x)\right)}{\left(f_{\{\sigma\}_n}\right)'\left(f_{\{\sigma\}_n}^{-1}(x)\right)} = \sum_{\{\sigma\}_n} \frac{1}{2^n} \left(f_{\{\sigma\}_n}^{-1}\right)'(x)\, p_0^{(x)}\left(f_{\{\sigma\}_n}^{-1}(x)\right) \tag{A.2}$$

where the sum extends over all $\{\sigma\}_n$ for which $f_{\{\sigma\}_n}^{-1}$ exists. Choosing

$$p_0^{(x)} := \begin{cases} 1/|I| & (x \in I) \\ 0 & (\text{otherwise}) \end{cases} \tag{A.3}$$

then yields

$$\mu_i^{\varepsilon_n} := \mu_n^{(x)}(b_i^{\varepsilon_n}) = \sum_{\{\sigma\}_n} \int_{x_i}^{x_{i+1}} p_n^{(x)}(x)\, dx = \sum_{\{\sigma\}_n} \frac{f_{\{\sigma\}_n}^{-1}(x_{i+1}) - f_{\{\sigma\}_n}^{-1}(x_i)}{|I|} \tag{A.4}$$

where $b_i^{\varepsilon_n} =: [x_i, x_{i+1}]$. The expression (A.4) can be calculated directly as the inverse functions $f_{\{\sigma\}_n}^{-1}$ are explicitly known.

Calculation of D_q

To calculate the D_q-spectrum from the set $\{\mu_i^{\varepsilon_n}\}$ of approximated measures of boxes the most obvious way is to calculate

$$\frac{1}{q-1} \frac{\log \sum_i (\mu_{i-1}^{\varepsilon_n} + \mu_i^{\varepsilon_n} + \mu_{i+1}^{\varepsilon_n})^q}{\log 3\, \varepsilon_n} \tag{A.5}$$

directly and take the average over all ε_n. Note that the sum of measures of boxes in the numerator corresponds to an enlarged box with enlargement $\delta = 2$.

For large boxes the result will be unsatisfactory because the asymptotic behaviour can not be seen. For very small boxes the result is also not good because the finite sampling or finite iteration depth does not allow arbitrarily good resolution of the measure. It is therefore crucial to find the correct range for the box sizes.

A better method to get an estimation for D_q therefore is to do a linear fit of

$$\log \sum_i (\mu_{i-1}^{\varepsilon_n} + \mu_i^{\varepsilon_n} + \mu_{i+1}^{\varepsilon_n})^q \tag{A.6}$$

as a function of $\log 3\, \varepsilon_n$ and choose the *scaling region* for ε_n by the quality of the fit, i. e. only fit the data in the region where it really depends linearly on $\log 3\, \varepsilon_n$. The estimation for D_q is then $1/(q-1)$ times the slope of the linear fit.

Error estimates

As error estimates one can use the standard deviation of the average in the one method and the standard deviation of the slope in the other. These error estimates are typically rather small and do not really give evidence of how far away from the real invariant measure the approximations are.

The comparison of numerical results shows that the second and third method for generating the measure of boxes leads to identical results for the high iteration depths of up to 21 iterations used for the effective field. The use of the more precise third method is necessary for the measure of the local magnetization though as in that case the iteration depth for the effective field is restricted to at most 10 iterations, cf section A.2.3 below.

A.1.2 Natural partition method

In this method the *new natural partition* is used instead of equally sized boxes. It is given by the intervals $[x_i^{(n)}, x_{i+1}^{(n)}]$ where $x_i^{(n)}$, $i = 1, \ldots, 2^{n+1}$, are the elements of the set $\{f_{\{\sigma\}_n}(x_\pm^*)\}$ ordered by size. This means that the new natural partition of order n is the set of intervals formed by the boundaries of the bands $I_{\{\sigma\}_n}$ [BL92]. It has 2^{n+1} intervals. In the non-overlapping case these intervals are simply the bands and the gaps. In the overlapping case the intervals of the new natural partition are the intervals with constant number of overlapping bands, i. e. the number of overlapping bands changes at the boundaries of the intervals of the new natural partition.

Generation of the measure

The measure of the intervals of the new natural partition can in principle be calculated with the same three methods used for calculating the measure of the boxes in the preceding subsection. The first method did not seem to be very appealing and was not realized though. The other two methods were realized. Note that in the non-overlapping case the only symbol set $\{\sigma\}_n$ entering the sum (A.2) is the symbol set of the band under consideration. Therefore equation (A.4) reduces to

$$\mu_n^{(x)}(I_{\{\sigma\}_n}) = \frac{1}{2^n} \frac{f_{\{\sigma\}_n}^{-1}(f_{\{\sigma\}_n}(x_+^*)) - f_{\{\sigma\}_n}^{-1}(f_{\{\sigma\}_n}(x_-^*))}{|I|} = \frac{1}{2^n} \tag{A.7}$$

such that both methods are equivalent in the non-overlapping case.

Determination of D_q

With the measures $\mu_i^{(n)} := \mu_n^{(x)}([x_{i+1}^{(n)}, x_i^{(n)}])$ of the intervals of the new natural partition of order n one can calculate the partition function

$$\Gamma(q, \tau, \{\mu_i^{(n)}\}) := \sum_i \frac{\left(\mu_i^{(n)}\right)^q}{l_i^{-\tau}} \tag{A.8}$$

where $l_i = |x_{i+1}^{(n)} - x_i^{(n)}|$. Then, in the spirit of definition 2.9, one tries to find the value τ_q for which $\Gamma_n(q, \tau_q, \{\mu_i^{(n)}\})$ neither diverges nor converges to 0 for $n \to \infty$. One way to do this is to determine the value $\tau_q^{(n)}$ with

$$\log \Gamma(q, \tau_q^{(n)}, \{\mu_i^{(n)}\}) \stackrel{!}{=} 0 \tag{A.9}$$

for each iteration depth n and take the average over iteration depths to obtain τ_q. As it is not clear which finite value the partition function takes at the correct τ_q, it is usually better to determine the stationarity of the partition function instead, i. e. determine $\tau_q^{(n)}$ by the condition

$$\log\Gamma\big(q,\tau_q^{(n)},\{\mu_i^{(n+1)}\}\big)-\log\Gamma\big(q,\tau_q^{(n)},\{\mu_i^{(n)}\}\big)\stackrel{!}{=}0 \tag{A.10}$$

and take the average over iteration depths n to obtain τ_q. Then, D_q is given by $D_q = 1/(1-q)\,\tau_q$.

Strictly speaking, the obtained estimate of D_q is a numerically estimated upper bound on D_q^{H} as the new natural partition is only one of the ε coverings with respect to which the supremum or infimum of $\Gamma(q,\tau,\varepsilon)$ for $q \geq 1$ and $q \leq 1$ has to be taken respectively. The general impression is however that it is a covering which is distinguished by the structure of the random iterated function system and should lead to the correct result. This really seems to be the case as the exact lower bounds of section 3.5 are practically identical with the numerical results in many cases.

For calculating D_0 it is not necessary to know the exact weights of the intervals of the new natural partition but only whether they are zero or not. Therefore, it is sufficient to count how many bands overlap in a given interval of the new natural partition. If this number is greater than zero the weight is non-zero and it is zero otherwise. In this way a lot of calculation time and memory can be saved such that for D_0 larger iteration depths than for the other dimensions are possible. This is especially important for the measure of the local magnetization.

Error estimates

As an error estimate the standard deviation in the average of the $\tau_q^{(n)}$ to various iteration depths n was used. It seems to give a rather good account of the precision of the result.

A.2 Local magnetization

As base for the convolution leading to the measure of the local magnetization one of the approximations of the invariant measure of the effective field on the new natural partition of the effective field is used. If densities are needed they are assumed to be approximatively constant on each interval of the new natural partition, i. e. $\tilde{p}_n^{(x)}(x) \approx \mu_i^{(n)}/l_i$ for $x \in [x_i^{(n)}, x_{i+1}^{(n)}]$ in the notation of the previous subsection. This piecewise constant measure densities are taken at iteration depths l for one and r for the other factor. This corresponds to l spins to the left and $r-1$ spins to the right of the site where the local magnetization is calculated.

A.2.1 Convolution

To obtain the measure of the local magnetization one needs to calculate the convolution of the measures of the effective field to the left and the right according to equation 4.5. It is given by

$$\begin{aligned}\mu_{l,r}^{(m)}([m_i, m_{i+1}]) &= (\tanh\beta)_\#(\mu_r^{(x)} * A_\#\mu_l^{(x)})([m_i, m_{i+1}]) \\ &= \int_{1/\beta\tanh^{-1}(m_i)}^{1/\beta\tanh^{-1}(m_{i+1})} p_l^{(x)}(y) \int p_r^{(x)}(x - A(y))\, dx\, dy\,. \end{aligned} \tag{A.11}$$

For $p_l^{(x)}$ and $p_r^{(x)}$ the piecewise constant approximations $\tilde{p}_l^{(x)}$ and $\tilde{p}_r^{(x)}$ are substituted and the inner integral is denoted as $F(y)$. This function is piecewise of the form $\kappa_j A(y) + \eta_j$ and thus can be represented by the coefficients κ_j, η_j and the end points y_j of the intervals $[y_j, y_{j+1}]$ on which the particular κ_j and η_j are valid. The outer integral in (A.11) is therefore approximately

$$\sum_j \int_{y_j}^{y_{j+1}} \tilde{p}_l^{(x)}(y)(\kappa_j A(y) + \eta_j)dy. \tag{A.12}$$

As $\tilde{p}_l^{(x)}$ is piecewise constant this integrals can easily be calculated provided $\int A(y)dy$ is known. This integral is given by

$$\int^x A(y)dy = \frac{1}{4\beta^2}(\mathrm{Li}_2(-e^{2\beta(x-J)}) - \mathrm{Li}_2(-e^{2\beta(x+J)})) - Jx + C \tag{A.13}$$

in which Li_2 denotes the second polylogarithmic function[1]. It turns out however that for the short intervals integrated on here the implementation of the polylogarithmic function Li_2 for double precision numbers is less precise than a simple fifth order Taylor expansion of $\int A(y)dy$ around the center of the intervals $[y_i, y_{i+1}]$. Therefore, the expansion is used in the numerical studies.

By the methods described thus far one can obtain the measure $\mu_{l,r}^{(m)}$ of any given interval $[m_i, m_{i+1}]$ and not too large iteration depths l and r. For the Cantor sets in 4.2 the method is in principal the same except that the extra difficulties of $A_\#$ and $(\tanh\beta)_\#$ are not present.

To estimate the D_q-spectrum of $\mu^{(m)}$ or the convoluted Cantor sets from the generated approximations the same two methods as for the measure of the effective field can be used.

A.2.2 Box method

As was done for the measure of the effective field one chooses boxes of size $\varepsilon_n = k^n\varepsilon_0$ with some scaling parameter $0 < k < 1$ and calculates the measures of these boxes with the convolution algorithm outlined above. The two techniques to obtain the generalized box dimensions D_q from this are then the same as for the measure of the effective field described above.

[1] The 2-nd polylogarithmic function is $\mathrm{Li}_2(z) := \sum_{k=1}^\infty \frac{z^k}{k^2} = -\int_0^z \frac{\log(1-t)}{t}\, dt$.

A.2.3 Natural partition method

When observing the process of the convolution of $\mu_r^{(x)}$ and $A_\#\mu_l^{(x)}$ more closely it becomes clear that there is a qualitative change whenever bands of $\mu_r^{(x)}$ and bands of $A_\#\mu_l^{(x)}$ start or cease to overlap, i.e. for values m_i of the magnetization obeying the condition

$$\frac{1}{\beta}\,\mathrm{artanh}(m_i) - g(x_{r,j}) = x_{l,k} \tag{A.14}$$

where $x_{r,j}$ and $x_{l,k}$ are points of the new natural partition of $\mu_r^{(x)}$ and $\mu_l^{(x)}$ respectively. This condition leads to

$$m_i = \tanh\beta\big(f_{\{\sigma\}_r}(x_\pm^*) + A(f_{\{\tilde\sigma\}_l}(x_\pm^*))\big). \tag{A.15}$$

These points m_i are obvious candidates for a new natural partition of the measure of the local magnetization. It turns out that there exists a natural degeneracy within the set $\{m_i\}$ induced by the trivial identity

$$A(a) + f_-(b) = A(b) + f_-(a) \tag{A.16}$$

and other such identities comprising higher iterations of f_+ and f_-. These degeneracies have to be removed 'by hand' by the algorithm. Then, as before for the measure of the effective field, the partition function

$$Z_{l,r}(q,\tau_q) = \sum_i \frac{\mu_{l,r}^{(m)}([m_{i+1},m_i])^q}{(m_{i+1}-m_i)^{\tau_q}} \tag{A.17}$$

is defined on this new natural partition and D_q is determined by one of the conditions (A.9) or (A.10) for various iteration depths l, r, l', r'. In all calculations the second condition provided better results and all shown results are based on this criterion.

Note that the memory and computation time requirements scale approximately like $2^l \cdot 2^r$ or worse. This restricted the use of the methods described to iteration depths up to $l = r = 10$. To obtain D_0 the algorithm can be simplified because $\mu_{l,r}^{(m)}([m_i,m_{i+1}])$ to the 0th power is 1 whenever at least two bands overlapped in the convolution for $m \in [m_i, m_{i+1}]$ and 0 otherwise. It is therefore sufficient to count the number of overlapping bands instead of evaluating the full convolution. For this simplified algorithm to calculate D_0, iteration depths up to $l = r = 13$ were achieved by distributed computations across the whole computer cluster.

Error estimates

As error estimates one uses again the standard deviation of the fit in case of the box method and the standard deviation of the average of τ_q over various iteration depths l and r in case of the method based on the new natural partition.

Appendix B

Additional proofs

The additional proofs in this chapter are of two different types. The sections B.1, B.3, B.4, B.10 and to some extent also B.2 and B.5 contain the proofs of known results and techniques which are difficult to be found in the literature in this form. They are provided for the convenience of the reader. The remaining sections B.6, B.7, B.8, B.9 and B.11 however contain original results which are integral parts of this thesis. They have been put into the appendix to avoid tiresome technicalities in the main text and therefore improve readability. The choice of the parts presented in the text and those presented in this appendix is no rating of their importance.

B.1 Monotonicity of D_q

Let μ be a bounded Borel measure on $\mathbb{R}^n$ for which D_q exists for all $q \in \mathbb{R}$ and let $\{\mu_i\}_{i\in\mathbb{N}}$ be defined as in definition 2.2. It is necessary to distinguish two cases. The first case is $1 < q' \leq q$. Define $x_i := \mu_i^{q-1}$ and let x be a random variable taking values x_i with probability μ_i. Furthermore, be $f : \mathbb{R} \to \mathbb{R}$, $f(x) = x^{(q'-1)/(q-1)}$ which is a concave function because $\frac{q'-1}{q-1} \leq 1$. Jensen's inequality yields

$$
\begin{aligned}
& f(\mathbb{E}x) \geq \mathbb{E}(f(x)) && \text{(B.1)}\\
\Rightarrow\quad & \Big(\sum_{i\in\mathbb{N}} \mu_i \mu_i^{q-1}\Big)^{\frac{q'-1}{q-1}} \geq \sum_{i\in\mathbb{N}} \mu_i \big(\mu_i^{q-1}\big)^{\frac{q'-1}{q-1}} && \text{(B.2)}\\
\Rightarrow\quad & \Big(\sum_{i\in\mathbb{N}} \mu_i^{q}\Big)^{\frac{1}{q-1}} \geq \Big(\sum_{i\in\mathbb{N}} \mu_i^{q'}\Big)^{\frac{1}{q'-1}} && \text{(B.3)}\\
\Rightarrow\quad & \frac{1}{q-1}\,\frac{\log\sum_{i\in\mathbb{N}}\mu_i^{q}}{\log\varepsilon} \leq \frac{1}{q'-1}\,\frac{\log\sum_{i\in\mathbb{N}}\mu_i^{q'}}{\log\varepsilon} && \text{(B.4)}
\end{aligned}
$$

which yields $D_q \le D_{q'}$ in the limit $\varepsilon \to 0$. In the second case $q' \le q < 1$ the function f is convex and Jensen's inequality now yields

$$\Big(\sum_{i\in\mathbb{N}} \mu_i^q\Big)^{\frac{q'-1}{q-1}} \le \sum_{i\in\mathbb{N}} \mu_i^{q'} \tag{B.5}$$

$$\Rightarrow \quad \Big(\sum_{i\in\mathbb{N}} \mu_i^q\Big)^{\frac{1}{q-1}} \ge \Big(\sum_{i\in\mathbb{N}} \mu_i^{q'}\Big)^{\frac{1}{q'-1}} \tag{B.6}$$

$$\Rightarrow \quad \frac{1}{q-1}\frac{\log \sum_{i\in\mathbb{N}} \mu_i^q}{\log\varepsilon} \le \frac{1}{q'-1}\frac{\log \sum_{i\in\mathbb{N}} \mu_i^{q'}}{\log\varepsilon} \tag{B.7}$$

and therefore $D_q \le D_{q'}$. As D_1 exists by assumption, D_q is continuous at $q = 1$ and these two cases are sufficient to prove $D_q \le D_{q'}$ for any $q \ge q'$.

B.2 Covariance of D_p with respect to bi-Lipschitz maps

Proof of Lemma 2.6. As f is bi-Lipschitz so is f^{-1} and therefore

$$L^{-1}\|y-x\| \le \|f^{-1}(y) - f^{-1}(x)\| \le L\|y-x\| \tag{B.8}$$

for some constant $L > 1$. Then

$$\|f^{-1}(f(x)+\varepsilon) - x\| = \|f^{-1}(f(x)+\varepsilon) - f^{-1}(f(x))\| \tag{B.9}$$

$$\le L\|f(x)+\varepsilon - f(x)\| = L\varepsilon \tag{B.10}$$

and

$$\|x - f^{-1}(f(x)-\varepsilon)\| \le L\|f(x) - (f(x)-\varepsilon)\| = L\varepsilon. \tag{B.11}$$

This implies $f^{-1}(B_\varepsilon(f(x))) \subseteq B_{L\varepsilon}(x)$. In the same way one obtains $B_{L^{-1}\varepsilon}(x) \subseteq f^{-1}(B_\varepsilon(f(x)))$ such that

$$\frac{\log \mu(B_{L^{-1}\varepsilon}(x))}{\log L^{-1}\varepsilon + \log L} \ge \frac{\log f_\#\mu(B_\varepsilon(f(x)))}{\log\varepsilon} \ge \frac{\log \mu(B_{L\varepsilon}(x))}{\log L\varepsilon - \log L}. \tag{B.12}$$

The left and the right hand side of the inequality converge to $D_p(x;\mu)$ such that the middle part which converges to $D_p(f(x); f_\#\mu)$ also has this limit. □

B.3 Reformulation of the partition function of the 1D RFIM

The main trick of the reduction of the partition function to a one-spin partition function in an effective field with otherwise only additive terms to the free energy is the simple identity

$$e^{\beta s A(x)} e^{\beta B(x)} = 2\cosh(\beta(x + Js)) \tag{B.13}$$

for $s = \pm 1$ which can directly be verified,

$$\begin{aligned} e^{\beta s A(x)} e^{\beta B(x)} &= \exp\Big(\beta s \frac{1}{2\beta} \log\Big[\frac{\cosh\beta(x+J)}{\cosh\beta(x-J)}\Big] \\ &\quad + \beta\frac{1}{2\beta}\log\big[4\cosh\beta(x+J)\cosh\beta(x-J)\big]\Big) && \text{(B.14)} \\ &= \Big[\frac{\cosh\beta(x+J)}{\cosh\beta(x-J)}\Big]^{s/2} 2[\cosh\beta(x+J)\cosh\beta(x-J)]^{1/2} && \text{(B.15)} \\ &= 2\cosh(\beta(x+Js)) && \text{(B.16)} \end{aligned}$$

where the last equality uses $s = \pm 1$ explicitly. With (B.13) the partition function can now be rewritten. For simplicity of notation the upper index (N) referring to the number of spins in the chain is suppressed here.

$$Z_N(\{h_i\}_{a\le i\le b}) = \sum_{\{s_i\}_{a\le i\le b}} \exp\beta\Big(\sum_{i=a}^{b-1} J s_i s_{i+1} + \sum_{i=a}^{b-1} h_i s_i + x_b s_b\Big) \tag{B.17}$$

where $x_b = A(x_{b+1}) + h_b = h_b$ has been used. Extracting all terms containing s_b leads to

$$Z_N = \sum_{\{s_i\}_{a\le i\le b-1}} \exp\beta\Big(\sum_{i=a}^{b-2} J s_i s_{i+1} + \sum_{i=a}^{b-1} h_i s_i\Big) \sum_{s_b=\pm 1} \exp\beta\big(J s_{b-1} s_b + x_b s_b\big)\,. \tag{B.18}$$

The sum on the right is $2\cosh\beta(x_b + Js_{b-1})$ which can be replaced by virtue of (B.13) to obtain

$$Z_N = \sum_{\{s_i\}_{a\le i\le b-1}} \exp\beta\Big(\sum_{i=a}^{b-2} J s_i s_{i+1} + \sum_{i=a}^{b-2} h_i s_i + x_{b-1}s_{b-1} + B(x_b)\Big) \tag{B.19}$$

where also $h_{b-1}s_{b-1} + A(x_b)s_{b-1} = x_{b-1}s_{b-1}$ has been used. Reiterating the procedure with the spin s_{b-1} yields

$$Z_N = \sum_{\{s_i\}_{a\le i\le b-2}} \exp\beta\Big(\sum_{i=a}^{b-3} J s_i s_{i+1} + \sum_{i=a}^{b-3} h_i s_i + x_{b-2}s_{b-2} + \sum_{i=b-1}^{b} B(x_i)\Big) \tag{B.20}$$

and after $N-1$ iterations the result is

$$Z_N(\{h_i\}_{a\le i\le b}) = \sum_{s_a=\pm 1} \exp\beta\Big(x_a s_a + \sum_{i=a+1}^{b} B(x_i)\Big) \tag{B.21}$$

which is the form given in equation (3.3).

B.4 Reformulation scheme for the RFIM on the Bethe lattice

The reformulation of the partition function of the random field Ising model on the Bethe lattice is very similar to the reformulation for the one-dimensional model. Starting from the partition function (5.2) one extracts all terms containing the spins at the successors of some vertex $y \in \partial V_{R-1}$ leading to

$$Z_N = \sum_{\{s_z\}_{y\in V_R\setminus\mathcal{S}(y)}} \exp\beta\Big(\sum_{\substack{z\in V_{R-1}\\ z'\in\partial V_R\setminus\mathcal{S}(y)}} Js_zs_{z'} + \sum_{z\in V_{R-1}} h_zs_z + \sum_{z\in\partial V_R\setminus\mathcal{S}(y)} x_z^bs_z\Big) \times \sum_{\{s_z\}_{z\in\mathcal{S}(y)}} \exp\beta\big(Js_ys_z + x_z^bs_z\big). \tag{B.22}$$

The last sum is

$$\sum_{\{s_z\}_{z\in\mathcal{S}(y)}} \exp\beta\big(Js_ys_z + x_z^bs_z\big) = \prod_{z\in\mathcal{S}(y)} 2\cosh\beta(x_z^b + Js_y) \tag{B.23}$$

which can be rewritten using (B.13) to yield

$$Z_N = \sum_{\{s_z\}_{y\in V_R\setminus\mathcal{S}(y)}} \exp\beta\Big(\sum_{\substack{z\in V_{R-1}\\ z'\in\partial V_R\setminus\mathcal{S}(y)}} Js_zs_{z'} + \sum_{z\in V_{R-1}} h_zs_z + \sum_{z\in\partial V_R\setminus\mathcal{S}(y)} x_z^bs_z + x_y^{(R)}s_y + \sum_{z\in\mathcal{S}(y)} B(x_z^b)\Big) \tag{B.24}$$

where $x_y^{(R)}$ is defined by (5.4). Reiterating this procedure for all $y \in \partial V_{R-1}$ and successively for all $y \in \partial V_l$ for $l = R-2, \dots 0$ then yields (5.3).

B.5 Structure of the RIFS

Let in this appendix the following notations be fixed. $\mathcal{I}_n$ denotes the union of all bands of order n,

$$\mathcal{I}_n := \bigcup_{\{\sigma\}_n\in\Sigma_n} I_{\{\sigma\}_n} \tag{B.25}$$

and $\mathcal{I} := \bigcap_{n\in\mathbb{N}}\mathcal{I}_n$ the intersection of all $\mathcal{I}_n$. Furthermore denote the set of all fixed points of order n by

$$F_n := \bigcup_{\{\sigma\}_n\in\Sigma_n} x^*_{\{\sigma\}_n} \tag{B.26}$$

and the union of all F_n by $F := \bigcup_{n\in\mathbb{N}} F_n$. Furthermore, $\{\sigma\}_n$ always denotes the head of the n leftmost symbols of a given sequence $\{\sigma\} \in \Sigma$. With these notations the following two lemmata can be formulated. B

Lemma B.1 Symbolic dynamics

1. *For any* $\{\sigma\} \in \Sigma$ *and any* $x_0 \in I$ *the limit* $\lim_{n\to\infty} f_{\{\sigma\}_n}(x_0)$ *exists and is independent of* x_0.

2. *Conversely, for any* $x \in \mathcal{I}$ *there exists a sequence* $\{\sigma\} \in \Sigma$ *such that* $\lim_{n\to\infty} f_{\{\sigma\}_n}(x_0) = x$ *for any* $x_0 \in I$.

Proof. Let $\{\sigma\} \in \Sigma$ be given and $\varepsilon > 0$. Then the interval $I_{\{\sigma\}_n}$ contains $f_{\{\sigma\}_m}(x_0)$ for any $x_0 \in I$ and any $m \geq n$. By the mean value theorem $|I_{\{\sigma\}_n}| \leq {A'}^n_{\max}|I|$ where $A'_{\max}$ denotes $\max_{x\in I} A'(x)$. As $A'_{\max} < 1$ this implies that $|f_{\{\sigma\}_m}(x_0) - f_{\{\sigma\}_{m'}}(x_0)| < \varepsilon$ for sufficiently large n and all $m, m' \geq n$ such that $(f_{\{\sigma\}_n}(x_0))_{n\in\mathbb{N}}$ is a Cauchy sequence of real numbers. As the real numbers are complete it thus converges in the limit $n \to \infty$.
Conversely let $x \in \mathcal{I}$ be given. Then it is contained in some $I_{\{\sigma\}_n}$ for all $n \in \mathbb{N}$. Beginning with $n = 1$ and following the prescription to choose $\sigma_n = +$ if $f^{-1}_{\{\sigma\}_{n-1}}(x) > 0$ and $\sigma_n = -$ otherwise one inductively obtains a well-defined increasing series of symbol sets $\{\sigma\}_n$ which are contained in each other thus defining an infinite sequence $\{\sigma\}$. This $\{\sigma\}$ fulfills $\lim_{n\to\infty} f_{\{\sigma\}_n}(x_0) = x$. In the non-overlapping case $\{\sigma\}$ is uniquely determined because x can be contained in only one band $I_{\{\sigma\}_n}$ for each n. $\square$

Lemma B.2 *The intersection of all bands is identical to the closure of the set of fixed points of finite compositions* $f_{\{\sigma\}_n}$ *and both are identical with the support of the invariant measure* $\mu^{(x)}$. *In symbols,*

$$\mathcal{I} = \overline{F} = \mathrm{supp}\ \mu^{(x)}\,. \tag{B.27}$$

Proof. Let $x \in \mathcal{I}$, $\{\sigma\} \in \Sigma$ be a corresponding symbolic sequence and $\varepsilon > 0$. Then $N \in \mathbb{N}$ exists such that $|I_{\{\sigma\}_n}| < \varepsilon$ for all $n \geq N$. This implies $|x - x^*_{\{\sigma\}_n}| < \varepsilon$ because both are elements of $I_{\{\sigma\}_n}$. Thus, $\lim_{n\to\infty} x^*_{\{\sigma\}_n} = x$ implying that x is an adherent point of F and therefore $\mathcal{I} \subset \overline{F}$. Conversely one has $F \subseteq \mathcal{I}$ and $\mathcal{I}$ is a closed set. As $\overline{F}$ is the smallest closed set containing F this implies $\overline{F} \subseteq \mathcal{I}$. This proves the first equality.
In the overlapping case $\mathrm{supp}\ \mu^{(x)} = I = \mathcal{I}$ and there is nothing to prove. In the non-overlapping case assume that some $x \in \mathcal{I}$ is not contained in $\mathrm{supp}\ \mu^{(x)}$. Then $\varepsilon > 0$ exists with $B_\varepsilon(x) \cap \mathrm{supp}\ \mu^{(x)} = \emptyset$ as the complement of $\mathrm{supp}\ \mu^{(x)}$ is open. On the other hand there exists $n \in \mathbb{N}$ and $\{\sigma\}_n \in \Sigma_n$ such that $x \in I_{\{\sigma\}_n} \subset B_\varepsilon(x)$ and therefore $\mu^{(x)}(B_\varepsilon(x)) \geq \mu^{(x)}(I_{\{\sigma\}_n}) = 2^{-n} > 0$ which is a contradiction. Therefore, $\mathcal{I} \subseteq \mathrm{supp}\ \mu$. The opposite inclusion is obvious because $\mu^{(x)}(\mathbb{R}\backslash\mathcal{I}_n) = 0$ and thus $\mathbb{R}\backslash\mathcal{I}_n \subseteq \mathbb{R}\backslash\mathrm{supp}\ \mu^{(x)}$ implying $\mathrm{supp}\ \mu^{(x)} \subseteq \mathcal{I}_n$ for all n and thus $\mathrm{supp}\ \mu^{(x)} \subseteq \mathcal{I}$. $\square$

From the two lemmata one immediately obtains that the existence of $\{\sigma\} \in \Sigma$ with $\lim_{n\to\infty} f_{\{\sigma\}_n}(x_0) = x$ follows for any $x \in \mathrm{supp}\ \mu^{(x)}$. Furthermore, F is never closed, i. e. $F \neq \overline{F}$, because F is countable but $\overline{F} = \mathcal{I}$ is uncountable.

B.6 Relation of $D_p(x;\mu^{(x)})$ and $D_p(f_\sigma^{-1}(x);\mu^{(x)})$

Let $x \in \operatorname{supp} \mu^{(x)}$ and $x \notin \mathcal{O}$, i.e. the predecessor of x under the iteration (3.4) is unique and therefore the Frobenius-Perron equation (3.7) has only one term. Denote $A'_{\max} := \max_{x\in I} A'(x) > 0$, $A'_{\min} := \min_{x\in I} A'(x) > 0$ and

$$\varepsilon_{\min} := \min_{x\in I} \left(f_-^{-1}\right)'(x)\,\varepsilon = \min_{x\in I} \left(f_+^{-1}\right)'(x)\,\varepsilon = \varepsilon/A'_{\max} \tag{B.28}$$

$$\varepsilon_{\max} := \max_{x\in I} \left(f_-^{-1}\right)'(x)\,\varepsilon = \max_{x\in I} \left(f_+^{-1}\right)'(x)\,\varepsilon = \varepsilon/A'_{\min}\,. \tag{B.29}$$

Then the mean value theorem applied to f_σ^{-1} implies

$$B_{\varepsilon_{\min}}(f_\sigma^{-1}(x)) \subseteq f_\sigma^{-1}(B_\varepsilon(x)) \subseteq B_{\varepsilon_{\max}}(f_\sigma^{-1}(x)) \tag{B.30}$$

such that the Frobenius-Perron equation (3.7) results in

$$\frac{1}{2}\mu^{(x)}(B_{\varepsilon_{\min}}(f_\sigma^{-1}(x))) \le \mu^{(x)}(B_\varepsilon(x)) \le \mu^{(x)}(B_{\varepsilon_{\max}}(f_\sigma^{-1}(x))) \tag{B.31}$$

and therefore

$$\begin{aligned}\frac{\log \mu^{(x)}(B_{\varepsilon_{\min}}(f_\sigma^{-1}(x))) - \log 2}{\log \varepsilon_{\min} - \log A'_{\max}} &\ge \frac{\log \mu^{(x)}(B_\varepsilon(x))}{\log \varepsilon} \\ &\ge \frac{\log \mu^{(x)}(B_{\varepsilon_{\max}}(f_\sigma^{-1}(x))) - \log 2}{\log \varepsilon_{\max} - \log A'_{\min}}\end{aligned} \tag{B.32}$$

which implies $D_p(x;\mu^{(x)}) = D_p(f_\sigma^{-1}(x);\mu^{(x)})$.

B.7 Proof of lemma 3.2

Set $\varepsilon_n := |I_{\{\sigma\}_n}|$. The sequence $(\varepsilon_n)_{n\in\mathbb{N}}$ is admissable because $\frac{\varepsilon_{n+1}}{\varepsilon_n} \ge A'_{\min}$. The mean value theorem for ϕ implies

$$\phi(\tilde{x}_i^{(n)}) = \phi(x_i^{(n)}) + \phi'(x_i^{(n)} + \delta_i^{(n)})(\tilde{x}_i^{(n)} - x_i^{(n)}) \tag{B.33}$$

with some $\delta_i^{(n)} \in [-\varepsilon_i, \varepsilon_i]$. Thus

$$\log\phi(\tilde{x}_i^{(n)}) - \log\phi(x_i^{(n)}) = \log\left(1 + \frac{\phi'(x_i^{(n)} + \delta_i^{(n)})}{\phi(x_i^{(n)})}\left(\tilde{x}_i^{(n)} - x_i^{(n)}\right)\right). \tag{B.34}$$

Denote the finite constant $\max\left\{\frac{\phi'(x)}{\phi(x)} : x \in I\right\}$ by $Q_{\max}$. Then $1 - Q_{\max}\,|\tilde{x}_i^{(n)} - x_i^{(n)}|$ is positive for sufficiently large $i \in \mathbb{N}$ and therefore (B.34) implies

$$\log\left(1 - Q_{\max}\,|\tilde{x}_i^{(n)} - x_i^{(n)}|\right) \le \log\phi(\tilde{x}_i^{(n)}) - \log\phi(x_i^{(n)}) \tag{B.35}$$

$$\le \log\left(1 + Q_{\max}\,|\tilde{x}_i^{(n)} - x_i^{(n)}|\right). \tag{B.36}$$

With $|\tilde{x}_i^{(n)} - x_i^{(n)}| \leq \varepsilon_i$ this yields

$$\log(1 - Q_{\max}\,\varepsilon_i) \leq \log\phi(\tilde{x}_i^{(n)}) - \log\phi(x_i^{(n)}) \leq \log(1 + Q_{\max}\,\varepsilon_i) \tag{B.37}$$

implying that the difference $\log\phi(\tilde{x}_i^{(n)}) - \log\phi(x_i^{(n)})$ converges to zero.

Let now $\varepsilon > 0$ and choose $N \in \mathbb{N}$ so large that $\big|\log\phi(\tilde{x}_i^{(n)}) - \log\phi(x_i^{(n)})\big| < \varepsilon$ for all $n > N$. Then one can choose $\tilde{N} \geq N$ such that also

$$\frac{1}{n}\Big|\sum_{i=1}^{N}\big(\log(\phi(\tilde{x}_i^{(n)}) - \log\phi(x_i^{(n)})\big)\Big| < \varepsilon \tag{B.38}$$

for all $n > \tilde{N}$ leading to

$$\begin{aligned}\frac{1}{n}\Big|\sum_{i=1}^{n}\big(\log(\phi\tilde{x}_i^{(n)}) - \log\phi(x_i^{(n)})\big)\Big| \;&\leq\; \frac{1}{n}\Big|\sum_{i=1}^{N}\big(\log\phi(\tilde{x}_i^{(n)}) - \log\phi(x_i^{(n)})\big)\Big| &\text{(B.39)}\\ &\quad+\frac{1}{n}\sum_{i=N+1}^{n}\big|\log(\phi(\tilde{x}_i^{(n)}) - \log\phi(x_i^{(n)})\big| \\ &\leq\; \varepsilon + \frac{n-N}{n}\,\varepsilon \;\leq\; 2\varepsilon &\text{(B.40)}\end{aligned}$$

for all $n > \tilde{N}$. This completes the proof.

B.8 Proof of lemma 3.4

Set $\varepsilon_n := |I_{\{\sigma\}_n}|$ like in appendix B.6 such that $(\varepsilon_n)_{n\in\mathbb{N}}$ is admissible. The fact that $x^*_{\{\sigma\}} \in I_{\{\sigma\}_n}$ for all $n \in \mathbb{N}$ and the choice of ε_n imply

$$B_{\varepsilon_n}(x^*_{\{\sigma\}}) \supseteq I_{\{\sigma\}_n} \tag{B.41}$$

such that

$$\mu^{(x)}(B_{\varepsilon_n}(x^*_{\{\sigma\}})) \geq \mu^{(x)}(I_{\{\sigma\}_n}) = \frac{1}{2^n} \tag{B.42}$$

leading to

$$\frac{\log\mu^{(x)}(B_{\varepsilon_n}(x^*_{\{\sigma\}}))}{\log\varepsilon_n} \leq \frac{-n\log 2}{\log\varepsilon_n}\,. \tag{B.43}$$

On the other hand $\varepsilon_n' := |f_{\{\sigma\}_n}(\Delta)|$ also defines an admissible sequence. The interval $I_{\{\sigma\}_n}$ is encompassed by two gaps. One of the adjacent gaps is always $f_{\{\sigma\}_{n-1}}(\Delta)$, the other is either $f_{\{\sigma\}_m}(\Delta)$ with $m < n-1$ or the complement of I. By contractivity of the random iterated function system $|f_{\{\sigma\}_m}(\Delta)| > |f_{\{\sigma\}_n}(\Delta)|$

for $m < n$, such that in either case the smallest gap next to $I_{\{\sigma\}_n}$ is $f_{\{\sigma\}_{n-1}}(\Delta)$. This implies

$$\mu^{(x)}(B_{\varepsilon'_n}(x^*_{\{\sigma\}})) \leq \mu^{(x)}(I_{\{\sigma\}_n}) = \frac{1}{2^n} \tag{B.44}$$

because $B_{\varepsilon'_n}(x^*_{\{\sigma\}})$ can not bridge any of the adjacent gaps and therefore only intersects $I_{\{\sigma\}_n}$. Thus,

$$\frac{\log \mu^{(x)}(B_{\varepsilon'_n}(x^*_{\{\sigma\}}))}{\log \varepsilon'_n} \geq \frac{-n \log 2}{\log \varepsilon'_n}. \tag{B.45}$$

The mean value theorem for $f_{\{\sigma\}_n}$ yields

$$\varepsilon_n = |I_{\{\sigma\}_n}| = f_{\{\sigma\}_n}(x^*_+) - f_{\{\sigma\}_n}(x^*_-) \tag{B.46}$$

$$= \big(f_{\{\sigma\}_n}\big)'(x^{(n)})\,(x^*_+ - x^*_-) = \prod_{i=1}^{n} A'\big(f^{-1}_{\{\sigma\}_i}(f_{\{\sigma\}_n}(x^{(n)}))\big)\ |I| \tag{B.47}$$

for some $x^{(n)} \in I$ and in the same way

$$\varepsilon'_n = \prod_{i=1}^{n} A'\big(f^{-1}_{\{\sigma\}_i}(f_{\{\sigma\}_n}(x'^{(n)}))\big)\ |\Delta| \tag{B.48}$$

for some other $x'^{(n)} \in I$. Combining (B.43) and (B.47) results in

$$\overline{D}_p(x^*_{\{\sigma\}};\mu^{(x)}) = \limsup_{n\to\infty} \frac{\log \mu^{(x)}(B_{\varepsilon_n}(x^*_{\{\sigma\}}))}{\log \varepsilon_n} \tag{B.49}$$

$$\leq \limsup_{n\to\infty} \frac{-\log 2}{\frac{1}{n}\sum_{i=1}^{n} \log A'\big(f^{-1}_{\{\sigma\}_i}(f_{\{\sigma\}_n}(x^{(n)}))\big) + \frac{1}{n}\log|I|}\,. \tag{B.50}$$

The assumption that the limit (3.35) exists and lemma 3.2 allow to replace $\sum_{i=1}^{n} \log A'\big(f^{-1}_{\{\sigma\}_i}(f_{\{\sigma\}_n}(x^{(n)}))\big)$ by $\sum_{i=1}^{n} \log A'\big(f^{-1}_{\{\sigma\}_i}(x^*_{\{\sigma\}})\big)$ such that

$$\overline{D}_p(x^*_{\{\sigma\}};\mu^{(x)}) \leq \limsup_{n\to\infty} \frac{\log 2}{\frac{1}{n}\sum_{i=1}^{n} \log A'\big(f^{-1}_{\{\sigma\}_i}(x^*_{\{\sigma\}})\big)}\,. \tag{B.51}$$

Using (B.45), (B.48) and lemma 3.2 yields in the same way

$$\underline{D}_p(x^*_{\{\sigma\}};\mu^{(x)}) = \liminf_{n\to\infty} \frac{\log \mu^{(x)}(B_{\varepsilon'_n})}{\log \varepsilon'_n} \tag{B.52}$$

$$\geq \liminf_{n\to\infty} \frac{-\log 2}{\frac{1}{n}\sum_{i=1}^{n} \log A'\big(f^{-1}_{\{\sigma\}_i}(f_{\{\sigma\}_n}(x'^{(n)}))\big) + \frac{1}{n}\log|\Delta|} \tag{B.53}$$

$$= \liminf_{n\to\infty} \frac{-\log 2}{\frac{1}{n}\sum_{i=1}^{n} \log A'\big(f^{-1}_{\{\sigma\}_i}(x^*_{\{\sigma\}})\big)}\,. \tag{B.54}$$

Inequalities (B.51) and (B.54) show that $D_p(x^*_{\{\sigma\}};\mu^{(x)})$ exists and is given by

$$D_p(x^*_{\{\sigma\}};\mu^{(x)}) = \lim_{n\to\infty} \frac{-\log 2}{\frac{1}{n}\sum_{i=1}^{n} \log A'\big(f^{-1}_{\{\sigma\}_i}(x^*_{\{\sigma\}})\big)}\,. \tag{B.55}$$

B.9 Proof of lemma 3.5

Let x_1, x_2, α_1 and α_2 be defined as in the sketch of proof. Assume without loss of generality $\alpha_1 \leq \alpha_2$. Using the notations $A'_{\max}$, $A'_{\min}$, $\varepsilon_{\min}$ and $\varepsilon_{\max}$ as in B.6 the mean value theorem applied to f_-^{-1} and f_+^{-1} implies

$$B_{\varepsilon_{\min}}(x_1) \subseteq f_-^{-1}(B_\varepsilon(x)) \subseteq B_{\varepsilon_{\max}}(x_1) \quad \text{and} \tag{B.56}$$
$$B_{\varepsilon_{\min}}(x_2) \subseteq f_+^{-1}(B_\varepsilon(x)) \subseteq B_{\varepsilon_{\max}}(x_2)\,. \tag{B.57}$$

The Frobenius-Perron equation (3.7) then yields

$$\mu^{(x)}(B_\varepsilon(x)) = \frac{1}{2}\mu^{(x)}(f_-^{-1}(B_\varepsilon(x))) + \frac{1}{2}\mu^{(x)}(f_+^{-1}(B_\varepsilon(x))) \tag{B.58}$$
$$\leq \frac{1}{2}\Big(\mu^{(x)}(B_{\varepsilon_{\max}}(x_1)) + \mu^{(x)}(B_{\varepsilon_{\max}}(x_2))\Big)\,. \tag{B.59}$$

Let $\delta > 0$. As α_1 and α_2 are the pointwise dimensions at x_1 and x_2 respectively one can find $\varepsilon_0 > 0$ such that for all $\varepsilon < \varepsilon_0$

$$\mu^{(x)}(B_{\varepsilon_{\max}}(x_1)) \leq \varepsilon_{\max}^{\alpha_1-\delta} \quad \text{and} \quad \mu^{(x)}(B_{\varepsilon_{\max}}(x_2)) \leq \varepsilon_{\max}^{\alpha_2-\delta} \tag{B.60}$$

and therefore

$$\log\mu^{(x)}(B_\varepsilon(x)) \leq \log(\varepsilon_{\max}^{\alpha_1-\delta} + \varepsilon_{\max}^{\alpha_2-\delta}) - \log 2 \tag{B.61}$$
$$= (\alpha_1-\delta)\log\varepsilon_{\max} + \log(1+\varepsilon_{\max}^{\alpha_2-\alpha_1}) - \log 2 \tag{B.62}$$
$$\leq (\alpha_1-\delta)(\log\varepsilon - \log A'_{\min}) \tag{B.63}$$

where in the last step $\alpha_2 - \alpha_1 \geq 0$ and thus $\log(1+\varepsilon_{\max}^{\alpha_2-\alpha_1}) \leq \log 2$ was used. Thus,

$$\frac{\log\mu^{(x)}(B_\varepsilon(x))}{\log\varepsilon} \geq (\alpha_1-\delta)\Big(1 - \frac{\log(A'_{\min})}{\log\varepsilon}\Big) \geq \alpha_1 - 2\delta \tag{B.64}$$

for sufficiently small ε. In an analogous way one can obtain the inequality

$$\frac{\log\mu^{(x)}(B_\varepsilon(x))}{\log\varepsilon} \leq \alpha_1 + 2\delta \tag{B.65}$$

Therefore, the pointwise dimension at x exists and is given by

$$D_p(x;\mu^{(x)}) = \lim_{\varepsilon\to 0}\frac{\log\mu^{(x)}(B_\varepsilon(x))}{\log\varepsilon} = \alpha_1 = \min\{\alpha_1,\alpha_2\} \tag{B.66}$$

which is the statement of lemma 3.5.

B.10 Equivalence of grid positions

In this appendix it is shown that for $q > 0$

$$\sum_i \mu(B_{\frac{\varepsilon}{2}}(x'_i))^q \leq 2^{q+1} \sum_i \mu(B_{\frac{\varepsilon}{2}}(x_i))^q. \tag{B.67}$$

for two grids $x_i = i\varepsilon$, $x'_i = x_i + y$, $i \in \mathbb{Z}$ which are shifted by y with respect to each other. Let $i \in \mathbb{Z}$ and denote $\mu_i := \mu(B_{\frac{\varepsilon}{2}}(x_i))$ and $\mu'_i := \mu(B_{\frac{\varepsilon}{2}}(x'_i))$. Clearly, $\mu'_i \leq \sum_{j\in J(i)} \mu_j$ where $J(i) = \{j \in \mathbb{Z} : B_{\frac{\varepsilon}{2}}(x_j) \cap B_{\frac{\varepsilon}{2}}(x'_i) \neq \emptyset\}$. As $B_{\frac{\varepsilon}{2}}(x'_i)$ intersects at most two $B_{\frac{\varepsilon}{2}}(x_j)$ the set $J(i)$ has at most two elements and one can write

$$\mu'^q_i \leq 2^q \max_{j\in J(i)} \mu_j^q. \tag{B.68}$$

On the other hand each $B_{\frac{\varepsilon}{2}}(x_j)$ intersects at most two $B_{\frac{\varepsilon}{2}}(x_i)$ for a fixed j such that any μ_j appears at most twice when summing (B.68) over all i. Therefore,

$$\sum_i \mu'^q_i \leq 2 \cdot 2^q \sum_i \mu_i^q \tag{B.69}$$

as claimed. As each sum is modulo constants bounded by the other the resulting D_q when using one grid are the same as when using the other. In this sense all grid positions are equivalent. It can be shown that in $\mathbb{R}^n$ also grids with differing orientation are equivalent [Rie95].

B.11 Calculation of $D_p(x^*_-; \nu)$ for the RFIM on the Bethe lattice

The invariant measure ν of the effective field of the RFIM on the Bethe lattice is a fixed point of the Frobenius-Perron equation (5.7), i.e.

$$\nu(X) = \sum_{\sigma=\pm} \tfrac{1}{2}(A_\#\nu * A_\#\nu)(X - \sigma h) \tag{B.70}$$

for the Bethe lattice of degree $k = 2$ and any measurable set X. Denote $A'_{\min} := \min_{x\in I} A'(x)$ and choose some $0 < \varepsilon_0 < h$. Then $\varepsilon_n := A'^n_{\min}\varepsilon_0$ defines an admissible sequence and as $\varepsilon_n < h$ the Frobenius-Perron equation for $\nu(B_{\varepsilon_n}(x^*_-))$ has only on term

$$\nu(B_{\varepsilon_n}(x^*_-)) = \tfrac{1}{2}(A_\#\nu * A_\#\nu)(B_{\varepsilon_n}(x^*_- + h)). \tag{B.71}$$

Because $x^*_- + h = A(x^*_-) + A(x^*_-)$ and $A(x^*_-)$ is the left boundary of $A_\#\nu$ the situation is like in the proof of lemma 4.3, cf also figure 4.1. Therefore,

$$\nu(B_{\varepsilon_n}(x^*_-)) \leq \tfrac{1}{2}\big(A_\#\nu(B_{\varepsilon_n}(A(x^*_-)))\big)^2 \tag{B.72}$$

$$= \tfrac{1}{2}\nu(A^{-1}(B_{\varepsilon_n}(A(x_-^*))))^2 \tag{B.73}$$
$$\leq \tfrac{1}{2}\nu(B_{\varepsilon_{n-1}}(x_-^*))^2 \tag{B.74}$$

where in the last step the mean value theorem for A^{-1} and the definition of ε_n was used to obtain $A^{-1}(B_{\varepsilon_n}(A(x_-^*))) \subseteq B_{\varepsilon_{n-1}}(x_-^*)$. Taking the logarithm this implies

$$\log \nu(B_{\varepsilon_n}(x_-^*)) \leq 2 \log \nu(B_{\varepsilon_{n-1}}(x_-^*)) \tag{B.75}$$

which leads to

$$\log \nu(B_{\varepsilon_n}(x_-^*)) \leq 2^n \log \nu(B_{\varepsilon_0}(x_-^*)) \tag{B.76}$$

after n-fold iteration. Dividing by $\log \varepsilon_n$ then results in

$$\frac{\log \nu(B_{\varepsilon_n}(x_-^*))}{\log \varepsilon_n} \geq \frac{2^n \log \nu(B_{\varepsilon_0}(x_-^*))}{n \log A'_{\min} + \log \varepsilon_0} \tag{B.77}$$

which diverges for $n \to \infty$. In the random field Ising model on the Bethe lattice the pointwise dimension of the invariant measure of the effective field at the boundary of its support is therefore infinite.

Bibliography

[AB83] G. Aeppli and R. Bruinsma, *Linear response theory and the one-dimensional Ising ferromagnet in a random field*, Phys. Lett. **97A** (1983), 117–120.

[ABJM97] A. Arneodo, E. Bacry, S. Jaffard, and J. F. Muzy, *Oszillating singularities on Cantor sets: A grand-canonical multifractal formalism*, J. Stat. Phys. **87** (1997), 179–209.

[ABJM98] A. Arneodo, E. Bacry, S. Jaffard, and J. F. Muzy, *Singularity spectrum of multifractal functions involving oscillating singularities*, J. Fourier Anal. Appl. **4** (1998), 159–174.

[AC90] L. Arnold and H. Crauel, *Iterated function systems and multiplicative ergodic theory*, Tech. Report 217, Institut für dynamische Systeme, Universität Bremen, 1990.

[And58] P. W. Anderson, *Absence of diffusion in certain random lattices*, Phys. Rev. **109** (1958), 1492–1505.

[And86] D. Andelman, *One-dimensional Ising model in a variety of random fields*, Phys. Rev. B **34** (1986), 6214–6218.

[AS97] R. F. S. Andrade and S. R. Salinas, *Ising model on a Cayley tree with competing and aperiodic interactions*, Phys. Rev. E **56** (1997), 1429–1436.

[AS99] R. F. S. Andrade and S. R. Salinas, *Diluted Ising model with competing interactions*, Physica A **270** (1999), 342–352.

[BA83] R. Bruinsma and G. Aeppli, *One-dimensional Ising model in a random field*, Phys. Rev. Lett. **50** (1983), 1494–1497.

[Bar93] M. F. Barnsley, *Fractals everywhere*, 2nd ed., Academic Press, San Diego, 1993.

[Bau90] H. Bauer, *Maß- und Integrationstheorie*, de Gruyter, Berlin, New York, 1990.

[Bax89] R. J. Baxter, *Exactly solved models in statistical mechanics*, Academic Press, London, 1989.

[Bel98] D. P. Belanger, *Experiments on the random field Ising model*, Spin glasses and random fields (Singapore) (A. P. Young, ed.), World Scientific, 1998, pp. 251–276.

[BG78] U. Brandt and W. Gross, *Exact results on random bond Ising chains in magnetic fields*, Z. Phys. B **31** (1978), 237–245.

[BL90] C. Barnes and J. M. Luck, *The distribution of the reflection phase of disordered conductors*, J. Phys. A **23** (1990), 1717–1734.

[BL92] U. Behn and A. Lange, *1D random field Ising model and nonlinear dynamics*, From Phase Transitions to Chaos (Singapore) (G. Györgyi, I. Kondor, L. Sasvári, and T. Tél, eds.), World Scientific, 1992, pp. 217–226.

[Ble90] P. M. Bleher, *Extremity of the disordered phase in the Ising model on the Bethe lattice*, Comm. Math. Phys. **128** (1990), 411–419.

[BPPV84] R. Benzi, G. Paladin, G. Parisi, and A. Vulpiani, *On the multifractal nature of fully developed tubulence and chaotic systems*, J. Phys. A **17** (1984), 3521–3531.

[BPZ90] U. Behn, V. B. Priezzhev, and V. A. Zagrebnov, *One-dimensional random field Ising model: Residual entropy, magnetization, and the "Perestroyka" of the ground state*, Physica A **167** (1990), 481–493.

[Bra80] U. Brandt, *Low temperature behaviour of a random-bond Ising chain*, J. Magn. Magn. Mater. **15** (1980), 223.

[Bru84] R. Bruinsma, *Random-field Ising model on a Bethe lattice*, Phys. Rev. B **30** (1984), 289–299.

[BRZ95] P. M. Bleher, J. Ruiz, and V. A. Zagrebnov, *On the purity of the limiting Gibbs state for the Ising model on the Bethe lattice*, J. Stat. Phys. **79** (1995), 473–482.

[BRZ96] P. M. Bleher, J. Ruiz, and V. A. Zagrebnov, *One-dimensional random-field Ising model: Gibbs state and structure of ground states*, J. Stat. Phys. **84** (1996), 1077–1093.

[BRZ98] P. M. Bleher, J. Ruiz, and V. A. Zagrebnov, *On the phase diagram of the random field Ising model on the Bethe lattice*, J. Stat. Phys. **93** (1998), 33–78.

[BS88] J. Bene and P. Szépfalusy, *Multifractal properties in the one-dimensional random-field Ising model*, Phys. Rev. A **37** (1988), 1703–1707.

[BvHK+93] U. Behn, J. L. van Hemmen, R. Kühn, A. Lange, and V. A. Zagrebnov, *Multifractality in forgetful memories*, Physica D **68** (1993), 401–415.

[BvHK+94] U. Behn, J. L. van Hemmen, R. Kühn, A. Lange, and V. A. Zagrebnov, *Multifractal properties of discrete stochastic mappings*, On three levels (New York) (M. Fannes, C. Maes, and A. Verbeure, eds.), Plenum Press, 1994, pp. 399–404.

[BY86] K. Binder and A. P. Young, *Spin glasses: Experimental facts, theoretical concepts, and open questions*, Rev. Mod. Phys. **58** (1986), 801–976.

[BZ87a] U. Behn and V. A. Zagrebnov, *One-dimensional random field Ising model and discrete stochastic mappings*, Tech. report, Joint Institute for Nuclear Research (JINR), Dubna, 1987.

[BZ87b] U. Behn and V. A. Zagrebnov, *One-dimensional random field Ising model and discrete stochastic mappings*, J. Stat. Phys. **47** (1987), 939–946.

[BZ88a] U. Behn and V. A. Zagrebnov, *Comment on "Random-field Ising model as a dynamical system"*, Phys. Rev. B **38** (1988), 7115–7116.

[BZ88b] U. Behn and V. A. Zagrebnov, *One-dimensional Markovian-field Ising model: Physical properties and characteristics of the discrete stochastic mapping*, J. Phys. A **21** (1988), 2151–2165.

[Can83] G. Cantor, *Grundlagen einer allgemeinen Mannichfältigkeitslehre*, Math. Anal. **21** (1883), 545–591.

[Can32] G. Cantor, *Gesammelte Abhandlungen mathematischen und philosophischen Inhalts*, Teubner, Berlin, 1932.

[CCC+90] J. M. Carlson, J. T. Chayes, L. Chayes, J. P. Sethna, and D. J. Thouless, *Bethe lattice spin glass: The effects of a ferromagnetic bias and external fields. I. Bifurcation analysis*, J. Stat. Phys. **61** (1990), 987–1067.

[CCST90] J. M. Carlson, J. T. Chayes, J. P. Sethna, and D. J. Thouless, *Bethe lattice spin glass: The effects of a ferromagnetic bias and external fields. II. Magnetized spin-glass phase and the de Almeida-Thouless line*, J. Stat. Phys. **61** (1990), 987–1067.

[Cip87] B. A. Cipra, *An introduction to the Ising model*, Amer. Math. Monthly **94** (1987), 937–959.

[CPRV99] M. Campostrini, A. Pelissetto, P. Rossi, and E. Vicari, *Improved high-temperature expansion and critical equation of state of three-dimensional Ising-like systems*, Phys. Rev. E **60** (1999), 3526–3563.

[Dom74] C. Domb, *Ising model*, Phase Transitions and Critical Phenomena (London, New York) (C. Domb and M. S. Green, eds.), vol. 3, Academic Press, 1974, pp. 357–484.

[DSS97] D. Dhar, P. Shukla, and J. P. Sethna, *Zero-temperature hysteresis in the random-field Ising model on a Bethe lattice*, J. Phys. A **30** (1997), 5259–5267.

[DVP78] D. Derrida, J. Vannimenus, and Y. Pomeau, *Simple frustrated systems: Chains, strips and squares*, J. Phys. C **11** (1978), 4749–4765.

[Dys53] F. J. Dyson, *The dynamics of a disordered linear chain*, Phys. Rev. **92** (1953), 1331–1338.

[EA75] S. F. Edwards and P. W. Anderson, *Theory of spin glasses*, J. Phys. F **5** (1975), 965.

[Eda95] A. Edalat, *Domain theory and integration*, Theoretical Computer Science **151** (1995), 163–193.

[Eda96] A. Edalat, *Power domains and iterated function systems*, Information and Computation **124** (1996), 182–197.

[Eda97] A. Edalat, *Domains for computation in mathematics, physics and exact real arithmetic*, The Bulletin of Symbolic Logic **3** (1997), 401–452.

[Egg74] T. P. Eggarter, *Cayley trees, the Ising problem, and the thermodynamic limit*, Phys. Rev. B **9** (1974), 2989–2992.

[Elt87] J. H. Elton, *An ergodic theorem for iterated maps*, Ergod. Th. & Dynam. Sys. **7** (1987), 481–488.

[Eva87] S. N. Evangelou, *Fractal measures in the random-field Ising model*, J. Phys. C **20** (1987), L511–L519.

[Fal75] H. Falk, *Ising spin system on a Cayley tree: Correlation decomposition and phase transition*, Phys. Rev. B **12** (1975), 5184–5189.

[Fal90] K. J. Falconer, *Fractal geometry*, John Wiley & Sons Ltd., Chichester, 1990.

[Fal97] K. J. Falconer, *Techniques in fractal geometry*, John Wiley & Sons Ltd., Chichester, 1997.

[Fal99] K. J. Falconer, *Generalized dimensions of measures on self-affine sets*, Nonlinearity **12** (1999), 877–891.

[FH91] K. H. Fischer and J. A. Hertz, *Spin glasses*, Cambridge University Press, Cambridge, 1991.

[FL91] A. M. Ferrenberg and D. P. Landau, *Critical behaviour of the three-dimensional Ising model: A high-resolution Monte Carlo study*, Phys. Rev. B **44** (1991), 5081–5091.

[FO99] K. J. Falconer and T. C. O'Neil, *Convolutions and the geometry of multifractal measures*, Math. Nachr. **204** (1999), 61–82.

[FOY83] J. D. Farmer, E. Ott, and J. A. Yorke, *The dimension of chaotic attractors*, Physica **7D** (1983), 153–180.

[Geo88] H. O. Georgii, *Gibbs measures and phase transitions*, de Gruyter, 1988.

[GP83] P. Grassberger and I. Procaccia, *Characterization of strange attractors*, Phys. Rev. Lett. **50** (1983), 346–349.

[GP87] G. H. Gunaratne and I. Procaccia, *Organization of chaos*, Phys. Rev. Lett. **59** (1987), 1377–1380.

[GR84] G. Györgyi and P. Ruján, *Strange attractors in disordered systems*, J. Phys. C **17** (1984), 4207–4212.

[GR00] J. M. Gutiérrez and M. A. Rodríguez, *A new exact method for obtaining the multifractal spectrum of multiscaled multinomial measures and IFS invariant measures*, Chaos, Solitons & Fractals **11** (2000), 675–683.

[Gra83] P. Grassberger, *Generalized dimensions of strange attractors*, Phys. Lett. **97A** (1983), 227–230.

[Hal67] B. I. Halperin, *Properties of a particle in a one-dimensional random potential*, Adv. Chem. Phys. **XIII** (1967), 123–177.

[Hau19] F. Hausdorff, *Dimension und äußeres Maß*, Math. Anal. **79** (1919), 157–179.

[HGH00] W. G. Hanan, J. Gough, and D. M. Heffernan, *Left-sided multifractality in a binary random multiplicative cascade*, Phys. Rev. E **63** (2000), 011109.

[HI98] C. K. Hu and N. S. Izmailian, *Exact correlation functions of Bethe lattice spin models in external magnetic fields*, Phys. Rev. E **58** (1998), 1644–1653.

[HIO99] C. K. Hu, N. S. Izmailian, and K. B. Oganesyan, *Exact phase diagram for an Ising model on a two-layer Bethe lattice*, Phys. Rev. E **59** (1999), 6489–6496.

[HJK+86] T. C. Halsey, M. H. Jensen, L. P. Kadanoff, I. Procaccia, and B. I. Shraiman, *Fractal measures and their singularities: The characterization of strange sets*, Phys. Rev. A **33** (1986), 1141–1151.

[HMP86] T. C. Halsey, P. Meakin, and I. Procaccia, *Scaling structure of the surface layer of diffusion-limited aggregates*, Phys. Rev. Lett. **56** (1986), 854–857.

[HP83] H. Hentschel and I. Procaccia, *The infinite number of generalized dimensions of fractals and strange attractors*, Physica **8D** (1983), 435–444.

[HR99a] J. Hausmann and P. Ruján, *The randomly driven Ising ferromagnet: I. General formalism and mean-field theory*, J. Phys. A **32** (1999), 61–74.

[HR99b] J. Hausmann and P. Ruján, *The randomly driven Ising ferromagnet: II. One and two dimensions*, J. Phys. A **32** (1999), 75–92.

[Hut81] J. E. Hutchinson, *Fractals and self similarity*, Ind. Univ. Math. J. **30** (1981), 713–747.

[Igl94] F. Igloi, *Correlations in random Ising chains at zero temperature*, J. Phys. A **9** (1994), 2995–3005.

[IH98] N. S. Izmailian and C. K. Hu, *Exact spin-spin correlation functions of Bethe lattice Ising and BEG models in external fields*, Physica A **254** (1998), 198–206.

[IJR99] F. Igloi, R. Juhasz, and H. Rieger, *Griffiths-McCoy singularities in the random transverse-field Ising spin chain*, Phys. Rev. B **59** (1999), 11308–11314.

[Isi24] E. Ising, *Beitrag zur Theorie des Ferro- und Paramagnetismus*, Ph.D. thesis, Universität Hamburg, 1924.

[KJTI99] D. Karevski, R. Juhasz, L. C. Turban, and F. Igloi, *Transverse-field Ising spin chain with inhomogeneous disorder*, Phys. Rev. B **60** (1999), 4195–4204.

[LB99] D. A. Lavis and G. M. Bell, *Statistical mechanics of lattice systems 1*, 2nd ed., Texts and Monographs in Physics, Springer, Berlin, Heidelberg, 1999.

[Len20] W. Lenz, *Beitrag zum Verständnis der magnetischen Erscheinungen in festen Körpern*, Phys. Zeitschr. **21** (1920), 613.

[LN89] J. M. Luck and Th. M. Nieuwenhuizen, *Correlation function of random-field Ising chains: Is it Lorentzian or not?*, J. Phys. A **22** (1989), 2151–2180.

[LN99] K. S. Lau and S. M. Ngai, *Multifractal measures and a weak separation condition*, Adv. Math. **141** (1999), 45–96.

[LP94] F. Ledrappier and A. Porzio, *A dimension formula for Bernoulli convolutions*, J. Stat. Phys. **76** (1994), 1307–1327.

[LP96a] F. Ledrappier and A. Porzio, *On the multifractal analysis of Bernoulli convolutions. I. Large-deviation results*, J. Stat. Phys. **82** (1996), 367–395.

[LP96b] F. Ledrappier and A. Porzio, *On the multifractal analysis of Bernoulli convolutions. II. Dimensions*, J. Stat. Phys. **82** (1996), 397–420.

[LR85] P. A. Lee and T. V. Ramakrishnan, *Disordered electronic systems*, Rev. Mod. Phys. **57** (1985), 287–337.

[Luc87] J. M. Luck, *Frustration effects in quasicrystals: An exactly soluble example in one dimension*, J. Phys. A **20** (1987), 1259–1268.

[Man83] B. B. Mandelbrot, *The fractal geometry of nature*, W. H. Freeman, New York, 1983.

[Man90] B. B. Mandelbrot, *New "anomalous" multiplicative multifractals: Left-sided $f(\alpha)$ and the modeling of DLA*, Physica A **168** (1990), 95–111.

[Mat74] H. Matsuda, *Infinite susceptibility without spontaneous magnetization. Exact properties of the Ising model on the Cayley tree*, Progr. Theor. Phys. **51** (1974), 1053–1063.

[MBA94] J. F. Muzy, E. Bacry, and A. Arneodo, *The multifractal formalism reviseted with wavelets*, Intern. J. Bifur. Chaos Appl. Sci. Engrg. **4** (1994), 245–302.

[ME91] B. B. Mandelbrot and C. J. G. Evertsz, *Exactly self-similar multifractals with left-sided $f(\alpha)$*, Fractals and Disordered Systems (New York) (A. Bunde and S. Havlin, eds.), Springer-Verlag, 1991, pp. 323–344.

[MEH90] B. B. Mandelbrot, C. J. G. Evertsz, and Y. Hayakawa, *Exactly self-similar left-sided multifractal measures*, Phys. Rev. A **42** (1990), 4528–4536.

[MHZ74] E. Müller-Hartmann and J. Zittartz, *New type of phase transition*, Phys. Rev. Lett. **33** (1974), 893–897.

[MP01] M. Mézard and G. Parisi, *The Bethe lattice spin glass revisited*, Eur. Phys. J. B **20** (2001), 217–233.

[MW73] B. M. McCoy and T. T. Wu, *The two-dimensional Ising model*, Harvard University Press, Cambridge, Massachusetts, USA, 1973.

[Nat98] T. Nattermann, *Theory of the random field Ising model*, Spin glasses and random fields (Singapore) (A. P. Young, ed.), World Scientific, 1998, pp. 277–298.

[NB01] T. Nowotny and U. Behn, *Convolution of multifractals and the local magnetization in a random field Ising chain*, J. Phys. A **34** (2001), 8057–8079.

[NMO85] J. M. Normand, M. L. Mehta, and H. Orland, *One dimensional random Ising models*, J. Phys. A **18** (1985), 621–639.

[NPB01a] T. Nowotny, H. Patzlaff, and U. Behn, *Orbits and phase transitions in the multifractal spectrum*, J. Phys. A **34** (2001), 1–23.

[NPB01b] T. Nowotny, H. Patzlaff, and U. Behn, *Phase diagram of the random field Ising model on the Bethe lattice*, cond-mat/0106074, submitted (2001).

[Ols95] L. Olsen, *A multifractal formalism*, Adv. in Math. **116** (1995), 82–196.

[Ols96] L. Olsen, *Multifractal dimensions of product measures*, Math. Proc. Camb. Phil. Soc. **120** (1996), 709–734.

[Ons44] L. Onsager, *Crystal statistics. I. A two-dimensional model with an order-disorder transition*, Phys. Rev. **65** (1944), 117–149.

[Ott93] E. Ott, *Chaos in dynamical systems*, Cambridge University Press, 1993.

[Pat97] H. Patzlaff, *Multifraktale Eigenschaften und Phasenübergänge diskreter stochastischer Abbildungen*, Ph.D. thesis, Universität Leipzig, 1997.

[PBL95] H. Patzlaff, U. Behn, and A. Lange, *Analytical explanation of a phase transition in the multifractal measure connected with a one-dimensional random field Ising model*, FRACTAL FRONTIERS, Fractals in the Natural and Applied Sciences (Singapore) (M. M. Novak and T. G. Dewey, eds.), World Scientific, 1995.

[Pea90] G. Peano, *Sur une courbe, qui remplit une aire plane*, Math. Anal. **36** (1890), 157–160.

[Pea73] G. Peano, *Selected works*, Toronto University Press, 1973.

[PSS00] Y. Peres, W. Schlag, and B. Solomyak, *Sixty years of Bernoulli convolutions*, Progress in Probability (Basel, Boston) (C. Bandt, S. Graf, and M. Zaehle, eds.), vol. 46, Birkhäuser, 2000, pp. 39–65.

[PW97] Y. Pesin and H. Weiss, *The multifractal analysis of Gibbs measures: Motivation, mathematical foundation, and examples*, Chaos **7** (1997), 89–106.

[Rad93] G. Radons, *A new transition for projections of multifractal measures and random maps*, J. Stat. Phys. **72** (1993), 227–239.

[Rad95] G. Radons, *Emergence of quenched phases and second order transitions for sums of multifractal measures*, Phys. Rev. Lett. **75** (1995), 2518–2521.

[Rén60] A. Rényi, *Some fundamental questions of information theory*, Magyar Tud. Akad. Mat. Fiz. Oszt. Közl **10** (1960), 251–282.

[Rén61] A. Rényi, *On measures of entropy and information*, Proceedings 4th Berkeley Symposium on Mathematical Statistics and Probability (Berkeley), Univ. of California Press, 1961.

[Rén70] A. Rényi, *Probability theory*, North-Holland, Amsterdam, 1970.

[Rie95] R. H. Riedi, *An improved multifractal formalism and self-similar measures*, J. Math. Anal. Appl. **189** (1995), 462–490.

[RM95] R. H. Riedi and B. B. Mandelbrot, *Multifractal formalism for infinite multinomial measures*, Adv. Appl. Math. **16** (1995), 132–150.

[RM98] R. H. Riedi and B. B. Mandelbrot, *Exceptions to the multifractal formalism for discontinuous measures*, Math. Proc. Camb. Phil. Soc. **123** (1998), 133–157.

[RS96] G. Radons and R. Stoop, *Superpositions of multifractals: Generators of phase transitions in the generalized thermodynamic formalism*, J. Stat. Phys. **82** (1996), 1063–1080.

[RSW93] G. Radons, H. G. Schuster, and D. Werner, *Fractal measures and diffusion as results of learning in neural networks*, Phys. Lett. A **174** (1993), 293–297.

[Ruj78] P. Ruján, *Calculation of the free energy of Ising systems by a recursion method*, Physica A **91** (1978), 549–562.

[Rya92] D. H. Ryan, *Recent progress in random magnets*, World Scientific, Singapore, 1992.

[Sat87] I. I. Satija, *Random-field Ising model as a dynamical system*, Phys. Rev. B **35** (1987), 6877–6879.

[SB87] P. Szépfalusy and U. Behn, *Calculation of a characteristic fractal dimension in the one-dimensional random field Ising model*, Z. Phys. B **65** (1987), 337.

[SC00] N. S. Skantzos and A. C. C. Coolen, *Random field Ising chains with synchronous dynamics*, J. Phys. A **33** (2000), 1841–1855.

[Sch57] H. Schmidt, *Disordered one-dimensional crystals*, Phys. Rev. **105** (1957), 425–441.

[Shu00] P. Shukla, *Exact solution of return hysteresis loops in a one-dimensional random-field Ising model at zero temperature*, Phys. Rev. E **62** (2000), 4725–4729.

[Shu01] P. Shukla, *Exact expressions for minor hysteresis loops in the random field Ising model on a Bethe lattice at zero temperature*, Phys. Rev. E **63** (2001), 027102.

[SK75] D. Sherrington and S. Kirkpatrick, *Solvable model of a spin glass*, Phys. Rev. Lett. **35** (1975), 1792.

[Sli99] M. B. Slimane, *Multifractal formalism for self-similar functions under the action of nonlinear dynamical systems*, Constr. Approx. **15** (1999), 209–240.

[SMCB94] M. R. Swift, A. Maritan, M. Cieplak, and J. R. Banavar, *Phase diagrams of random-field Ising systems*, J. Phys. A **27** (1994), 1525–1532.

[SRR00] P. Shukla, R. Roy, and E. Ray, *Hysteresis in one-dimensional anti-ferromagnetic random field Ising model at zero-temperature*, Physica A **276** (2000), 365–375.

[SS97] R. Stoop and F. H. Steeb, *Convex hull violation by superposition of multifractals*, Phys. Rev. E **55** (1997), 6589–6592.

[SSD00] S. Sabhapandit, P. Shukla, and D. Dhar, *Distribution of avalanche sizes in the hysteretic response of the random-field Ising model on a Bethe lattice at zero temperature*, J. Stat. Phys. **98** (2000), 103–129.

[SSU98a] K. Simon, B. Solomyak, and M. Urbanski, *Parabolic iterated function systems with overlaps I*, Mathematica Gottingensis Preprint Series **8** (1998).

[SSU98b] K. Simon, B. Solomyak, and M. Urbanski, *Parabolic iterated function systems with overlaps II*, preprint (1998).

[SSU00] K. Simon, B. Solomyak, and M. Urbanski, *Invariant measures for parabolic IFS with overlaps and random continued fractions*, preprint (2000).

[ST86] P. Szépfalusy and T. Tél, *New approach to the problem of chaotic repellers*, Phys. Rev. A **34** (1986), 2520–2523.

[TAP77] D. J. Thouless, P. W. Anderson, and R. G. Palmer, *Solutions of 'solvable model of a spin glass'*, Philos. Mag. **35** (1977), 593–601.

[Tél86] T. Tél, *Characteristic exponents of chaotic repellers as eigenvalues*, Phys. Lett. A **119** (1986), 65–68.

[Tél87] T. Tél, *Escape rate from strange sets as an eigenvalue*, Phys. Rev. A **36** (1987), 1502–1505.

[TFI89] T. Tanaka, H. Fujisaka, and M. Inoue, *Free-energy fluctuations in a one-dimensional random Ising model*, Phys. Rev. A **39** (1989), 3170–3172.

[TFI90] T. Tanaka, H. Fujisaka, and M. Inoue, *Scaling structures of free-energy fluctuations in a one-dimenional dilute Ising model*, Prog. Theor. Phys. **84** (1990), 584.

[vHKK88] J. L. van Hemmen, G. Keller, and R. Kühn, *Forgetful memories*, Europhys. Lett. **5** (1988), 663–668.

[vHT74] J. von Heimburg and H. Thomas, *Phase transitions of the Cayley tree with Ising interaction*, J. Phys. C **7** (1974), 3433–3443.

[vK04] H. von Koch, *Sur une courbe continue sans tangente, obtenue par une construction géométrique élémentaire*, Arkiv för Matematik, Astronomi och Fysik **1** (1904), 681–704.

[Wei72] K. Weierstraß, *Über continuierliche Functionen eines reellen Arguments, die für keinen Wert des letzteren einen bestimmten Differentialquotienten besitzen*, [Wei95] (first publication), 1872, pp. 71–74.

[Wei95] K. Weierstraß, *Mathematische Werke*, Mayer & Müller, Berlin, 1895.

[Wu82] F. Y. Wu, *The Potts model*, Rev. Mod. Phys. **54** (1982), 235–268.

[You82] L. S. Young, *Dimension, entropy, and Lyapunov exponents*, Ergod. Th. & Dynam. Sys. **2** (1982), 109–124.

Curriculum Vitae

Surname	Nowotny
First Name	Thomas
Place and Date of Birth	Kassel, September 17, 1971
Nationality	German
Marital Status	Single
Current Address	Lauchstädter Str. 33 04229 Leipzig

September 1978–July 1982	Elementary School Heiligenrode
August 1982–June 1991	Highschool Engelsburg Gymnasium, Kassel
June 11, 1991	Abitur
August 1991–September 1992	Zivildienst, Caritas-Verband Kassel
October 1992–July 1994	Undergraduate studies in physics, Georg-August Universität Göttingen
July 8, 1994	Diplomvorprüfung in physics
August 1994–July 1998	Graduate studies in physics, Georg-August Universität Göttingen
September 1995–August 1996	Studies in physics, University of California, Riverside (Education Abroad Program)
Winter semester 1996/97	Teaching assistant, Institut für Theoretische Physik, Göttingen
March 1997–September 1998	Assistant, data processing group, Max-Planck Institut für Strömungsforschung, Göttingen
July 9, 1998	Diplom in physics
since October 1998	PhD student in theoretical physics, Graduiertenkolleg Quantenfeldtheorie, Universität Leipzig
since June 1999	Network administrator, Institut für Theoretische Physik, Leipzig

Acknowledgements

After nearly three years of research work on this thesis acknowledgements are due to numerous colleagues and friends. First of all I thank Ulrich Behn for his support, our regular and helpful discussions and his general good humour which makes working with him so pleasant. Furthermore I thank my colleagues in the Graduiertenkolleg Quantenfeldtheorie for the numerous tea time discussions and the homely atmosphere. Thanks are due to Elisabeth Leps, all other friends and my parents for continous support and encouragement. I want to use this opportunity to also thank all developers of free software in particular Linux, X, Emacs, TeX/LaTeX, GCC, Condor, CLN and all the other software without which this work would not have been possible. The work was financially supported by the Graduiertenkolleg "Quantenfeldtheorie" of the Deutsche Forschungsgemeinschaft (DFG).

Index